THE UNIVERSITY OF CHICAGO

DECIPHERING THE MECHANISMS OF SONIC HEDGEHOG DISPERSAL AND GRADIENT FORMATION IN THE EMBRYONIC LIMB BUD MESENCHYME

A DISSERTATION SUBMITTED TO
THE FACULTY OF THE DIVISION OF THE BIOLOGICAL SCIENCES
AND THE PRITZKER SCHOOL OF MEDICINE
IN CANDIDACY FOR THE DEGREE OF
DOCTOR OF PHILOSOPHY

COMMITTEE ON DEVELOPMENT, REGENERATION, AND STEM CELL BIOLOGY

BY
SEAN MACKENZIE CORCORAN

CHICAGO, ILLINOIS
DECEMBER 2026

© 2026 Sean Mackenzie Corcoran

For my family, friends, and wife for the support and joy that pushed me to achieve this milestone.

"The chemical basis of morphogenesis depends upon the interaction of substances which diffuse through tissues." — Alan Turing, The Chemical Basis of Morphogenesis (1952)

TABLE OF CONTENTS

LIST OF FIGURES vii

LIST OF TABLES viii

ACKNOWLEDGMENTS ix

ABSTRACT xi

1 INTRODUCTION TO TISSUE PATTERNING, MORPHOGEN GRADIENTS, AND THE UNRESOLVED REGULATION OF SONIC HEDGEHOG DISPERSAL . . 1
1.1 Preface 1
1.2 Embryological and Theoretical Foundations of Pattern Formation 2
1.3 Morphogens: the Conduits of Tissue Patterning 5
1.3.1 The Identification of the First Morphogen 5
1.3.2 Secreted Morphogens and the Principles of Tissue Patterning 7
1.3.3 The Establishment of Morphogen Gradients is Tightly Regulated . . 10
1.4 Sonic Hedgehog: Developmental Roles, Signal Transduction, and Biogenesis 12
1.4.1 Diverse Roles of Shh in the Neural Tube Epithelium 13
1.4.2 Sonic Hedgehog Signal Transduction 13
1.4.3 Shh Biogenesis and Intrinsic Limitation in Diffusion 16
1.5 Specialized Mechanisms for Long-Range Hedgehog Dispersal 17
1.5.1 Carrier-Assisted Diffusion 17
1.5.2 Direct-Delivery Along Cytonemes 21
1.6 Tissue Architecture and the Regulation of Hedgehog Dispersal 23
1.7 Limb Development and the Role of Shh Signaling in Anterior-Posterior Patterning 25
1.7.1 Signaling Centers of the Limb Bud 27
1.7.2 Anterior-Posterior Specification Models in the Chicken and Mouse Limb Bud 30
1.7.3 Mechanisms of Sonic Hedgehog Dispersal in the Limb Bud 32
1.8 Overview of Dissertation 34

2 EXOSOME SECRETION IS REQUIRED FOR SONIC HEDGEHOG DISPERSAL AND SIGNAL GRADIENT FORMATION IN THE EMBRYONIC LIMB BUD MESENCHYME 35
Abstract 35
2.1 Introduction 36
2.2 Results 39
2.3 Discussion 66
2.4 Materials and Methods 71

3 CONCLUSION AND FUTURE DIRECTIONS 103
3.1 Preface 103
3.2 MVB packaging and exosome release represents a central Shh secretion pathway 103
3.3 A complex Shh trafficking route is shared between mesenchymal and epithelial tissues 105
3.4 Exosome secretion is required for mesenchymal cells to establish Shh gradients 106
3.5 Transport along cytonemes provides an alternative mode of exosome-mediated Shh dispersal 109
3.6 Extracellular vesicles serve as broad mediators of cell-cell signaling in both development and disease 114

APPENDIX A SYNTHETIC CYTONEME MANIPULATION AND THE ROLE OF CYTONEMES IN SKELETAL PATTERNING OF THE LIMB 118
A.1 Preface 118
A.2 Introduction 118
A.3 Results and Discussion 120
A.3.1 ATV- can deplete GFP-tagged cargo from PLMC cytonemes 120
A.3.2 ATV- and EGFP-Myosin10-Tail coexpression can greatly reduce cytoneme formation in PLMCs 121
A.3.3 Cytoneme loss of function in the limb bud in vivo causes variable skeletal defects 122
A.4 Materials and Methods 125
A.4.1 Image Analysis and Quantification 127

REFERENCES 129

LIST OF FIGURES

1.1 Reaction-diffusion and positional information models of pattern formation . . . 4
1.2 Bcd Morphogen Gradient in the *Drosophila* syncytial embryo 6
1.3 Secreted morphogens share similar design principles and work in concert 8
1.4 Shh signal transduction and biogenesis 15
1.5 Carrier-assisted diffusion mechanisms 18
1.6 Extracellular vesicles share similar composition but differ in biogenesis. 20
1.7 Cytonemes mediate direct delivery of Shh between cells via synapse like connections 22
1.8 A complex trafficking route promotes multiple potential modes of Hh dispersal in *Drosophila* imaginal wing disc epithelial cells 25
1.9 Vertebrate models of limb development and the roles of Shh signaling in the limb bud 26

2.1 Primary Limb Mesenchymal Cell (PLMC) culture provides a tractable model to study Shh trafficking and dispersal dynamics 41
2.2 Shh-FL-msfGFP overexpression does not alter cytoneme production or subcellular localization 42
2.3 CDH release system provides tight ER trapping in vitro and in vivo 45
2.4 A CDH synchronous release system reveals that Shh rapidly accumulates in MVB-like structures after leaving the Golgi Apparatus. 47
2.5 Shh fusion proteins colocalize in endocytosis-derived CD63-positive MVBs . . . 49
2.6 Shh-positive endosomal structures are bona fide multivesicular bodies (MVBs) that fuse to the plasma membrane to release Shh-bound exosomes. 50
2.7 MVB-plasma membrane fusion events in PLMC cell bodies generate extracellular CD63-pHluo labeled exosomes. 52
2.8 Shh-bound secreted exosomes associate with and travel along cytonemes 55
2.9 Exosome secretion contributes to Shh association along cytonemes 57
2.10 Exosome secretion is required for Shh dispersal and signal gradient formation. . 59
2.11 Controls related to Shh signaling gradients 61
2.12 Exosomes are transported along the external surface of cytonemes and are required to establish Shh concentration gradients in vivo. 62
2.13 Ultrastructural views of limb bud mesenchymal cells in vivo highlight narrow cytoneme diameters 64
2.14 Embryonic injection of Nexinhib20 in vivo does not affect cell morphology or cell death in the limb bud mesenchyme 65

A.1 ATV- can pull GFP-tagged cargo to the minus end of cytonemes 121
A.2 ATV- and EGFP-Myosin10-Tail coexpression in PLMCs reduces cytoneme formation 122
A.3 ATV- mediated cytoneme inhibition causes variable skeletal defects in the limb . 124

LIST OF TABLES

2.1 Key Resource Table 71

ACKNOWLEDGMENTS

First and foremost, I would like to thank my advisor, Dr. Edwin Munro, for his guidance and support. Although my research project was unique within his lab, I am deeply grateful that he gave me the space and freedom to chart my own path as a scientist. Ed your passion for microscopy (and pottery), is something I deeply admire.

To my thesis committee, Dr. Ellie Heckscher, Dr. Victoria E. Prince, and Dr. Timothy Sanders, thank you for your time, questions and advice, and encouraging discussions over the years. In moments when I doubted the scope of my work, your feedback consistently challenged me to make claims confidently and use my skepticism as a strength and not a crutch. Thank you all for your steady support through every stage of this process. Ellie, thank you for your kindness, and trust in allowing me to TA the DNUFO course for many years. Vicky, thank you for giving me the opportunity to help build the UChicago Embryology course. Additionally, you were always a resource whether for science or for navigating grad school. Lastly, Tim, thank you for taking me into your lab early on and introducing me to the world of chick limb bud development. I still fondly remember the excitement of learning new techniques and building tools together in those early years, and I am grateful for the opportunity we had to work together.

I would like to thank Pulin Li, Alissa Weaver, Benjamin Glick, Miriam Domowicz, Bruno Correia, and Sailan Shui for genetic constructs, cell lines, and general reagents that made this work possible. Additionally, I would like to thank Christine Labno (Director of the Integrated Light Microscopy Core) for advice both on microscopy and FIJI macro writing.

To my lab mates, past and present: thank you for creating a vibrant day-to-day work environment. From eating lunch together, wordling, and playing pickleball, I feel very fortunate to be surrounded by great scientists who also love life.

To my friends and colleagues, thank you for making this PhD journey infinitely more fun. To Jake and Thea, from simple hangouts at the point to traveling to Tulum together,

I always enjoy spending time with you. To Rob, you are an inspiration of extremes. You work harder than anyone I know but also spend the most time on vacation. To members of the Pierogi Princes (Annisa, Sierra, Matt, Amrita, and Kierstin), thank you for making Chicago feel like home.

I am deeply grateful to my family. Mom and Dad, thank you for your constant love, support, and encouragement. I consider myself lucky to have grown up in a loving home that empowered me to pursue my goals and seek out new opportunities. You believed in me even when I doubted myself, and everything I have achieved in this degree is built on the foundation you gave me. I also appreciate your and Evan's attempts to learn about my project, even though Evan thought I worked with kumquots instead of aliquots.

To my wife Tiffany, you have made my life better in every way. Your ambition and confidence consistently push me to become the best version of myself. Your kindness, love, and support accept me when I fail to be my best version. Thank you.

ABSTRACT

Embryos use a small number of conserved developmental signaling molecules called morphogens to pattern a broad range of cell fates across varied tissues. Morphogens are secreted by source cells and disperse across target tissues to shape signaling activity gradients which, in turn, are interpreted by target cells to mediate fate decisions. Because these gradients must be precise across tissues of different sizes and architectures, morphogen dispersal must be tightly regulated.

Hedgehog (Hh) signaling is a highly conserved pathway that controls diverse cellular behaviors during development, homeostasis, and disease. Like other morphogens, Hh and its vertebrate ortholog Sonic Hedgehog (Shh), disperse over long distances to form gradients and pattern tissues. However, during biogenesis, Hedgehog morphogens gain two covalent lipid modifications that promote membrane tethering and intrinsically limit diffusivity in the aqueous extracellular environment. Cells therefore must adopt specialized mechanisms to increase the distance of signal dispersal.

Several such mechanisms have been proposed. Carrier-assisted diffusion, mediated by extracellular vesicles and carrier proteins, shields the hydrophobic lipid modifications of Hh morphogens and thereby promotes their diffusion in the hydrophilic extracellular space. Another mechanism proposed bypasses diffusion altogether. Specialized signaling filopodia called cytonemes can directly transport morphogens from cell to cell in a synapse-like manner. However, the molecular regulation of these mechanisms, how they coordinate and interact with one another, and how they are utilized across diverse tissue architectures remains poorly understood.

In this thesis, I investigate the mechanisms governing Shh dispersal and gradient formation in the embryonic chicken limb bud mesenchyme. In the limb bud, Shh patterns the anterior-posterior axis to regulate digit specification. Specifically, Shh is expressed in a small posterior region of the limb bud and undergoes long-range dispersal across the mesenchyme

to form a signaling activity gradient that instructs differential cell fate.

My work establishes exosome secretion as a central pathway for Shh dispersal and gradient formation in the limb bud mesenchyme. I created and optimized a novel synchronous release tool that allowed me to dissect the intracellular trafficking of Shh in primary limb bud mesenchymal cells with high spatiotemporal resolution. Using this tool, I found that Shh is rapidly packaged into exosomes for release into the extracellular space. Live imaging revealed that Shh-bound exosomes can both diffuse in the extracellular space and bind to and travel along the external surface of cytonemes for directed transport. Futhermore, I determined that exosome secretion is required for the formation of Shh signaling gradients both in 2D reconstituted co-culture assays and in the 3D limb bud mesenchyme *in vivo*. My findings suggest that exosome secretion serves as a primary Shh dispersal strategy and can be tuned by changing the mode of transport (e.g. diffusion vs cytoneme delivery) to sculpt signaling gradients and pattern diverse tissues. In summary, this work has helped unify key aspects of Shh signaling by highlighting the coordination of dispersal mechanisms.

CHAPTER 1

INTRODUCTION TO TISSUE PATTERNING, MORPHOGEN GRADIENTS, AND THE UNRESOLVED REGULATION OF SONIC HEDGEHOG DISPERSAL

1.1 Preface

A fundamental question in developmental biology is how seemingly uniform tissues gain spatial pattern and specialized function. During embryogenesis, cells communicate to coordinate higher-order biological processes, such as growth and morphogenesis. One of the predominant forms of cell-cell communication relies on the secretion of signaling molecules that bind to receptors on target cells to elicit a cellular response. Morphogens are a small class of developmental signaling molecules that are produced at a local source, form concentration gradients across tissues, and instruct differential cell fate in a concentration-dependent manner. In order to achieve the correct tissue pattern, cells must coordinate the distribution of morphogens across space and time with high precision and modulate the interpretation of morphogen signaling. This chapter outlines the history, theory, and experimental evidence of general morphogen-mediated tissue patterning and delves into the regulation of Hedgehog as an example morphogen. Despite its well-characterized roles in tissue patterning, how Hedgehog ligands are dispersed across a tissue and establish a gradient remains poorly understood. This chapter will highlight the biophysical challenges of setting up a Hedgehog gradient, the known mechanisms of extracellular transport, and the open-ended questions in how Sonic Hedgehog is transported across the developing vertebrate limb bud mesenchyme.

1.2 Embryological and Theoretical Foundations of Pattern Formation

How cells organize into tissues with specialized pattern and function serves as one of the most fundamental questions in developmental biology. In this section, I will lay out the historical groundwork that morphogen-mediated tissue patterning was built upon.

The concept that embryogenesis relied on cell-cell communication grew from classical embryology experiments from the late 19th and early 20th centuries. Hans Driesch performed experiments in which he separated or re-arranged the position of sea urchin blastomeres and found that they had a remarkable ability to compensate for missing parts and re-organize to develop into complete sea urchin larvae (Driesch, 1891). These experiments were the first demonstrations of regulative development, which emphasizes that cell fate is not fixed, but rather dependent on position and interactions with external cues.

This idea was greatly built upon by a series of amphibian transplantation experiments performed by Hans Spemann and Hilde Mangold. Together, they transplanted the dorsal blastopore lip of a donor newt gastrula to the opposite side of a host gastrula and observed the formation of an entire second body axis (Spemann and Mangold, 1924). They concluded that regions of an embryo, called organizers or organizing centers, could organize other regions through some type of inductive signal. Years later, Conrad Waddington coined the term evocators for the chemical agents produced by organizers that can induce an embryonic tissue (Needham et al., 1934). The majority of the 20th century was spent both theoretically and mathematically modeling how embryonic patterns can arise as well as searching to identify the chemical agents responsible for embryonic induction.

In the second half of the 20th century, two key models were established that sought to model and conceptualize how embryonic patterning could occur: Turing's Reaction-Diffusion model and Wolpert's Positional Information (French Flag) model.

Reaction-Diffusion, or the Turing model, sought to address the question of how asym-

metry and pattern originate from a homogeneous, symmetric group of cells? In his 1952 "Chemical basis of morphogenesis", the mathematician Alan Turing proposed that two chemical species, which he named morphogens, could generate stable, periodic patterns of concentration using just chemical reactions and diffusion after an initial stochastic fluctuation in concentration (Turing, 1952). In 1972, Gierer and Meinhardt expanded Turing's reaction-diffusion model by modifying the morphogen parameters to include short-range activators and long-range inhibitors (Gierer and Meinhardt, 1972). In this model, stochastic local increases in the activator can promote positive feedback mediated increases in the activator, which in turn increase the local concentration of a faster diffusing inhibitor. The faster diffusing inhibitor prevents neighboring increases of the activator but allows the initial peak of the activator to stabilize. In regions at distance where the level of the inhibitor is low, local increases of the activator can emerge, repeating the cycle until spatially periodic concentrations of morphogens stabilize (Figure 1.1A). Conceptually, reaction-diffusion can be described as local self-enhancement paired with lateral inhibition (Green and Sharpe, 2015). Overall, reaction-diffusion models provided key insights into self-organization and how patterns of morphogens can arise.

The second key model of embryonic patterning, the positional information model, arose while attempting to address how complexity of pattern can derive from pre-patterned asymmetry and how this complex pattern can scale with size. In 1968, Lewis Wolpert initially posed his conceptual "French Flag Problem", asking how cells could organize into a simple linear pattern represented by the colors and proportions of the French Flag (blue, white, and red) and maintain the scaling of the pattern regardless of tissue size (Wolpert, 1968). One of the key conceptual solutions to this model was the fixed gradient model in which cells at the boundary of the line of cells produce and secrete a type of inductive signal called a morphogen, initially coined by Turing (Turing, 1952), that forms a concentration gradient over the developmental field in a tissue. Based on coordinate position within the tissue, cells

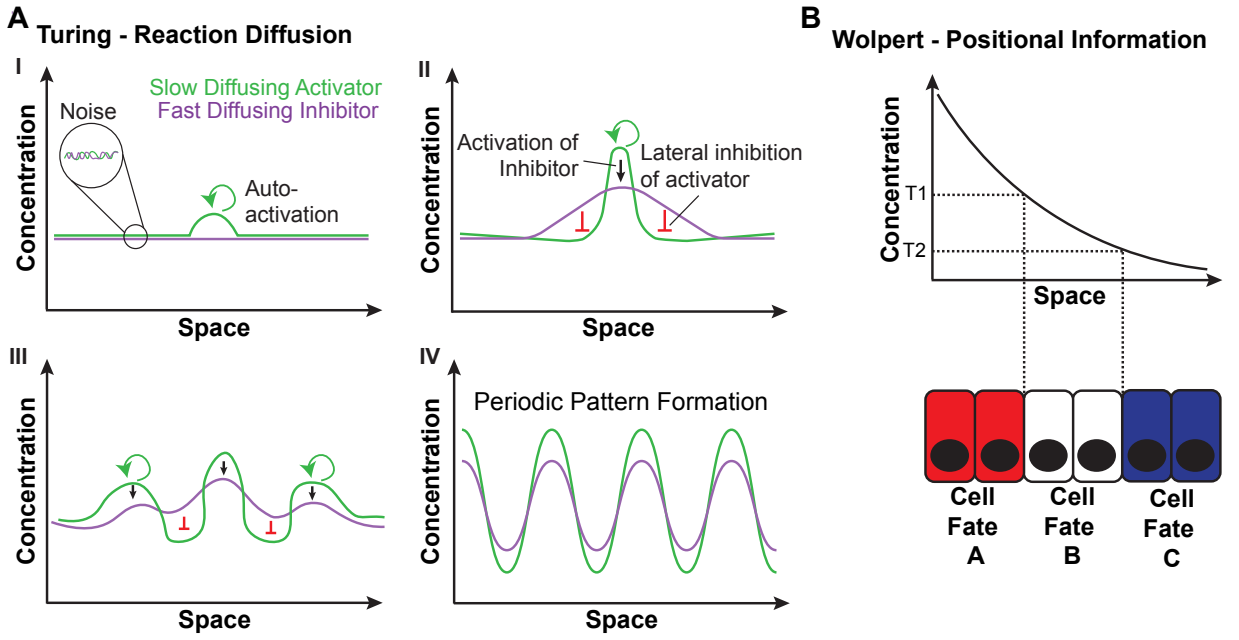


Figure 1.1: Reaction-diffusion and positional information models of pattern formation *(Adapted from Green and Sharpe, 2015).* (A) Diagram illustrating steps (I-IV) of reaction-diffusion generation of periodoic pattern (B) Diagram illustrating Wolpert's positional information model. Note the concentration thresholds (T1) and (T2) that promote differential cell fate.

are exposed to different thresholds of the morphogen, triggering differentiation into distinct cell types (i.e. blue, white, or red cells) forming the pattern of the French Flag (Figure 1.1B) (Wolpert, 1969). Francis Crick used mathematical modeling to demonstrate that diffusion of small, organic chemical species across a developmentally relevant sized field (less than a millimeter of distance) could generate linear gradients within a biologically relevant time frame (a few hours) (Crick, 1970). Together, the positional information created by morphogen gradients provided a simple, intuitive model to pattern tissues.

Both reaction-diffusion and morphogen gradient-positional information models remained conceptual until the discovery and identification of morphogens in the late 20th century. The discovery of bonafide morphogens helped validate and unify these models. However, subsequent experimental work revealed an incredible amount of biochemical, biophysical, and cellular complexity that requires a deeper evaluation of how morphogen gradients are

established and how patterning is integrated with other developmental processes, like growth and cell survival.

1.3 Morphogens: the Conduits of Tissue Patterning

In this section, I will describe the discovery of the first morphogen, followed by a brief survey of identified morphogens, their functions, and the challenges of dispersing morphogens across tissues.

1.3.1 The Identification of the First Morphogen

With the theoretical framework of morphogen gradients, positional information, and spatial patterning established, researchers in the last half of the 20th century aimed to discover the morphogens hypothesized to mediate this patterning. In the 1980s, Christine Nüsslein-Volhard and Eric Weischaus performed large-scale genetic screens that uncovered 120 zygotic genes and around 30 maternal genes required for the development of the *Drosophila melanogaster* embryonic body plan (Nüsslein-Volhard and Wieschaus, 1980; Nüsslein-Volhard et al., 1984, 1987; Jürgens et al., 1984). Based on the severity of the patterning defect, the maternally deposited gene *bicoid (bcd)* became a candidate for a morphogen.

Wolfgang Driever and Nüsslein-Volhard showed that maternally deposited *bcd* mRNA localized to the anterior pole of the egg, and when later translated, the Bcd protein formed an anterior to posterior gradient in the early syncytial embryo (Figure 1.2A) (Driever and Nüsslein-Volhard, 1988b). They found that modifying *bcd* gene dosage could modify the resulting Bcd protein gradients and cause spatial shifts in morphological features along the anterior-posterior axis (Driever and Nüsslein-Volhard, 1988a). Lastly, they found that injection of *bcd* mRNA into the anterior region of *bcd* deficient embryos could be rescue patterning, while ectopic, posterior injection of *bcd* mRNA could induce ectopic anterior structures (Fig-

ure 1.2B) (Driever et al., 1990). Together, these papers provided experimental evidence for Wolpert's positional information model, demonstrating that Bcd acts as a morphogen by diffusing away from a local source to form a spatial gradient and instructing cell fate in a dose-dependent manner.

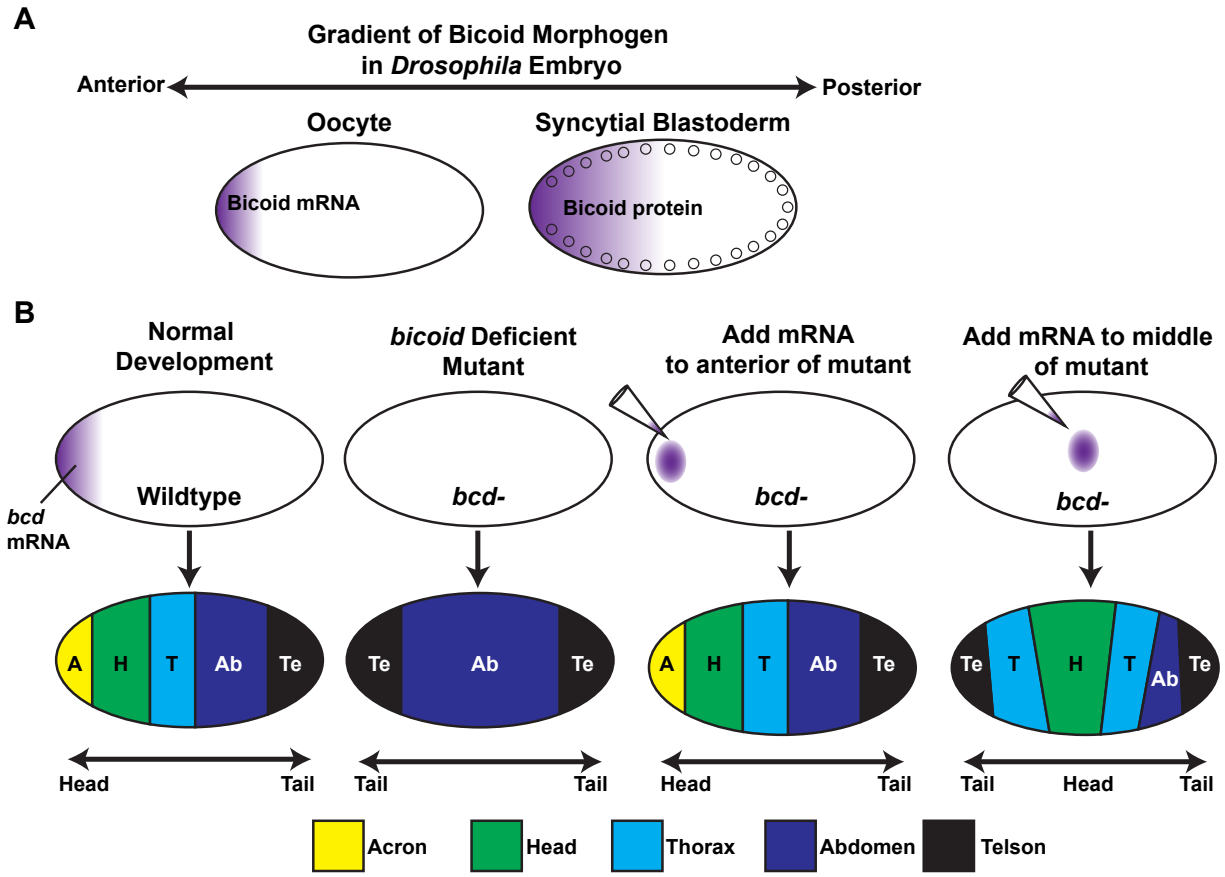


Figure 1.2: Bcd Morphogen Gradient in the *Drosophila* syncytial embryo *(Adapted from Gilbert, 2003).* (A) Diagram of anterior localization of maternally deposited *bcd* mRNA and the resulting Bcd protein gradient. (B) Diagram highlighting set of experiments and phenotypes performed by Driever and Nüsslein-Volhard in the 1980s to establish the function of Bcd as a morphogen.

Although identified first, Bcd is somewhat of a unique morphogen. Unlike the highly conserved morphogens later discovered, Bcd arose relatively recently in evolution, and it is restricted to *Diptera* (Mulhair et al., 2025). Additionally, Bcd is a maternally deposited transcription factor that forms spatial gradients across the shared cytoplasm between the

nuclei within the Drosophila embryonic syncytium, bypassing the need for extracellular transport. By comparison, in most tissues, cells are partitioned by distinct plasma membranes, which transcription factors cannot move across. Thus, most morphogens must be secreted and transported across the extracellular space to form concentration gradients and mediate tissue patterning.

1.3.2 Secreted Morphogens and the Principles of Tissue Patterning

Despite the diversity of body plans and tissue types across the animal kingdom, a relatively small suite of highly-conserved morphogens have been identified. With the exception of retinoic acid, most identified morphogens are secreted protein ligands (Schilling et al., 2012). These secreted ligands belong to distinct groups or families based on their structural and functional identity, including Bone Morphogenetic Proteins (Bmps) of the TGF-β superfamily, the Wingless-related integration site (Wnt) Family, the Fibroblast Growth Factor (Fgf) Family, and the Hedgehog (Hh) Family.

Regardless of the differences in structural and functional identity, all secreted morphogens follow a shared design principle for tissue patterning (Figure 1.3A). Morphogens are produced and secreted in a small, local region of cells often known as a signaling center or organizer (Basson, 2012). Morphogens undergo specialized transport across a tissue, interacting with other cells, extracellular matrix molecules, and secreted inhibitors to form a concentration gradient (Müller et al., 2013). Through ligand-receptor binding on the plasma membrane, morphogen signals are transduced through biochemical cascades and complex gene regulatory networks to instruct cell fate decisions in a graded manner (Rogers and Schier, 2011; Briscoe and Small, 2015). Thus, the diversity of tissue pattern can be attributed to differential cellular competence, the regulation of morphogen dispersal, and specific interpretation and feedback (Sagner and Briscoe, 2017).

Morphogens can have highly conserved roles in early embryonic axis determination. For

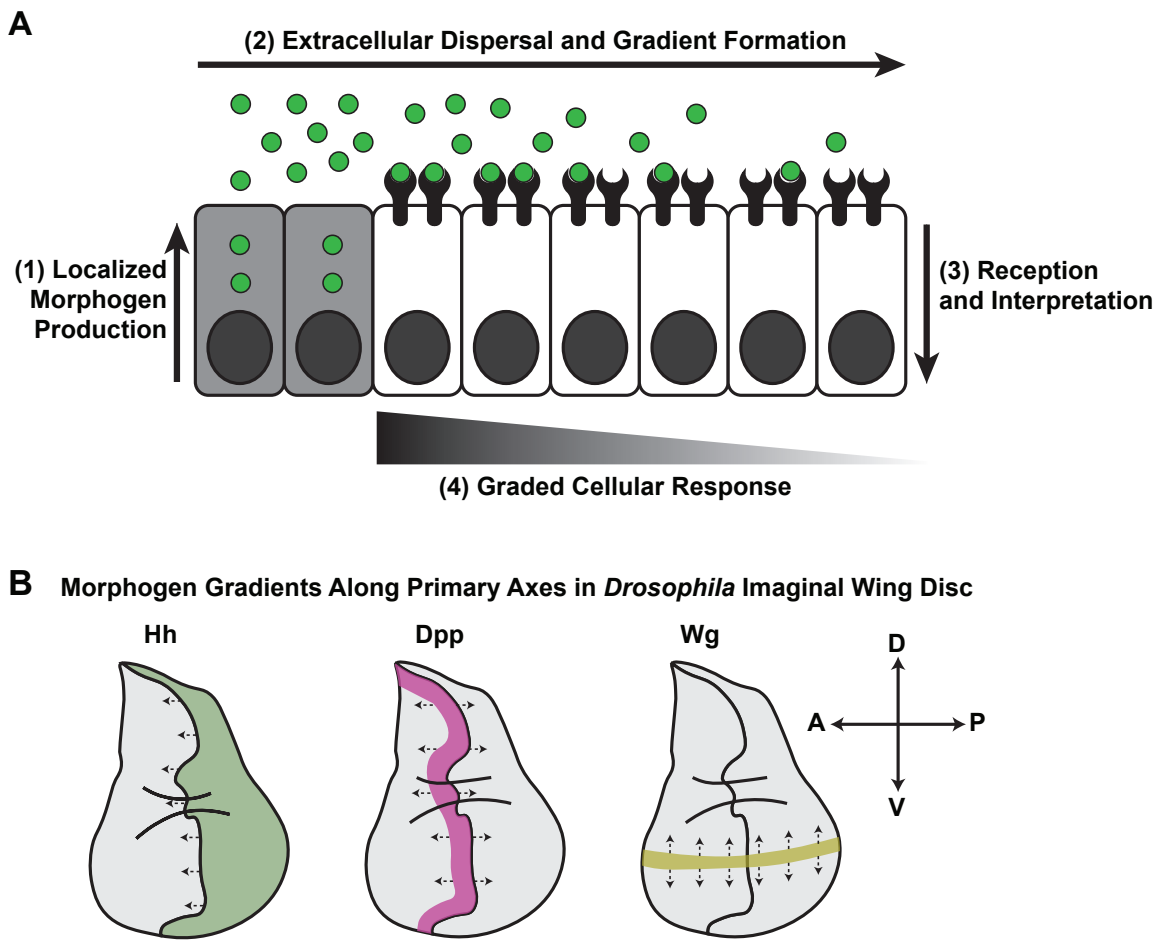


Figure 1.3: Secreted morphogens share similar design principles and work in concert. (A) Diagram of general steps of secreted morphogen-mediated tissue patterning. (B) Diagram of 3 morphogen gradients regulating different axes of the *Drosophila* imaginal wing disc.

example, in Bilaterians, there are highly conserved roles for Wnt signaling gradients in patterning the anterior-posterior body axis and Bmp signaling gradients in patterning the dorsal-ventral body axis (Petersen and Reddien, 2009; Niehrs, 2010; Yan and Wang, 2021). These morphogens also have ancient functions in patterning primary body axes in radially symmetric animals. For example, Wnt signaling patterns the oral-aboral axis in cnidarians (Leclère et al., 2016).

The same morphogens are re-used later in development to drive unique tissue patterning

and organogenesis. For example, Bmps help pattern the sensory and interneuron fates in the dorsal neural tube (Barth et al., 1999), the regionalization of the gut (Roberts et al., 1995; Wang et al., 2025), the morphogenesis of the kidney (Oxburgh et al., 2004), and are essential in the differentiation of osteoblasts and general skeletal development(Kronenberg, 2003). Similarly, Wnts also help pattern multiple tissues and organs, including the skin, lungs, heart, gut, and nervous system (Lim and Nusse, 2013; Ren et al., 2026; Li et al., 2022; Verzi and Shivdasani, 2008; Patapoutian and Reichardt, 2000).

Importantly, many morphogens are used in concert with one another. For example, in the *Drosophila* imaginal wing disc, Hh, Dpp (a BMP ortholog), and Wg (a Wnt ortholog) all function together to pattern different tissue axes to give rise to the specialized adult wing (Figure 1.3C). Specifically, *Hh* is expressed in the posterior compartment of the wing disc epithelium, disperses across to the posterior compartment, and induces a thin stripe of *Dpp* at the midline (Basler and Struhl, 1994; Tabata and Kornberg, 1994). Dpp then diffuses long-range to pattern the anterior-posterior axis and positions the wing veins (Nellen et al., 1996; Lecuit et al., 1996). An orthogonal stripe of Wg (a Wnt ortholog) helps pattern the dorsal ventral axis and promote growth (Neumann and Cohen, 1997).

Beyond the true morphogen function in graded cell fate specification, many of these signaling molecules have diverse functions during development and homeostasis often driving proliferation, cell-survival, stem-cell renewal, and cell migration (Mehlen et al., 2005; Dekanty and Milán, 2011; Eggington et al., 2022; Gibney and Pani, 2025). Whether these secondary functions also have graded responses remains unclear and will be discussed in Chapter 3. From this point forward, these signaling molecules will be referred to as morphogens, regardless of their tissue-specific function.

1.3.3 The Establishment of Morphogen Gradients is Tightly Regulated

There are many factors that can control the shape of a gradient, including tissue growth, morphogen production rates, mechanisms of dispersal or spread across a tissue, receptor binding, internalization, recycling, and both intracellular and extracellular degradation (Wartlick et al., 2009). All of these parameters are context-specific and regulated by tissue architecture and intrinsic properties of morphogens themselves.

Theoretically, gradients can be generated by growth alone. If one considers morphogen producing cells to be a unit of volume and if they continuously grow and divide, the concentration of the morphogen will be diluted as volume increases, causing a temporal gradient. For example, *Fgf8* mRNA is expressed in the posterior pre-somitic mesoderm, and as these cells divide and expand out of the expression region, they dilute the *Fgf8* mRNA, forming a gradient (Dubrulle and Pourquié, 2004).

In addition, the tissue environment itself can regulate morphogen gradients. Tissues have unique architectures with varying cell type compositions, such as tightly-packaged, polarized epithelial cells or loosely connected mesenchymal cells that can impact overall tortuosity and geometry of the extracellular space in which morphogens must travel (Nicholson and Syková, 1998; Zhu et al., 2025). Moreover, tissues can vary the densities and compositions of extracellular matrix molecules, such as Heparan sulfate proteoglycans, receptors, and secreted inhibitors, to shape gradients by sequestering or degrading morphogens (Wang et al., 2016). For example, by introducing uniform receptor-mediated degradation of morphogens across a tissue, a linear gradient seen in source-sink models can transform into one of exponential decay (Lewis et al., 1977).

Perhaps the most debated aspect of morphogen gradient formation lies in how morphogens actually move across tissues. Diffusion across a tissue has been touted as the most straightforward mechanism to generate concentration gradients. Using both theoretical and complex modeling with empirical biophysical parameters, it has been demonstrated

that diffusion is fully capable of generating gradients over the time scales and distances for known developmental patterning fields (Crick, 1970; Schwank et al., 2011; Zhou et al., 2012; Müller et al., 2013). However, simple diffusion models struggle to explain how hydrophobic morphogens are dispersed across tissues. Additionally, a growing body of experimental work suggests that morphogens are dispersed through highly regulated modes of secretion, carrier-assisted diffusion, and cytoneme-based active transport mechanisms.

Each morphogen has intrinsic physical and chemical properties that modify the way it moves across tissues. Functional morphogens span a wide range of physical sizes. For example, Fgfs vary in size from 17-34 kDa in vertebrates, while *Drosophila* Fgf homologs exceed 80 kDa (Ornitz and Itoh, 2001; Tulin and Stathopoulos, 2010). Similarly, mature Bmp2 homodimers are roughly 30 kDa, with individual monomers measured to be much smaller at 14-16 kDa (Suzuki et al., 2020). Relatedly, the diffusion coefficients between morphogens can vary dramatically within the same tissue environment. For instance, Fluorescence Recovery After Photobleaching (FRAP) experiments in the *Drosophila* imaginal wing disc demonstrate that Wg-GFP moves roughly twice as slow as Dpp-GFP with diffusion coefficients of 0.05 $\mu m^2/s$ and 0.1 $\mu m^2/s$, respectively (Kicheva et al., 2007). Additionally, the biochemical properties of morphogens can alter dispersal across a tissue. While FGF and BMPs are hydrophilic ligands capable of simple diffusion in the extracellular space, Wnt and Hh ligands contain lipid modifications that increase their intrinsic hydrophobicity and limit their extracellular spread (Willert et al., 2003; Mann and Beachy, 2004). Overall, the regulation of morphogen gradient formation is a complex process governed by tissue properties and the physical and chemical properties of the morphogens.

Hedgehog-mediated tissue patterning exemplifies the need for tight regulation of extracellular dispersal remarkably well. Hedgehog signaling is an essential pathway that regulates the organization of numerous tissues across most animal species (Jiang and Hui, 2008). Paradoxically, long-range Hh dispersal is required for patterning, yet the lipid modifications of

Hh ligands inherently limit spread across the aqueous extracellular space. This regulatory challenge demonstrates why Hh dispersal serves as a key model to extract general principles for morphogen transport. The following sections introduce the Hedgehog signaling pathway, with a focus on vertebrate Sonic Hedgehog, and the mechanisms postulated to disperse Hh ligands across tissues.

1.4 Sonic Hedgehog: Developmental Roles, Signal Transduction, and Biogenesis

Originally discovered as a segment polarity gene in the Nüsslein-Volhard and Wieschaus saturation screen (1980), Hedgehog (Hh) was later identified as a morphogen that patterns diverse tissues. Core components of the Hh signaling pathway are highly conserved across most metazoans, from cnidarians to humans (Matus et al., 2008).

Vertebrates specifically have three Hedgehog ligand homologs: *Desert Hedgehog* (*Dhh*), *Indian Hedgehog* (*Ihh*), and *Sonic Hedgehog* (*Shh*). *Dhh* has the most restricted expression with primary functions in the reproductive system and peripheral nervous system (Bitgood et al., 1996; Clark et al., 2000; Kawai et al., 2011; Dilower et al., 2023; Parmantier et al., 1999; Sharghi-Namini et al., 2006). *Ihh* has broader expression and plays key roles in patterning the hematopoietic and vascular systems, extraocular orbital structures of the mammalian eye, and skeletal development (Dyer et al., 2001; Dakubo et al., 2008; Ohba, 2020). *Shh* has the broadest expression and regulates the development of almost every organ system of the vertebrate body plan (Varjosalo and Taipale, 2008).

Given the essential role of Shh in development, dysregulated Shh signaling causes many human pathologies. Mutations in the Shh signaling pathway can lead to congenital birth defects, including Holoprocencephaly, Pallister-Hall syndrome, and Gorlin syndrome (Nieuwenhuis and Hui, 2005). In addition, ectopic activation of Shh signaling can promote certain cancers, including basal cell carcinoma and medulloblastoma (McMahon et al., 2003). Thus,

understanding the regulation of Shh dispersal is of both biological and medical importance.

1.4.1 Diverse Roles of Shh in the Neural Tube Epithelium

The vertebrate neural tube serves as a key model of how Shh functions in morphogen-mediated tissue patterning. After neurulation, Shh expressed by the notochord induces *Shh* expression in the ventral floorplate of the neural tube (Echelard et al., 1993; Roelink et al., 1995). Ventral floorplate cells disperse Shh to form a concentration gradient and a corresponding signaling activity gradient along the DV axis of the neural tube (Gritli-Linde et al., 2001; Chamberlain et al., 2008; Cohen et al., 2015). Both the concentration and duration of signaling regulate the combinatorial expression of transcription factors that drive neural progenitors to differentiate into distinct motor neuron and interneuron identities (Briscoe et al., 2000). Progressively higher duration and intensity of signaling drive neural progenitors to more ventral fates (Ribes and Briscoe, 2009).

Interestingly, beyond its role as a bona fide morphogen, Shh performs additional roles in the embryonic neural tube. Shh acts as a mitogen promoting the proliferation and survival of neural progenitor cells in the neural tube (Cayuso et al., 2006). Furthermore, floor-plate produced Shh also functions as an axon guidance cue for dI1 commissural neurons (Charron et al., 2003; Bourikas et al., 2005).

1.4.2 Sonic Hedgehog Signal Transduction

Similar to other secreted morphogens, the cellular response is mediated through reception and a downstream biochemical signaling cascade that results in transcriptional activation of key target genes. In vertebrates, Shh signaling takes place at a specialized signaling organelle: the primary cilium (Goetz and Anderson, 2010).

In the absence of Shh signals in receiving cell populations (Figure 1.3B), the trans-membrane receptor Patched-1 (Ptch1) accumulates in the primary cilium and inhibits the

accumulation and activity of the main Hedgehog transducer Smoothened (Smo) by reducing available cholesterol in the ciliary membrane (Kinnebrew et al., 2021). Without Smo, the orphan G-protein coupled receptor Gpr161 accumulates in the primary cilia and activates Protein Kinase A (PKA) through increased cAMP production (Bachmann et al., 2016; Cai et al., 2022). Active ciliary PKA phosphorylates Suppressor of Fused (Sufu) and the Glioma-associated oncogene (Gli2/3) transcription factors (Pan et al., 2006; Zhuang, 2025). The phosphorylation of the Sufu and Gli2/3 stabilizes the complex in the cytoplasm and promotes the proteasome-mediated cleavage of Gli2 and Gli3 into their repressor forms, Gli2R and Gli3R, that translocate to the nucleus to repress Shh target gene expression (Pan et al., 2006).

In the presence of Shh ligands, the signaling pathway is activated; or more accurately, the pathway inhibition is relieved (Figure 1.3C). First, Shh binds to the semi-redundant co-receptors Cell Adhesion Associated Oncogene Regulated (Cdo), Brother of CDO (Boc), and/or Growth Arrest-Specific 1 (Gas1), which then transfer Shh ligands to Ptch1 (Izzi et al., 2011). Shh inhibits Ptch1 in multiple ways. First, the lipid moieties of Shh bind key hydrophobic regions of the Ptch1, preventing its function in cholesterol transport and thereby relieving Ptch1's repression of Smo (Qi et al., 2018; Qian et al., 2019; Kinnebrew et al., 2021). Second, Shh binding to Ptch1 promotes the endocytosis and degradation of the receptor-ligand complex, allowing active Smo to accumulate in the primary cilia (Yue et al., 2014). Active Smo promotes the removal of Gpr161 from the primary cilia and physically inhibits the catalytic subunit of PKA (Pal et al., 2016; Happ et al., 2022). Without PKA phosphorylation, Gli2/3 dissociates from Sufu and bypasses proteolytic processing into the repressor forms. Full length transcriptional activator forms of Gli2 (Gli2A) and Gli3 (Gli3A) translocate into the nucleus and promote the expression of Shh targets. These targets include the transcription factor *Gli1*, the Shh receptor *Ptch1*, and the membrane-associated and secreted Shh antagonist *Hhip*. *Ptch1* and *Hhip* upregulation establishes a negative feedback

loop through increased Shh ligand sequestration (Holtz et al., 2013).

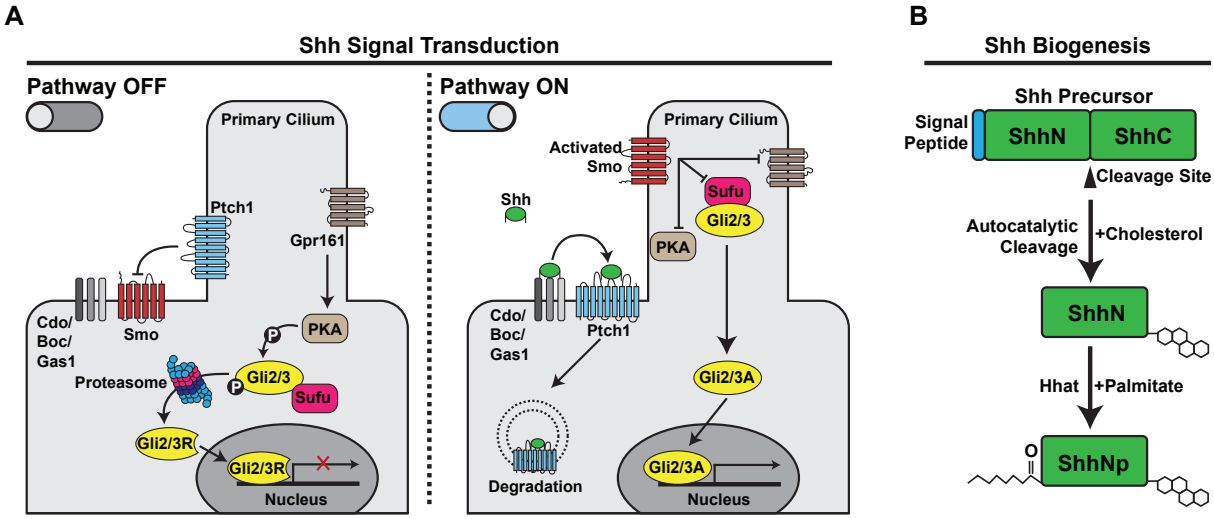


Figure 1.4: Shh signal transduction and biogenesis. (A) Diagram of the biochemical signaling when when Shh signaling is OFF vs ON. When the pathway is OFF, Ptch1 accumulates in the primary cilium and inhibits Smo. Ciliary Gpr161 promotes the PKA-dependent phosphorylation of Gli2/3-Sufu complexes. Phosphorylated Gli-Sufu complexes are targeted for partial proteolysis resulting in Gli2/3R repressors that translocate to the nucleus for transcriptional repression. To turn the pathway ON, Cdo/Boc/Gas1 co-receptors bind and transfer Shh to Ptch1 driving its internalization and degradation. Smo then accumulates in the primary cilium and inhibiting PKA, Gpr161, and Sufu allowing free, full length Gli2/3A activators to translocate to the nucleus for transcriptional activation. (B) Diagram showing the autocatalytic cleavage and the lipid modification steps during Shh biogenesis.

Although both Gli2 and Gli3 can exist as either transcriptional activators or repressors, they functionally serve in separate roles. In the absence of Shh signal, Gli2 is often fully degraded by the proteasome, making Gli3R the dominant transcriptional repressor (Persson et al., 2002). On the other hand, upon Shh stimulation, full-length Gli2A provides far greater transcriptional activation activity than Gli3A, making Gli2 the dominant transcriptional activator.

1.4.3 Shh Biogenesis and Intrinsic Limitation in Diffusion

As alluded to above, Hh ligands share a complex biogenesis involving autocatalytic cleavage followed by dual lipid modification (Figure 1.3A). In the endoplasmic reticulum, Shh is produced as a 45 kDa precursor protein comprising a 19 kDa N-terminal signaling domain (Shh-N) and a 25 kDa C-terminal autoprocessing domain (Shh-C). In murine Shh, the thiol group of Cysteine199 (first amino acid of Shh-C) undergoes a nucleophilic attack on the preceding Glycine198 (last amino acid of Shh-N), creating a thioester intermediate. The hydroxyl group of a free cholesterol attacks the thioester to form an ester-linked bond to the C-terminus of Shh-N, releasing Shh-C (Porter et al., 1996a). Hedgehog Acyltransferase (Hhat) then catalyzes the attachment of palmitate from palmitoyl Co-A to the N-terminal Cysteine of Shh-N via an amide bond (Pepinsky et al., 1998) (Pepinsky et al., 1998; Buglino and Resh, 2008). After processing and dual lipid modification, the signaling active N-terminal fragment is designated as ShhNp.

Although required for efficient Ptch1 inhibition and proper bioactivity, the dual lipid modifications tether Shh to the plasma membrane of producing cells, limiting its spread across the aqueous extracellular space. The sterol-sensing domain of the 12-pass transmembrane protein Dispatched-1 (Disp1) is thought to alleviate the membrane tethering of Shh by extracting the cholesterol-modified C-terminal end of ShhNp. Once released, Hh ligands disperse across tissues and form signaling gradients of various length scales. For example, in the *Drosophila* imaginal wing disc, Hh signaling gradients often extend around 10 cells, or roughly 30-40 microns away, from the Hh-producing posterior compartment (Basler and Struhl, 1994; Chen and Struhl, 1996; Strigini and Cohen, 1997), while the Shh signaling gradients in vertebrate neural tube and limb buds extend between 100-300 microns (Balaskas et al., 2012; Cohen et al., 2015; Lewis et al., 2001; Sanders et al., 2013). Uncovering how cells functionally solubilize Hh ligands or shield the lipid moieties for extracellular dispersal and gradient formation has emerged as a central question in the field. Although simple diffusion

is often described as the likely mechanism of morphogen dispersal (Schwank et al., 2011; Müller et al., 2013), there remains great debate regarding how morphogens are transported across a tissue.

1.5 Specialized Mechanisms for Long-Range Hedgehog Dispersal

The lipid moieties of Hh ligands limit diffusion, yet long-range gradients are still formed; thus, cells must utilize additional dispersal mechanisms.

Many mechanisms have been postulated to help mediate the long-range dispersal of Hh ligands. Initial studies demonstrated that Hh ligands, via their Cardin-Weintraub motifs and glycosaminoglycan binding sites, interact with cell surface heparan sulfate proteoglycans (HSPGs) and oligomerize into high order multimers (Vyas et al., 2008; Farshi et al., 2011). These Hh multimers were hypothesized to form micellar-like organizations that shield the lipid moieties of Hh to allow for soluble, long-range diffusion. However, these oligomeric Hh particles may, in fact, associate with other extracellular carriers reviewed below and in (Figure 1.5).

1.5.1 Carrier-Assisted Diffusion

Scube Proteins

Recent studies have revealed extracellular chaperones or carriers that bind and shield the hydrophobic lipid moieties of Hh ligands to promote long range diffusion. The signal peptide-CUB domain EGF-like (Scube) family proteins have been identified as one of the key extracellular carriers in vertebrates. Scube1, Scube2, Scube3 are secreted proteins that have variable expression in vertebrate embryos, but all three paralogs can bind to the lipid moieties of Shh (Lin et al., 2023; Schlissel et al., 2024).

Scube proteins act as a shuttle between Shh-producing cells and Shh-receiving cells. For

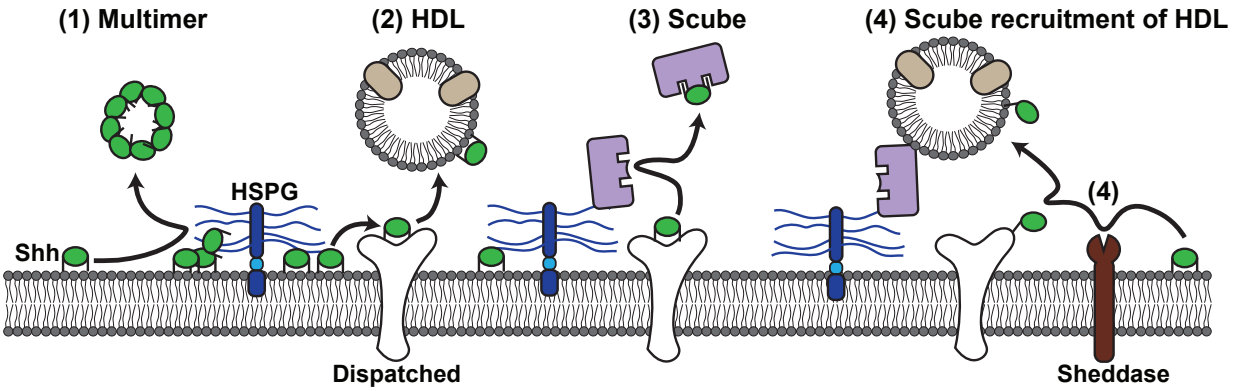


Figure 1.5: Carrier-assisted diffusion mechanisms. This diagram highlights four key mechanisms posed to mediate Shh diffusion via extracellular interactions. First, Shh can form high-order multimers through interactions with heparan sulfate proteoglycans (HSPGs). HSPGs and Dispatched coordinate the transfer of Shh to extracellular chaperones including HDL particles (2) or Scube protein carriers (3). ADAM10-sheddases can cleave the N-terminal palmitate of Shh to promote the Dispatched-mediated transfer to Scube2-recruited HDL particles (4).

example, Scube2 expression increases Disp-1 mediated release of Shh into the media via palmitate and cholesterol binding (Tukachinsky et al., 2012). Co-purification experiments found that Scube2-Shh complexes were stable in the media, suggesting that Scube2 functions as an extracellular carrier of Shh (Wierbowski et al., 2020). Weirbowski et al. reported a relay in which Cdo/Boc recruit Scube2-Shh complexes and mediate the transfer of Shh to Gas1, which transfers Shh to Ptch1 for downstream signal activation. Additionally, a recent report found that Scube1 increases the spatial extent of Shh signaling activity in synthetic co-culture gradient assays by increasing the transition rates of membrane-bound and freely diffusing Shh (Schlissel et al., 2024).

High Density Lipoprotein

High density lipoproteins (HDL) serve as another key, and highly conserved, extracellular carrier that promotes long-range Hh dispersal. HDL are 8-10 nm phospholipid monolayer particles enriched with apolipoproteins and other scaffolding proteins that transport cholesterol

between cells (Ben-Aicha et al., 2020; Sloop et al., 1987; Palm et al., 2013). In *Drosophila*, Hh ligands colocalize with lipophorin particles (Lpp), analogs to HDL (Panakova et al., 2005). Knocking down *Lpp* in the imaginal wing disc epithelium reduces the long-range Hh signaling but doesn't affect short-range Hh signaling (Panáková et al., 2005). Recent reports in cell culture models suggest that Scube2 recruits HDL to HSPGs, where Disp1 and a sheddase cleave the N-terminal palmitate of Shh for transfer to HDL (Puschmann et al., 2026). However, the proposed delipidation of Hh ligands remains controversial.

Extracellular Vesicles

In addition to soluble protein carriers, Hh ligands can be packaged onto the external membranes of extracellular vesicles (EVs) for long-range transport. EVs are membrane-bound vesicles secreted by nearly all cell types that transport proteins, lipids, and nucleic acids between cells (van Niel et al., 2018). EVs are quite heterogenous in size, molecular composition, cellular origin and function (Schank et al., 2026). Generally, EVs can be subdivided into two major types based on their subcellular origin: 1) Exosomes and 2) Ectosomes (Figure 1.6).

Exosomes undergo a complex biogenesis dependent on the endosomal pathway before secretion (Figure 1.5A). Specifically, when endosomes mature, the limiting outer membrane of the endosome can bud inward and pinch off within the lumen to form intralumenal vesicles (ILVs). This process can be driven in either an Endosomal Sorting Complex Required for Transport (ESCRT)-dependent or a neutral sphingomyelinase (nSMase)-dependent manner (van Niel et al., 2018). The process of ILV generation concentrates specific cytoplasmic nucleic acids and proteins within the lumens of ILVs. Late endosomes that accumulate multiple ILVs are called multivesicular bodies (MVBs). MVBs have two potential fates: degradation via Rab7 GTPase mediated fusion with lysosomes or Rab11, Rab27a/b, Rab35 mediated fusion to the plasma membrane (Kowal et al., 2014; Stenmark, 2009). Plasma membrane fusion releases ILVs into the extracellular space as diffusible exosomes. Exosomes,

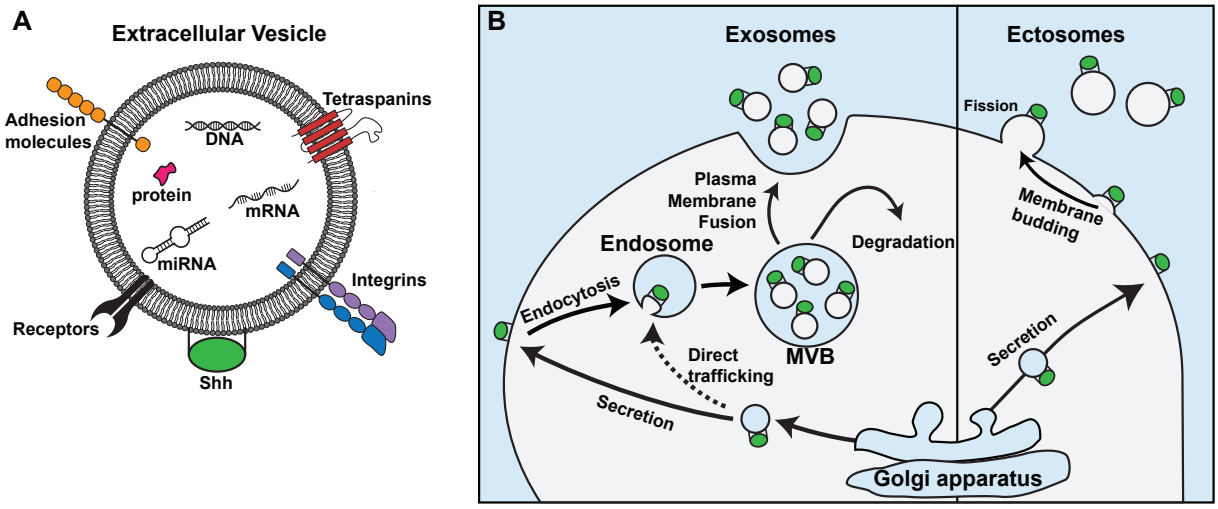


Figure 1.6: Extracellular vesicles share similar composition but differ in biogenesis. (A) Diagram highlighting the basic structure and composition of extracellular vesicles. (B) Diagram highlighting the differences in biogenesis between exosomes and ectosomes. Exosomes are derived from the endosomal system, while ectosomes are derived from plasma membrane shedding.

which range from 30-150 nm in diameter, are enriched in a diverse composition of cargo sorted by tetraspanin proteins (CD63, CD9, CD81) (van Niel et al., 2018). Secretory cargo, such as transmembrane proteins and secreted signaling molecules (e.g. Hh ligands) are packaged within MVBs/ILVs through either direct trafficking from the Golgi apparatus to the endosomal membrane or endocytosis of cargo from the plasma membrane into an early endosome.

Hh ligands associate with secreted exosomes in multiple cell and tissue contexts. In *Drosophila* wing disc cells, immuno-electron microscopy revealed that Hh localized to both intralumenal vesicles within MVBs and in secreted EVs in the adjacent extracellular space. Perturbations of intralumenal vesicle formation, via ESCRT(I-III) and nSMase RNAi, significantly reduced spatial extent of the Hh signaling activity gradient measured by *Ptc1*, *Dpp*, *Ci* target gene expression in the wing disc (Gradilla et al., 2014; Parchure et al., 2015). It is important to note that ESCRTI, ESCRTIII as well as nSMase may promote ectosome formation, thus Hh gradients might, in part, be regulated by exosome and ectosome secretion

(Cocucci and Meldolesi, 2015).

In addition, immuno-EM revealed Shh and CD63 localized on the membrane of small (30-60 nm in diameter) secreted EVs (Vyas et al., 2014). Inhibiting endocytosis, through Rab5a dominant negative overexpression, reduced the level of Shh in the secreted EV fractions, suggesting that these EVs were exosomes.

Ectosomes, also referred to as microvesicles or shedding vesicles, are derived from the outward budding and fission of the plasma membrane and can range between 100-1000 nm in diameter (Muralidharan-Chari et al. 2010). Unlike exosome biogenesis, ectosome formation does not rely on the endosomal pathway (Figure 1.5B). Specifically, during nucleation, transmembrane proteins and lipid-anchored proteins (e.g. Shh) cluster into discrete lipid microdomains, promoting outward curvature of the plasma membrane (Muralidharan-Chari et al., 2010). The GTPase ARF6 recruits cargo to budding ectosomal vesicles, while ESCRT-(I,III) proteins and ARF6-regulated actomyosin contractility facilitate the fission and release of these ectosomes into the extracellular space (Cocucci and Meldolesi, 2015; Muralidharan-Chari et al., 2009).

While less is known about ectosomal packaging of Hh ligands, in the *Drosophila* wing disc, specialized apical ectosomes derived from the microvilli are enriched in Hh and have been reported to function in long-range signaling (Hurbain et al., 2022).

Overall, Scube, HDL, and EVs all work to shield the hydrophobic lipid moieties of Hh ligands to allow for soluble diffusion in the hydrophilic extracellular space. However, their overlapping roles make it difficult to determine their individual functions and precise coordination.

1.5.2 Direct-Delivery Along Cytonemes

A growing body of work challenges the diffusion paradigm of morphogen dispersal, providing evidence of a direct-delivery mechanism mediated by cytonemes. Cytonemes are thin

(∼200 nm in diameter) F-actin composed filipodial protrusions that can extend up to 200 microns in length and transport morphogens, co-receptors, and receptors from cell-to-cell in a fashion similar to neuronal synapses (Figure 1.7) (Kornberg, 2014; Ma et al., 2025). Although discovered in the *Drosophila* wing disc mediating Dpp dispersal (Ramírez-Weber and Kornberg, 1999), cytonemes have now been observed in diverse tissues and organisms, mediating the transport and reception of multiple morphogens including Fgfs, Bmps, Wnts, and Hhs (Gradilla et al., 2014; Kornberg, 2014; Stanganello and Scholpp, 2016).

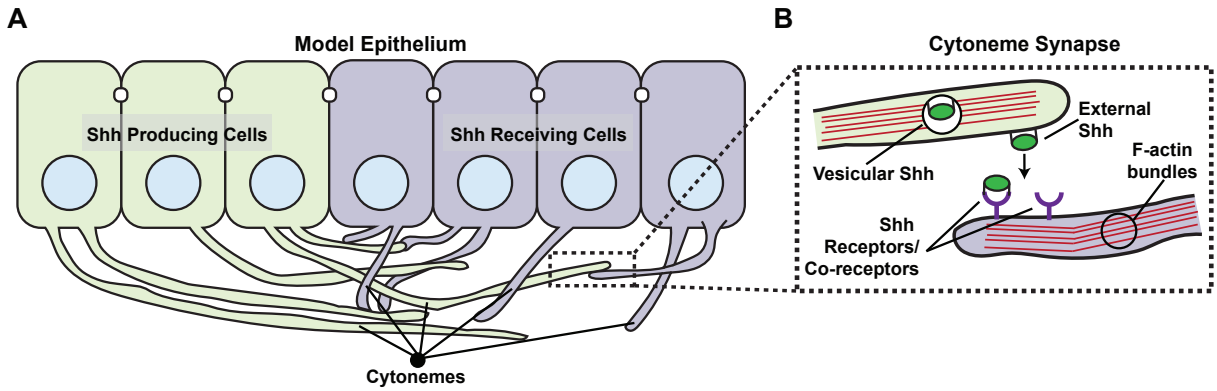


Figure 1.7: Cytonemes mediate direct delivery of Shh between cells via synapse like connections. Diagram highlighting cytonemes projecting from Shh producing and receiving cells at the basolateral surface of a hypothetical epithelial tissue. They form synapse-like connections where Shh signal transfer takes place.

Cytonemes provide a direct route for dispersal, bypassing the limitations of extracellular diffusion, and play important roles in Hh signaling in varied, developmental contexts. In *Drosophila*, cytonemes are critical for the juxtracrine Hh signaling that maintains the germ stem cell niche, and promote long-range dispersal that patterns the imaginal wing disc and abdominal epidermis (Rojas-Ríos et al., 2012; Bischoff et al., 2013). In vertebrates, Shh ligands have been observed along cytonemes emanating from the Shh-producing cells of the neural tube and the limb bud (Hall et al., 2024; Sanders et al., 2013). Moreover, Hh receptors and co-receptors localize to cytonemes, highlighting the roles of cytonemes in mediating Hh reception (Bischoff et al., 2013; Sanders et al., 2013; Chen et al., 2017; Hall et al., 2019).

Importantly, cytonemes seem to be required for tissue patterning as inhibition of cytoneme formation, through manipulation of actin regulators, reduces signaling activity gradients in both the *Drosophila* wing disc epithelium and in the mouse neural tube epithelium (Bischoff et al., 2013; Hall et al., 2024).

However, the mechanisms governing Hh transport along cytonemes remains poorly understood. In the *Drosophila* wing disc, Hh is postulated to be transported along cytonemes in two potential ways: 1) inside of the cytoneme packaged within a small MVB or other vesicular carrier or 2) externally along the cytoneme bound to an EV (Gradilla et al., 2014). In cultured mouse fibroblasts, Shh appears to travel inside cytonemes associated with CD9-positive vesicles (Hall et al., 2021). However, split-GFP reconstitution experiments in the chicken limb bud mesenchyme provide evidence of external transport of Shh puncta (Sanders et al., 2013). While the exact mechanism of how Hh ligands are actively transported along cytonemes remains unclear, the unconventional actin motor, Myosin10, seems to play a role in facilitating transport in vertebrates (Hall et al., 2021).

In summary, a variety of different mechanisms have been proposed to regulate Hh ligand dispersal. However, the relative contributions and the potential coordination of these mechanisms *in vivo* remains ambiguous.

1.6 Tissue Architecture and the Regulation of Hedgehog Dispersal

The bulk of our understanding of Hh dispersal *in vivo* comes from studies using polarized epithelial tissues, such as the *Drosophila* imaginal wing disc and the vertebrate neural tube. Epithelia have a very distinct tissue architecture. They are composed of tightly packed cells organized into sheets with apicobasal polarity. Epithelial cells secrete a stiff laminin and collagen IV rich extracellular matrix, called a basement membrane at their basal surface and often form an apical lumen (Bonnans et al., 2014).

The *Drosophila* imaginal wing disc epithelium has served as the most extensively studied

model for Hh dispersal *in vivo*. The wing disc originates through the invagination of the embryonic ectoderm to form a sac-like epithelium composed of a pseudostratified, columnar epithelium known as the disc proper, where Hh signaling takes place, and a supporting squamous epithelium known as the peripodial epithelium (Tripathi and Irvine, 2022).

There are conflicting reports of how and where Hh is dispersed for long-range signaling in the disc proper, but it is generally accepted that Hh undergoes primary secretion apically where it is immediately endocytosed in a Dispatched-dependent manner. However, the exact route of long-range transport is debated (Figure 1.8). Some reports claim Hh is re-secreted to the apical microvilli plasma membrane and secreted on microvilli-derived ectosomes/EVs for long-range signaling in the lumen (Hurbain et al., 2022). Other groups have demonstrated that endocytosed Hh is transcytosed to the basolateral domain where Hh can be secreted and bind Lpp (Panáková et al., 2005), packaged into MVBs for exosome secretion (Gradilla et al., 2014; Parchure et al., 2015), or loaded along cytonemes for long-range mediated dispersal Gradilla et al. (2014).

In the vertebrate neural tube, floor plate cells utilize a similar secretory route of primary apical secretion, Disp1-mediated internalization and transcytosis to the basolateral domain for loading on cytonemes (Hall et al., 2024). Interestingly, many of these cytonemes project into the lumen near the primary cilia on the apical face of receiving neural progenitor cells.

Mesenchymal tissues, such as cartilage, bone, and connective tissue, represent a large fraction of the vertebrate body plan. Unlike epithelial tissues, mesenchymal tissues are characterized by loosely packed cells that lack apicobasal polarity, embedded in a porous, 3-dimensional extracellular matrix often consisting of fibronectin, collagen-I, proteoglycans, and hyaluronic acid (Ferrer-Vaquer et al., 2010; Galiè, 2024; Toole, 2004; Frantz et al., 2010). Mesenchymal tissues lack an apical lumen but possess dynamic and interconnected extracellular spaces between cells. Overall, the tissue architecture differences between epithelial and mesenchymal tissues pose different obstacles in morphogen dispersal, so the mechanisms in

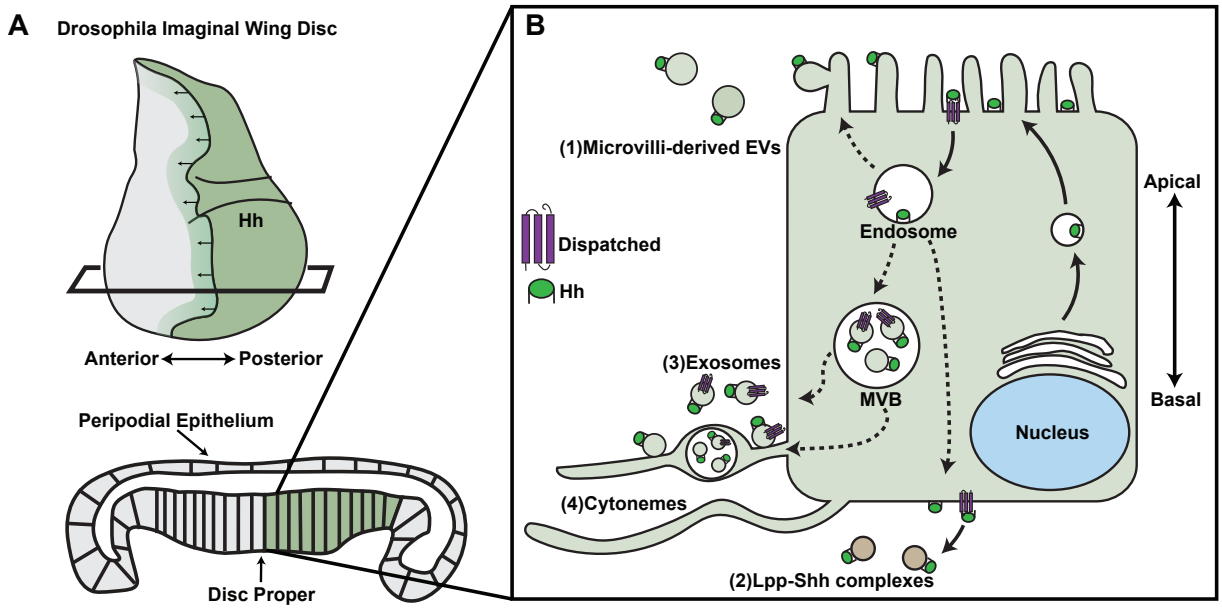


Figure 1.8: A complex trafficking route promotes multiple potential modes of Hh dispersal in *Drosophila* imaginal wing disc epithelial cells. (A) Diagram of the signaling compartment of the wing disc and a cross sectional view of the epithelium. (B) Diagram highlighting the secretory route and potential dispersal mechanisms of Hh in the wing disc cells. Hh undergoes primary secretion apically followed by internalization into endosomes. The dashed arrows highlight the numerous reported routes for secondary secretion and dispersal.

which Shh dispersal is regulated may vary in these tissues. Although Shh signaling is known to mediate the patterning of many mesenchymal tissues, including the face and limb (Hu and Helms, 1999; Riddle et al., 1993), the mechanisms that govern Shh dispersal in these tissues have yet to be elucidated.

1.7 Limb Development and the Role of Shh Signaling in Anterior-Posterior Patterning

Since 1948, the developing vertebrate limb has become a classic model to investigate tissue cell signaling, tissue patterning, and morphogenesis (Saunders, 1948). The limb bud is the primordial structure that gives rise to the adult limb, and it's composed of a 3D meshwork of mesenchymal progenitor cells derived from the somatopleural layer of the lateral plate

mesoderm sheathed in an outer epithelial ectodermal layer (Tickle, 2015). The mesenchymal progenitor cells give rise to the cartilage, perichondrium, tendons, ligaments, and dermis of the adult limb, while the epithelial layer becomes the epidermis (Pearse et al., 2007).

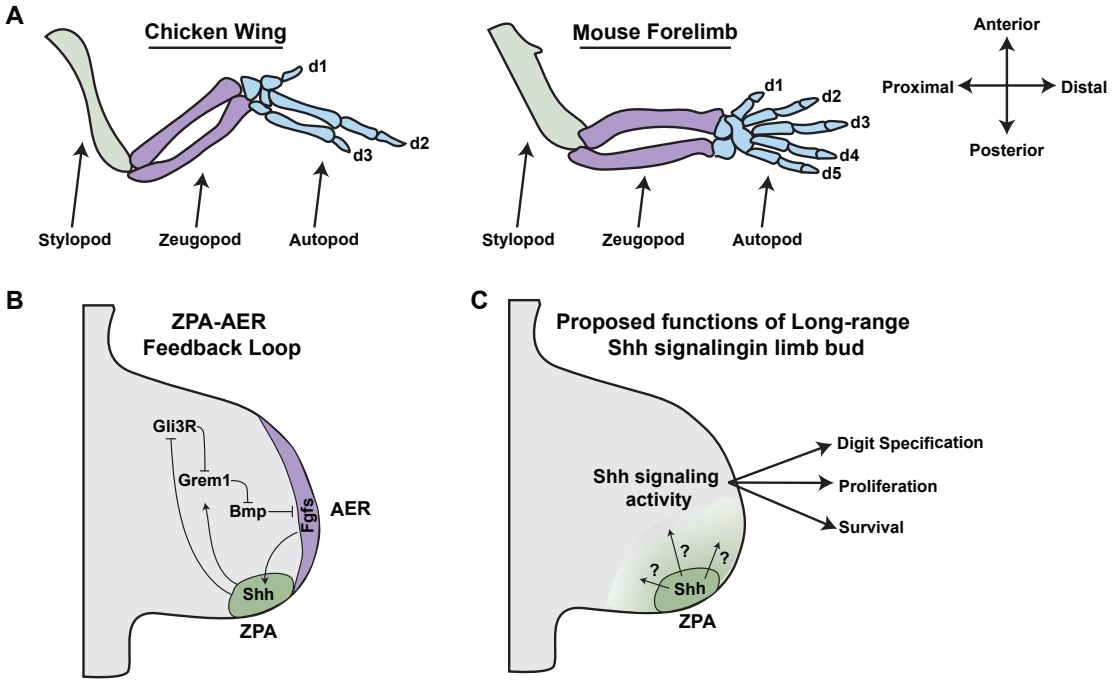


Figure 1.9: Vertebrate models of limb development and the roles of Shh signaling in the limb bud. (A) Diagrams of the skeletal elements in the chicken wing and mouse forelimb. Note the similarities in stylopod and zeugopod elements, but the differences in the number and shape of the autopod digits (d). (B) Diagram of the ZPA-AER feedback loop. Fgfs from the AER promote Shh expression in the ZPA. Shh signaling represses Gli3R and activates Grem1. Grem1 inhibits Bmp which inhibits Fgf expression in the AER. (C) Diagram of the Shh signaling activity gradient in the limb bud and its regulation of multiple developmental processes. The question marks represent the uncertainties in Shh dispersal to generate the signaling activity gradient

Before the limb bud is fully formed, polarization of the presumptive limb field helps establish key signaling centers that organize the three major axes of the limb: Proximal-Distal (shoulder to finger), Dorsal-Ventral (fingernail/back of hand to palm), and Anterior-Posterior (thumb to pinkie finger) (McQueen and Towers, 2020). After patterning and outgrowth, the limb bud mesenchyme condenses into cartilage and undergoes endochondral

ossification. In proximal to distal order, the resulting skeletal elements are categorized in three distinct segments: stylopod (humerus/femur), zeugopod (radius/ulna or fibula/tibia, and autopod (wrist/ankle and digits) (Figure 1.9A).

Importantly, in the limb bud mesenchyme, Shh signaling is critical for regulating tissue patterning and growth. Thus, the limb bud mesenchyme serves as an exemplary model for investigating the mechanisms regulating Shh transport in non-epithelial tissues. In the following sections, I will highlight what is known about limb development, the multifunctional roles of Shh in the limb, the two models of digit specification, and the candidate mechanism hypothesized to mediate Shh dispersal.

1.7.1 Signaling Centers of the Limb Bud

Two key signaling centers, the Apical Ectodermal Ridge (AER) and the Zone of Polarizing Activity (ZPA), regulate limb bud development. Below I describe their discovery, induction, and functions in development.

The Apical Ectodermal Ridge (AER) Regulates Proximal-Distal Specification and Limb Bud Outgrowth via FGF Signaling

In 1948, John Saunders observed a thick ectodermal ridge at the distal end of the limb bud and questioned if it might regulate the outgrowth of the limb. After he dissected and removed what he coined as the apical ectodermal ridge (AER) of the limb bud, he observed halted limb development. By removing the AER at increasingly later stages of development, he also observed loss of increasingly distal structures, suggesting that the AER served as a signaling center that controlled the proximal to distal outgrowth of the limb (Saunders, 1948).

Decades later, the molecular signaling that induces the AER and the signals derived from the AER were discovered. Early lateral plate mesodermal cells secrete Fgf10 to the

overlying ectoderm, promoting the expression of *Fgf8* in the ectoderm. *Fgf8* expressing ectodermal cells begin to cluster at the dorsal/ventral boundary or the distal edge of the limb bud to form a pseudostratified AER structures (Yonei-Tamura et al., 1999; Sekine et al., 1999). The AER continues to express and secrete Fgf8 and Fgf4, which drives high levels of proliferation in the underlying mesenchyme causing limb bud growth along the proximal-distal axis (Niswander et al., 1993; Fallon et al., 1994; Crossley et al., 1996; Sun et al., 2002). Based on these discoveries, the specification of the proximal-distal skeletal elements is now thought to be controlled by a "signal-time" model. This model proposes that proximal-distal specification is mediated by opposing gradients of retinoic acid (from mesodermal flank) and Fgf8 (from AER) and by intrinsic timing mechanisms controlling sequential Hox gene expression (Saiz-Lopez et al., 2015).

The Zone of Polarizing Activity (ZPA) Regulates Anterior-Posterior Patterning and Mesenchymal Expansion via Shh Signaling

Similar to the discovery of the AER, classic embryology experiments led to the discovery of the second signaling center of the limb bud. While investigating apoptotic regions in the limb, Saunders and Gasseling dissected a small posterior region of chick limb bud and grafted it to the anterior portion of a host limb bud, and they subsequently observed a mirror-image duplication of the digits (Saunders and Gasseling, 1968). From this discovery, they hypothesized that this region was an organizer capable of patterning the anterior-posterior axis or polarizing the limb bud and named it accordingly as the Zone of Polarizing Activity (ZPA). By characterizing the digit duplications that result from grafting ectopic ZPAs at varied positions along the anterior-posterior axis of the limb bud, Tickle et al. showed that digit identity depends on the distance from the nearest ZPA (Tickle et al., 1975). Overall, this work suggested that a gradient of positional information, likely produced by a diffusible morphogen from the ZPA, specifies the digits of the limb.

A seminal study identified Shh as the primary morphogen expressed in the ZPA that mediates the polarizing or patterning activity of the ZPA (Riddle et al., 1993). Retinoic acid expressed early in the embryonic flank induces expression of the transcription factor *Hand2* in the early limb bud mesenchyme (Mic et al., 2004; Fernandez-Teran et al., 2000). Posterior restriction of Hand2, via Gli3 repression, acts as an essential activator with Hoxd13, binding to a specific enhancer known as the ZPA Regulatory Sequence (ZRS) to drive the expression of *Shh* in the mesenchymal cells of the ZPA (Galli et al., 2010; te Welscher et al., 2002; Lettice et al., 2003).

A large body of work has demonstrated that Shh is required for anterior-posterior patterning of the limb bud. Global genetic knockout of Shh in the mouse causes loss of all digits, except for the most anterior digit 1, as well as severe truncations along the proximal-distal axis (Chiang et al., 1996). In *oligozeugodactyly* (*ozd*) mutant chickens, a large portion of the ZRS is deleted which prevents *Shh* expression in the limb bud and subsequently causes severe loss of posterior structures, including the ulna and all digits (1-3) in the wing (Ros et al., 2003). Conversely, grafting Shh-coated beads or Shh-expressing cells to the anterior limb bud could phenocopy the mirror image duplication of the digits caused by ZPA grafts (Yang et al., 1997).

Shh Acts as both a Morphogen and a Mitogen in the Limb Bud

Although exclusively expressed in the ZPA, immunohistochemistry has shown that Shh protein can form a gradient emanating away from the ZPA (Li et al., 2006; Wang et al., 2022). Additionally, direct target genes of Shh signaling, *Ptch1* and *Gli1*, have graded expression across the AP axis of the limb bud, again emanating away from the ZPA (Marigo et al., 1996a,b). As mentioned in previous sections, Shh signaling regulates the proteolysis of Gli2/3, thus Shh directly regulates an inverse gradient of Gli3R in the anterior limb bud (Wang et al., 2000, 2007). The ratio of Gli activator and repressor in the limb bud is re-

ported to help specify the digits along the anterior-posterior axis (Wang et al., 2000, 2007; Litingtung et al., 2002). Altogether, this collection of work suggests Shh satisfies the criteria of a classic morphogen: Shh is produced locally, disperses to form a long-range gradient, and promotes graded Gli processing to specify digit identity.

Shh also assists in promoting proliferation and limb bud expansion. ZPA-derived Shh participates in a key positive feedback loop with the AER and limb bud outgrowth (Figure 1.9B) (Niswander et al., 1994). Shh expression in the ZPA is promoted and maintained by FGF signaling from the AER. In return, paracrine Shh signaling induces *Gremlin1* (*Grem1*) expression, a secreted inhibitor of BMP, in the limb bud mesenchyme. Gremlin1 functions to inhibit mesenchymally expressed BMPs that repress FGF signaling in the AER. Therefore, the positive feedback between Shh and FGF couples limb bud outgrowth along the proximal-distal axis and tissue patterning along the anterior-poster axis. Independent of interactions with the AER, Shh signaling in the chick limb bud promotes proliferation in mesenchyme through regulating expression of cell cycle genes, including D cyclins (Towers et al., 2008; Pickering et al., 2019).

While a Wolpertian spatial concentration gradient was initially assumed to mediate anterior-posterior patterning and digit specification, this assumption doesn't take account for the highly complex and dynamic nature of the developing limb bud.

1.7.2 Anterior-Posterior Specification Models in the Chicken and Mouse Limb Bud

How Shh specifies digit identity along the anterior-posterior axis is still actively debated. The role of Shh as a pro-proliferative signal can complicate its function in specifying digit identity. Additionally, there appears to be species-specific differences between how Shh functions in the developing chick and mouse limb buds, preventing a clear, unified model. Below, I will summarize the leading models of how Shh is mediating the patterning of the AP axis from

work in both chick and mouse embryos.

The Promotion Model in Chick Embryos

Experimental evidence suggests that Shh functions as a classic morphogen in the chick limb bud. The specification of digit identity across the AP axis relies on both concentration and duration of Shh signaling and is deeply interconnected with growth. Both ZPA and Shh-coated bead grafting experiments showed that the time the graft was left in place determined how completely the digits were mirror duplicated (Smith, 1980; Yang et al., 1997). This suggested that the increasing concentration of Shh exposure over time is what confers positional information to specify digit identity in a mechanism known as promotion (Gurdon et al., 1995). This was experimentally demonstrated by inhibiting Shh signaling rapidly after the onset of expression in chick limb buds through use of timed application of cyclopamine, a small molecule inhibitor of Smo (Towers et al., 2011). Here, they found that inhibition of Shh signaling 4 hours after Shh onset led to the specification of only the most anterior digit 1, while inhibition after 8 hours specified digit 2 and after inhibition after 12 hours specified digit 3. Additionally, through fate-mapping experiments, they determined that the Shh-expressing cells of the ZPA did not contribute to any cartilage/bone which provided strong evidence of a long-ranged signaling prerequisite. Thus, every 4 hours chick wing bud mesenchymal cells are promoted through anterior to posterior positional values by increased paracrine Shh signaling.

The Biphasic and Secondary Relay Model in Mouse Embryos

Although many aspects of Shh signaling are shared between chick and mouse, the way Shh patterns the anterior-posterior axis and specifies digit identity appears different in mouse. In particular, there is growing evidence that Shh may not act as a true long-range, graded morphogen in the mouse limb bud.

Unlike the chick limb bud, genetic lineage tracing experiments demonstrated that the most posterior 2 digits (digit 4-5) of the mouse limb are derived from the descendents of the Shh-expressing ZPA (Harfe et al., 2004). This indicated that digit specification, at least in part, is mediated through the duration of short-range Shh signaling, not through long-range concentration gradients. By genetically deleting Shh at various time points during development, Zhu et al. observed that only a short period of Shh signaling was required to specify digits, and that the loss of digits caused by Shh deletion mirrored a dramatic increase in apoptosis and decreased proliferation (Zhu et al., 2008). To explain the role of Shh in anterior-posterior patterning, they proposed a biphasic model in which an early transient phase of Shh signaling specifies digit identity and a later phase of signaling promotes the proliferation and cell survival of the limb mesenchyme to produce enough cells to form the digits (Zhu et al., 2008). To uncouple the role of cell survival from patterning, Zhu et al. conditionally knocked out Shh and pro-apoptotic genes Bax/Bak to reinforce cell survival without the need for Shh (Zhu et al., 2022). Interestingly, they found that only a brief, two-hour period of early Shh signaling was required to specify all five digits when cell survival was reinforced, and that extent of Shh signaling activity was short-range within the ZPA. Since only digits 4-5 are directly derived from the ZPA, these results imply that digits 2-3 were specified indirectly by a secondary relay signal induced by short-range Shh signaling. Furthermore, this suggests that the long-range Shh signaling seen later in limb development is primarily for promoting cell survival.

1.7.3 Mechanisms of Sonic Hedgehog Dispersal in the Limb Bud

Although the exact mechanism of how Shh confers positional information and how its "non-morphogen" secondary functions play into limb development are hotly contested, one principle is clear: Shh ligands must be dispersed across the dynamically growing, convoluted limb bud mesenchyme to regulate limb development.

However, whether the same dispersal mechanisms characterized in polarized epithelia (e.g. the wing disc and neural tube) also operate within the mesenchyme, and to what extent, remain open questions.

Cytonemes have been identified as a possible Shh dispersal mechanism in the chicken limb bud. Live imaging of mosaically labeled cells in the limb bud mesenchyme revealed that ZPA cells and Shh-receiving cells both project numerous cytonemes that reach up to 150 microns in length theoretically covering the distance of the digit forming field in the limb bud (Sanders et al., 2013). Using live imaging, they showed that diffraction limited Shh puncta travel along ZPA-derived cytonemes in a net anterograde manner. Cytonemes on Shh-receiving cells are enriched in Shh co-receptors with the ability to form synapse-like connections with cytonemes from the ZPA. However, it remains unclear what regulates the loading of Shh on cytonemes and whether cytonemes are even required for Shh gradient formation and mesenchymal tissue patterning.

A recent study in embryonic mouse limb buds suggests that Shh gradients may be shaped by a combination of cytonemes and secreted EVs. Wang et al. observed that a distal-to-proximimal gradient of FGF/PI3K signaling correlated with two morphologically distinct populations of Shh in the limb: a diffuse population distally and a punctate population proximally (Wang et al., 2022). They found that the levels of PI3K signaling in immortalized NIH-3T3 fibroblasts could drive either cytoneme transport of Shh (PI3K low) or the secretion of Shh on large exosome-like particles (PI3K high). Overall, they hypothesized that the gradient of Shh protein in the limb bud was shaped by long-range, highly mobile exosome-like particle diffusion in distal compartments and low mobility, cytoneme trapping in proximal compartments. However, the exosome-like particles observed in the NIH-3T3 cells were atypically large and shared few common characteristics with typical exosomes, making their identity unclear. Additionally, the differential sorting of Shh to cytonemes vs EVs was never explicitly demonstrated in the limb.

Altogether our understanding of how Shh is dispersed across mesenchymal tissues remains poorly understood. While cytonemes and EVs may assist in dispersing Shh in the limb bud, their molecular regulation and their contribution to tissue patterning are yet to be defined. This thesis aims to examine the fundamental cell biology regulating Shh dispersal in the limb bud and identify universal principles governing tissue patterning.

1.8 Overview of Dissertation

In this thesis, I investigate the mechanisms that regulate Shh dispersal and gradient formation in the limb bud mesenchyme.

In Chapter 2, I describe my published findings on the role of exosomes and their relationship to cytonemes in the chicken limb bud mesenchyme. I reveal a complex intracellular trafficking route that packages Shh in MVBs primed for exosome secretion. I show that exosome secretion is required for Shh gradient formation. Lastly, I highlight an interconnected mechanism of exosome secretion and cytoneme transport.

In Chapter 3, I present conclusions from my work, discuss their relation to current views on cell communication, and propose key future directions.

In Appendix A, I present preliminary results highlighting the use of a synthetic tool to manipulate cytoneme formation in limb bud mesenchymal cells, and ask if mosaic manipulation of cytonemes can affect limb development.

CHAPTER 2

EXOSOME SECRETION IS REQUIRED FOR SONIC HEDGEHOG DISPERSAL AND SIGNAL GRADIENT FORMATION IN THE EMBRYONIC LIMB BUD MESENCHYME

The work presented in this chapter has been accepted in:

Corcoran, S., Fisher, J., Sanders, T.A., Munro, E.M. In press. Exosome secretion is required for Sonic Hedgehog dispersal and signal gradient formation in the embryonic limb bud mesenchyme. *Cell Reports.*

AUTHOR CONTRIBUTIONS: S.C., J.F, and T.S. contributed to genetic construct cloning. S.C. performed all cell culture, RT-qPCR, *in vitro* and *in vivo* electroporation, immunofluorescence staining, and light microscopy-based experiments. J.F. dissected limb buds and performed scanning electron microscopy. S.C. performed all data analysis. T.S. and E.M. supervised the project. S.C., T.S., and E.M. wrote the manuscript.

Abstract

Carrier-assisted diffusion and cytoneme transport help disperse Hedgehog morphogens across diverse embryonic tissues, yet their relative contributions to patterning mesenchymal tissues remain poorly understood. Here, we combine signaling assays with quantitative microscopy to establish exosome secretion as a major mechanism for Sonic Hedgehog (Shh) dispersal. Using a synchronous release system to visualize Shh trafficking, we demonstrate that Shh traffics through the exosome biogenesis pathway in limb bud mesenchymal cells. Shh-bound exosomes diffuse through extracellular space and also bind and travel along cytonemes, providing two alternative modes of transport. We show that exosome secretion is essential to establish short-range Shh signaling gradients *in vitro* and contributes to shaping Shh protein gradients in the limb bud *in vivo*. We propose that exosome-based Shh secretion, combined with different modes of extracellular transport, provides a tunable mechanism to sculpt Shh gradients across different length and time scales.

2.1 Introduction

Hedgehog (Hh) signaling patterns many different tissues during development (Varjosalo and Taipale, 2008). Like other morphogens, Hedgehog (Hh) ligands are secreted by source cells and dispersed across tissues to form gradients of signaling activity that instruct many cellular processes including: differentiation, proliferation, survival, migration, and stem cell maintenance (Balordi and Fishell, 2007; Briscoe et al., 2000; Hu and Helms, 1999; Petrova and Joyner, 2014; Riddle et al., 1993).

Hh ligands, including the well-conserved vertebrate paralog, Sonic Hedgehog (Shh), are synthesized as precursor proteins that undergo autocatalytic cleavage and acquire two lipid modifications: an N-terminal palmitate and C-terminal cholesterol. These hydrophobic lipid moieties are required for proper spatial distribution and bioactivity, but they also tether Hh ligands to cell membranes, restricting their spatial spread (Grover et al., 2011; Lee et al., 2001; Lewis et al., 2001; Porter et al., 1996b). Thus, cells must harness additional mechanisms to overcome this restriction, promote ligand dispersal and shape longer-range signaling gradients across tissues.

One class of mechanisms involves the association of Hh with diffusible extracellular carriers. For example, release of membrane-tethered Hh by Dispatched proteins and transfer to molecular carriers, such as Signal peptide-CUB domain EGF-like (SCUBE) proteins or high density lipoproteins (HDL) can promote Hh solubility and extracellular diffusion(Burke et al., 1999; Kawakami et al., 2002; Ma et al., 2002; Panáková et al., 2005; Tukachinsky et al., 2010; Vyas et al., 2008). Alternatively, Hh ligands can be packaged onto extracellular vesicle (EV) carriers for secretion and dispersal. Although EVs vary widely in size and composition, they belong to two major types, distinguished by mode of biogenesis. Exosomes are generated by endocytosis of cargo and endosomal packaging, followed by inward budding of endosomal membranes to produce intraluminal vesicles within specialized late endosomes called multivesicular bodies (MVBs). These intralumenal vesicles are then re-

leased as exosomes when MVBs fuse with the plasma membrane (Han et al., 2022; Welsh et al., 2024). Ectosomes, or microvesicles, are formed by outward budding from the plasma membrane (Rädler et al., 2023). Hh associates with MVB-derived exosomes in a variety of contexts, including the Drosophila imaginal wing disc, chick notochord, developing mouse brain, and in human cell lines (Coulter et al., 2018; Eitan et al., 2016; Vyas et al., 2014). Inhibiting MVB biogenesis reduces Hh secretion and the spatial extent of Hh signaling gradients in many of these contexts, suggesting key roles for MVB-derived exosomes in tissue patterning (Gradilla et al., 2014; Matusek et al., 2014; Parchure et al., 2015; Vyas et al., 2014; Walvekar et al., 2025). In Drosophila imaginal wing discs, both apically secreted ectosomes and basolaterally secreted exosomes have been implicated in Hh dispersal, although their relative contributions to Hh gradient formation and tissue patterning remain a topic of debate (Gradilla et al., 2014; Hurbain et al., 2022; Matusek et al., 2014).

In addition to carrier-assisted diffusion, a growing body of work suggests that cells harness specialized signaling filopodia, known as cytonemes, to transport morphogens and their receptors across developing tissues. Hh ligands and receptor/co-receptors travel along cytonemes in the vertebrate limb bud mesenchyme, in Drosophila imaginal disc epithelia, in mouse neural tubes, and in various cell culture models (Bischoff et al., 2013; Gradilla et al., 2014; Hall et al., 2021; Sanders et al., 2013; Wang et al., 2022; Hall et al., 2024). Inhibiting cytonemes reduces Hh signaling gradients in epithelial tissues, but has no apparent effect on gradients produced by fibroblast cells cultured *in vitro* (Bischoff et al., 2013; Schlissel et al., 2024; Hall et al., 2024). Studies in different organisms and cultured cell types suggest that Hh may travel inside of cytonemes, in association with secretory vesicles or small MVBs, or on the surfaces of cytonemes, either as naked oligomers or in association with exosomes (Gradilla et al., 2014; Sanders et al., 2013; Hall et al., 2021). Thus, in general, the relevant modes and contributions of cytoneme-based transport remain poorly defined.

Studies of Hh trafficking and dispersal *in vivo* have focused on epithelial tissues composed

of close-packed cells with well-defined apical and basal domains facing distinct extracellular compartments. However, Hh signaling also patterns many mesenchymal tissues which are formed by loosely connected networks of apolar cells embedded in a complex extracellular matrix, and therefore may require different strategies to control Hh dispersal and shape signaling gradients (Hu and Helms, 1999; Riddle et al., 1993).

The vertebrate limb bud is a well-established *in vivo* model for Shh-mediated patterning of mesenchymal tissues. Within the posterior margin of the limb bud mesenchyme, a region known as the zone of polarizing activity (ZPA) provides a local source of Shh, which is dispersed over hundreds of microns to form anterior-posterior gradients of protein concentration and signaling activity (Goodrich et al., 1996; Li et al., 2006; Marigo et al., 1996a; Riddle et al., 1993; Wang et al., 2022). A large body of work establishes clear roles for spatiotemporally graded Shh signaling in anterior-posterior patterning (Chiang et al., 1996; Ros et al., 2003; Scherz et al., 2007; Towers et al., 2011; Zhu et al., 2022), promoting proliferation and survival (Towers et al., 2008; Zhu et al., 2008), and regulating the outgrowth of the limb bud through reciprocal interactions with a distal FGF-expressing signaling center known as the apical ectodermal ridge (AER) (Chiang et al., 2001; Niswander et al., 1994). Previous work suggested that cytonemal transport of Shh puncta may contribute to shaping gradients of Shh activity in chick limb buds, although the magnitude of this contribution and the nature of the Shh puncta remain unclear. More recent work in embryonic mouse limb buds suggests that Shh gradients may be shaped by a combination of diffusion of Shh on exosome-like particles and local trapping and directed transport of Shh along cytonemes (Wang et al., 2022). However, the mechanisms that govern intracellular trafficking and release of Shh within the limb bud mesenchyme, the nature of the extracellular carriers that mediate Shh dispersal, and the mechanisms by which Shh is transported within and/or along cytonemes, all remain poorly understood.

Here, we exploit primary limb bud mesenchymal cell cultures (PLMCs) as a develop-

mentally relevant, and experimentally tractable, model system for functional analysis of Shh trafficking and dispersal. We deploy a chemically disruptable heterodimer synchronous release system to visualize Shh trafficking with high spatial and temporal resolution in cultured PLMCs, and we adapt a reconstituted tissue reporter assay to measure Shh signaling gradients made by single PLMCs *in vitro*. Using these approaches, we identify exosome-based secretion as a major pathway for Shh dispersal from limb bud mesenchymal cells. We demonstrate that exosome secretion is required to form short-range signaling gradients *in vitro* and contributes to shaping Shh protein gradients *in vivo*. We show that Shh-containing exosomes, produced by PLMCs *in vitro,* can either diffuse freely through extracellular space, or they can bind to and travel along the outer surfaces of cytonemes. Additionally, we confirm that Shh-containing exosomes can also bind and travel along cytonemes *in vivo*. We suggest that while the shorter cytonemes formed by cultured PLMCs are dispensable for signaling *in vitro*, the transport of Shh-bound secreted exosomes along the lengthier cytonemes observed *in vivo* may play a more important role in promoting longer-range, directed, or sustained signaling during normal limb development. Overall, our study establishes exosome-mediated Shh dispersal as a fundamental and versatile basis for Shh signaling and mesenchymal tissue patterning.

2.2 Results

Primary Limb Bud Mesenchymal Cells provide a developmentally relevant in vitro model for Shh trafficking and dispersal

Efforts to study the cell biology of Shh secretion and transport in intact limb buds have been limited by the difficulty of combining high-resolution imaging with specific manipulations. To overcome this limitation, we optimized cultures of primary limb bud mesenchymal cells (PLMCs) as a tractable *in vitro* model for Shh trafficking and dispersal with direct relevance to limb bud patterning *in vivo* (Barna and Niswander, 2007; DeLise et al., 2000).

We dissected limb buds from chick embryos at Hamburger and Hamilton (HH) stage ~22 (Embryonic Day 3.5), dissociated them into single cells, introduced plasmids of interest via electroporation, and seeded the cells at confluency to generate high-density cultures of PLMCs (Figure 2.1A, Methods). Using palmitoylated-EGFP (pm-EGFP) and mIRFP682 tagged Utrophin-Calponin Homology Domain (UCHD-mIRFP682) to label plasma membranes and filamentous actin (F-actin), respectively, we confirmed that cultured PLMCs project numerous F-actin based filopodia (Figure 2.1B-B"), resembling cytonemes made by limb bud mesenchymal cells *in vivo*, albeit with shorter lengths (Figure 2.1D) (Sanders et al., 2013). As *in vivo*, these cytonemes undergo dynamic cycles of extension and retraction (Video S1), and they accumulate the motor domain of the atypical motor Myosin10 (Myo10-HMM-msfGFP) at their tips (Figure 2.1C).

To characterize Shh localization in PLMCs, we inserted monomeric superfolder GFP (msfGFP) into full length Shh just before the cholesterol modification site to ensure proper processing, cholesterol modification, and bioactivity (Figure 2.2A, See Methods) (Chamberlain et al., 2008; Quijada and Guerrero, 2007; Sanders et al., 2013; Vincent et al., 2003). Upon overexpression of Shh-FL-msfGFP in PLMCs, we observed small diffraction-limited Shh puncta within cell bodies, along cytonemes and at their tips. Time lapse analysis revealed both anterograde and retrograde transport of Shh puncta along cytonemes, as previously reported for limb bud mesenchyme cells *in vivo* (Figure 2.1E and Video S2) (Sanders et al., 2013). Importantly, while over-expression of Shh can induce cytoneme formation in immortalized cell culture lines (Hall et al., 2021), it did not affect the number, and only slightly affected the length, of cytonemes in cultured PLMCs (Figure 2.2B-D), as previously shown for limb bud mesenchymal cells *in vivo*. We also observed Shh puncta in the extracellular space surrounding individual Shh-expressing PLMCs, suggesting that these cells release a diffusible form of Shh. Finally, we observed accumulation of Shh-FL-msfGFP within large, spherical endosome-like structures in the cell bodies of PLMCs (Figure 2.1E').

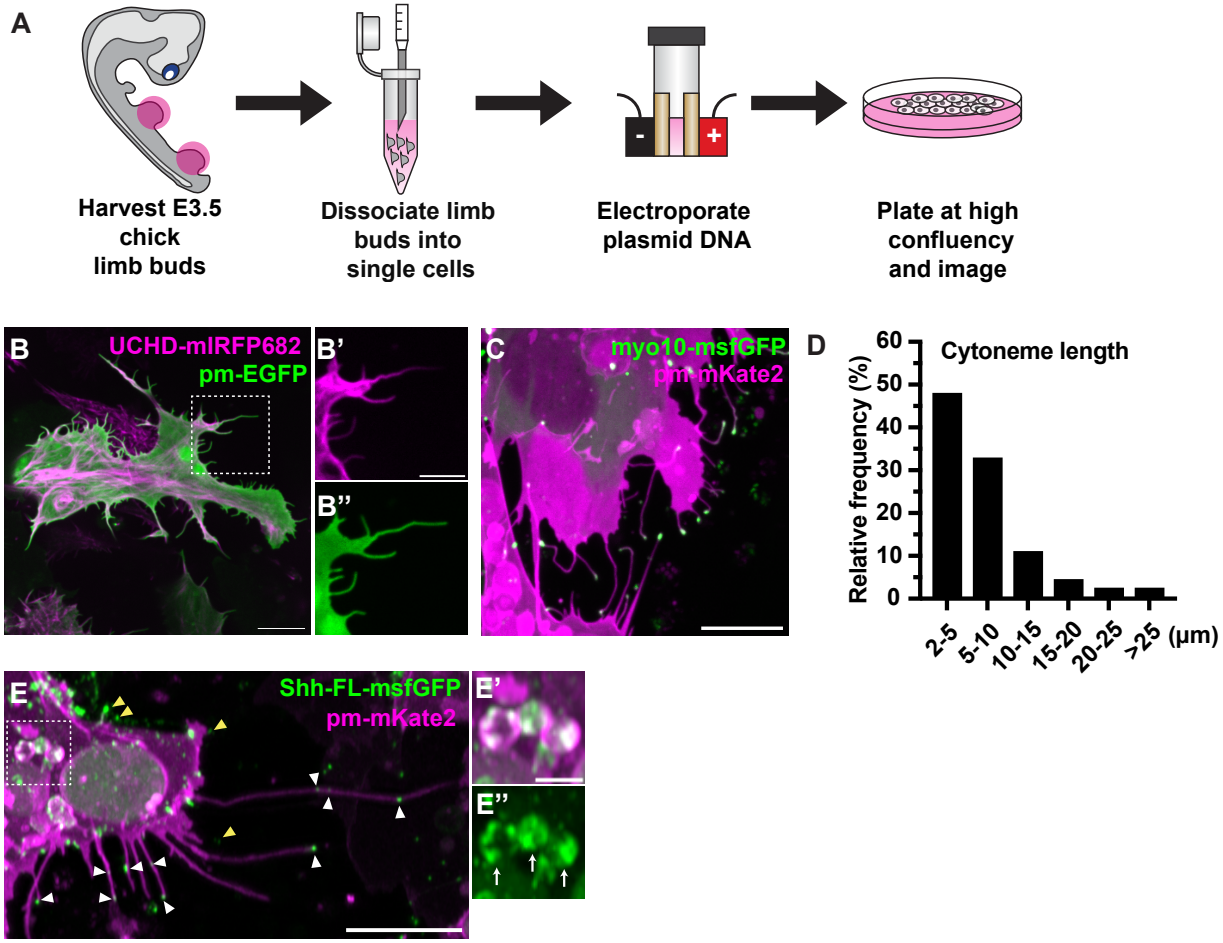


Figure 2.1: Primary Limb Mesenchymal Cell (PLMC) culture provides a tractable model to study Shh trafficking and dispersal dynamics. (A) Protocol for generating PLMC cultures. (B) PLMC electroporated with plasmids encoding palmitoylated (pm)-EGFP (membrane) and mIRFP682 tagged Utrophin-Calponin Homology Domain (F-Actin). White box indicates region which is magnified in B′ and B″ to display protrusions labeled with F-Actin (B′) and membrane (B″). C) PLMC expressing pm-mKate2 (membrane) and Myosin10-(HMM)msfGFP. D) Histogram displaying the relative frequency of the lengths of all cytonemes over 2 microns from control data in Figure S1D (n = 31 cells, 490 cytonemes pooled from 2 independent experiments). E) Micrograph depicting PLMC electroporated with pm-Kate2 to mark cell membranes and Shh-FL-msfGFP. White arrowheads mark Shh puncta localized to cytonemes. Yellow arrowheads mark extracellular Shh puncta. E′–E″) Magnified white box highlights large, spherical Shh-positive endosome/MVB-like structures in the cell soma (arrows). Scale Bars in (B, C, E) = 10 μm, (B′–B″) = 5 μm, (E′) = 2 μm.

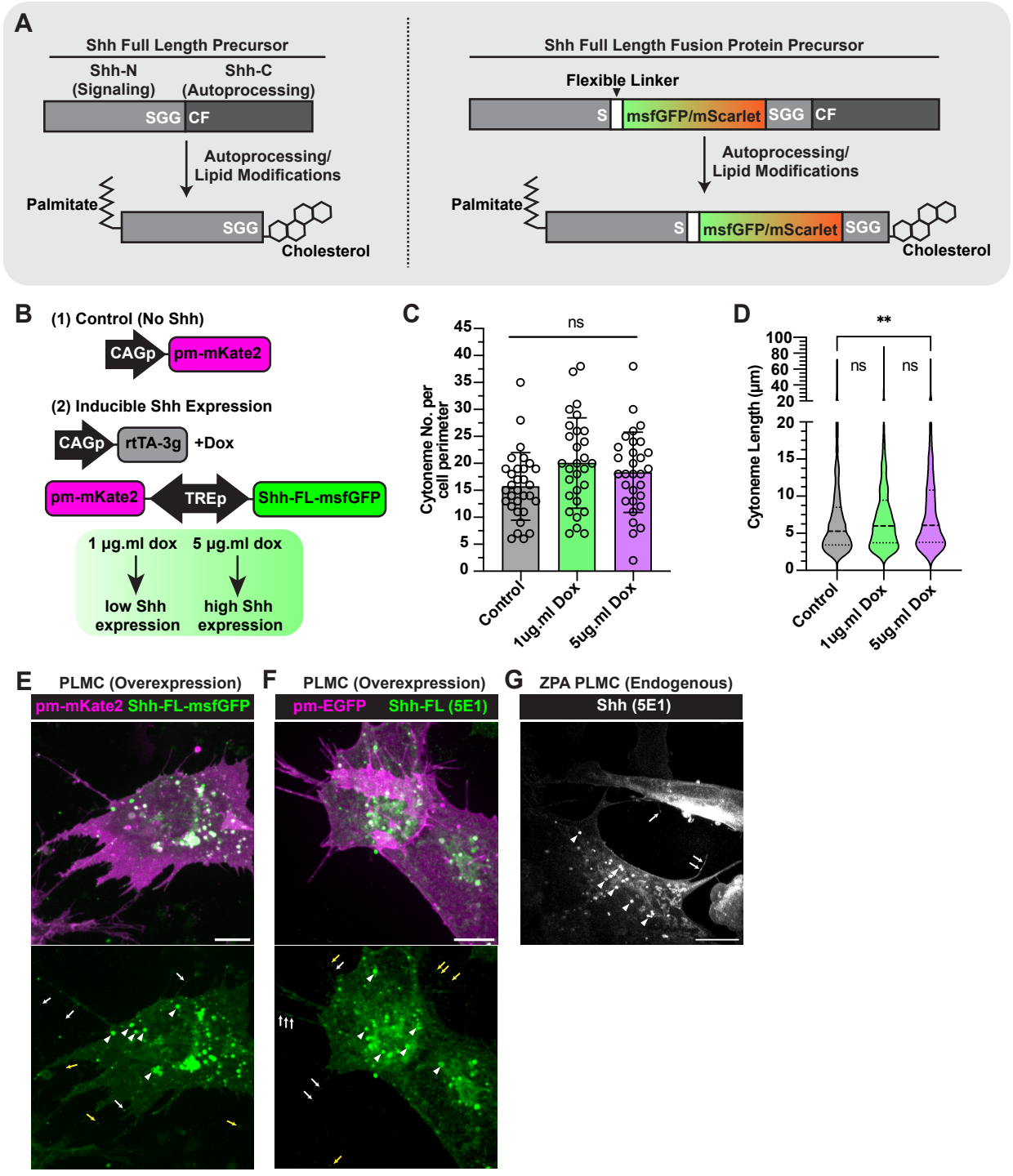


Figure 2.2: Shh-FL-msfGFP overexpression does not alter cytoneme production or subcellular localization.

(Figure 2.2 continued) (A) Overview of precursor and lipid modified protein for wild-type and internally tagged Shh. (B) Experimental strategy for overexpression of Shh in anterior limb bud derived PLMCs, which lack endogenous Shh expression (see Methods for details). C–D) Quantifications of number (C) and length (D) of cytonemes made by PLMCs under the indicated Shh overexpression conditions (C): $n = \sim 30$ cells per condition, pooled from 2 independent experiments; (D): $n > 90$ cytonemes per condition, ± SD). Shh control dataset was used to produce the histogram shown in Figure 1.1D and for comparison with cytonemes *in vivo* in Figure 6C (E) PLMC overexpressing pm-mKate2 and Shh-FL-msfGFP. (F) PLMC overexpressing pm-mKate2 and Shh-FL stained with anti-Shh (5E1) antibody (non-specific secondary antibody signal was subtracted from Shh channel). (G) PLMC derived from ZPA region of limb bud stained with anti-Shh (5E1) antibody. White arrows in (E–G) point to cytoneme-localized Shh, yellow arrows point to extracellular Shh puncta, and white arrowheads point to Shh accumulated in endosome/MVB-like structures. Scale Bars = 10 μm. Significance testing was performed using one-way ANOVA with Tukey's Multiple Comparisons.

These structures are ˜1 µm in diameter, and they contain smaller intralumenal patches of Shh-FL-msfGFP signal, suggesting that they may be multivesicular bodies (MVBs). We observed similar localization of immunostained Shh in PLMCs overexpressing untagged Shh or in ZPA-derived PLMCs endogenously expressing Shh (Figure 2.2E-G), confirming that they are not artifacts of Shh-FL-msfGFP overexpression. We conclude that cultured PLMCs provide a useful model in which to study mechanisms that govern Shh secretion and dispersal, with direct relevance to Shh gradient formation *in vivo*.

Shh traffics to both cytonemes and MVB-like structures rapidly after synthesis

To gain deeper insights into the dynamics of Shh secretion and transport by PLMCs, we developed methods to observe passage of Shh through the secretory pathway in limb bud mesenchymal cells. One common method, known as Retention Using Selective Hooks (RUSH) (Boncompain et al., 2012), uses high affinity binding of streptavidin binding protein (SBP) to streptavidin to trap secretory cargo in the endoplasmic reticulum (ER), which is released upon addition of biotin. Unfortunately, the high levels of endogenous biotin in chicken yolk/embryos prevents the constitutive retention of cargo using RUSH in this system

(Figure 2.3A-B top panel) (Taniguchi and Watanabe, 2007).

As an alternative strategy, we designed a functionally analogous ER trap and synchronous release system using Chemically Disruptable Heterodimer (CDH) protein binding switches (Giordano-Attianese et al., 2020). CDH switches consist of a truncated Bcl-xL receptor and a synthetic CDH Binder moiety (referred to here as CB), that bind one another with high affinity, but dissociate upon addition of a small molecule inhibitor of Bcl-xL (A1155463) (Giordano-Attianese et al., 2020; Shui et al., 2021). To implement an ER trap, we added the ER localization sequence from the STIM1 gene and the ER retention signal (KDEL) to the Bcl-xL receptor. To make a trappable form of Shh, we inserted the CB moiety upstream of the msfGFP into our full length, msfGFP tagged Shh (Shh-CB-msfGFP; see Methods). When both constructs are expressed in the same cell, Shh-CB-msfGFP should be trapped in the ER until released by the addition of A1155463 (Figure 2.4A). We screened a panel of published point-mutated variants of the CB moiety, with varying affinities for the Bcl-xL receptor (Shui et al., 2021), and identified a variant (Shh-CB(D138A)) that is tightly trapped in the ER in both PLMCs and *in vivo*, but is rapidly and efficiently released upon exposure to A1155463 (Figure 2.3B bottom panels, 2.3C-2D). We used the CB(D138A) variant (hereon CB) for all subsequent experiments.

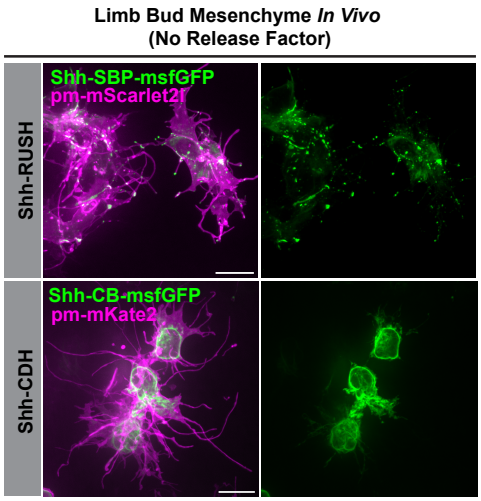
To confirm that the Shh-CB-msfGFP fusion protein is secreted and retains normal bioactivity, we collected conditioned media from HEK-293FT cells transfected with plasmids encoding either a pm-EGFP negative control, Shh-FL-msfGFP as a positive control, or our new Shh-CB-msfGFP. Then we incubated Shh-responsive NIH-3T3 cells with conditioned media for 40 hours and performed RT-qPCR against the Shh target gene *Ptch1* (Figure 2B). Conditioned media from cells expressing either Shh-FL-msfGFP or Shh-CB-msfGFP upregulated *Ptch1* expression compared to the pm-EGFP control, confirming that Shh-CB-msfGFP is properly secreted and remains biologically active (Figure 2.4C).

To characterize the kinetics of Shh release and post-release trafficking, we expressed

A

	RUSH	CDH
Trap/Hook	Streptavidin	truncated Bcl-xL
Binding Moiety	Streptavidin Binding Protein (SBP)	CDH Binding Moiety CB(D138A)/LD3
Release Factor	Biotin	A-1155463
Trap *In Vivo*	NO	YES

B



C

CB Isoform (LD3)	Binding Affinity (K_d)	Release?
LD3	4 pM	NO
LD3(E22A)	270 pM	NO
LD3(D138A)	22 nM	YES

(Shui et al., 2021)

D

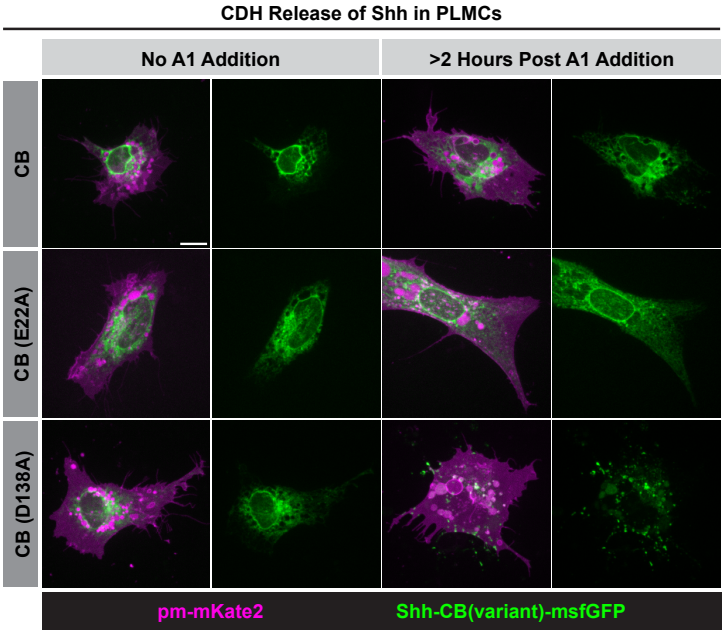


Figure 2.3: CDH release system provides tight ER trapping in vitro and in vivo. (A) Comparison between RUSH and CDH synchronous release systems. (B) Representative micrographs of limb bud mesenchymal cells in vivo, electroporated with either RUSH (ER-localized streptavidin and Shh-SBP-msfGFP) or CDH (ER-localized Bcl-xL and Shh-CB-msfGFP) release systems without any addition of release factors (Biotin or A1155463, respectively). Shh-SBP-msfGFP (RUSH) is distributed as punctate structures throughout the cell body and cytonemes, whereas Shh-CB-msfGFP (CDH) remains in the ER.

(Figure 2.3 continued) C) Previously published point mutated variants of the LD3 (CB) moiety and their binding affinity with Bcl-xL, scored for rapid release (under 2 hours) from an ER based trap in PLMCs. D) Micrographs showing PLMCs that were electroporated with the ER-localized Bcl-xL trap and a Shh-CB/LD3(variant)-msfGFP with and without 2 hours of A1155463 incubation. Scale Bars = 10 μm.

the ER-localized trap, Shh-CB-msfGFP, and a Golgi apparatus marker (GalNAcT2-HALO) in chicken embryonic fibroblasts. We added A1155463 and visualized release of Shh-CB-msfGFP in live cells using spinning disk confocal microscopy (Figure 2.4D, Video S3). At the earliest timepoint examined (5 minutes after exposure to A1155463), Shh-CB-msfGFP remained tightly trapped in the ER, indicating that the CDH trap does not leak (Figure 2.4D, left panel). By 20 minutes post release, Shh-CB-msfGFP began to colocalize with the GalNacT2-Halo signal, indicating its entry into the Golgi apparatus (Figure 2.4D, middle panel). Starting 30 minutes post release, we observed Shh-CB-msfGFP puncta moving throughout the cell body, indicating rapid progress through the secretory system (Figure 2.4D, right panel, Video S3). Quantifying Golgi-associated Shh-CB-msfGFP signal vs time confirmed that Shh is released with similar kinetics across multiple cells (Figure 2.4E). Thus, the CDH system provides a reproducible way to follow secretory trafficking of Shh.

We then expressed the CDH trap and Shh-CB-msfGFP in PLMCs, induced synchronous release, fixed at 90 minutes post-release (MPR) using cytoneme-preserving Fidelis Fixative (See Methods), and imaged using Airyscan Super-Resolution microscopy. As described above for un-trapped Shh-FL-msfGFP, we observed accumulation of Shh-CB-msfGFP puncta in cell bodies, along cytonemes and within MVB-like structures in association with outer membranes and intralumenal vesicles (Figure 2.4F). To determine where and when these Shh-positive MVB-like structures originate, we released Shh-CB-msfGFP in PLMCs and used super-resolution spinning disk microscopy to follow its intracellular dynamics. Shh-enriched MVB-like structures (yellow arrowheads) began to appear about 30-40 minutes post-release, often in the perinuclear region, and continued to accumulate over the next 30 minutes,

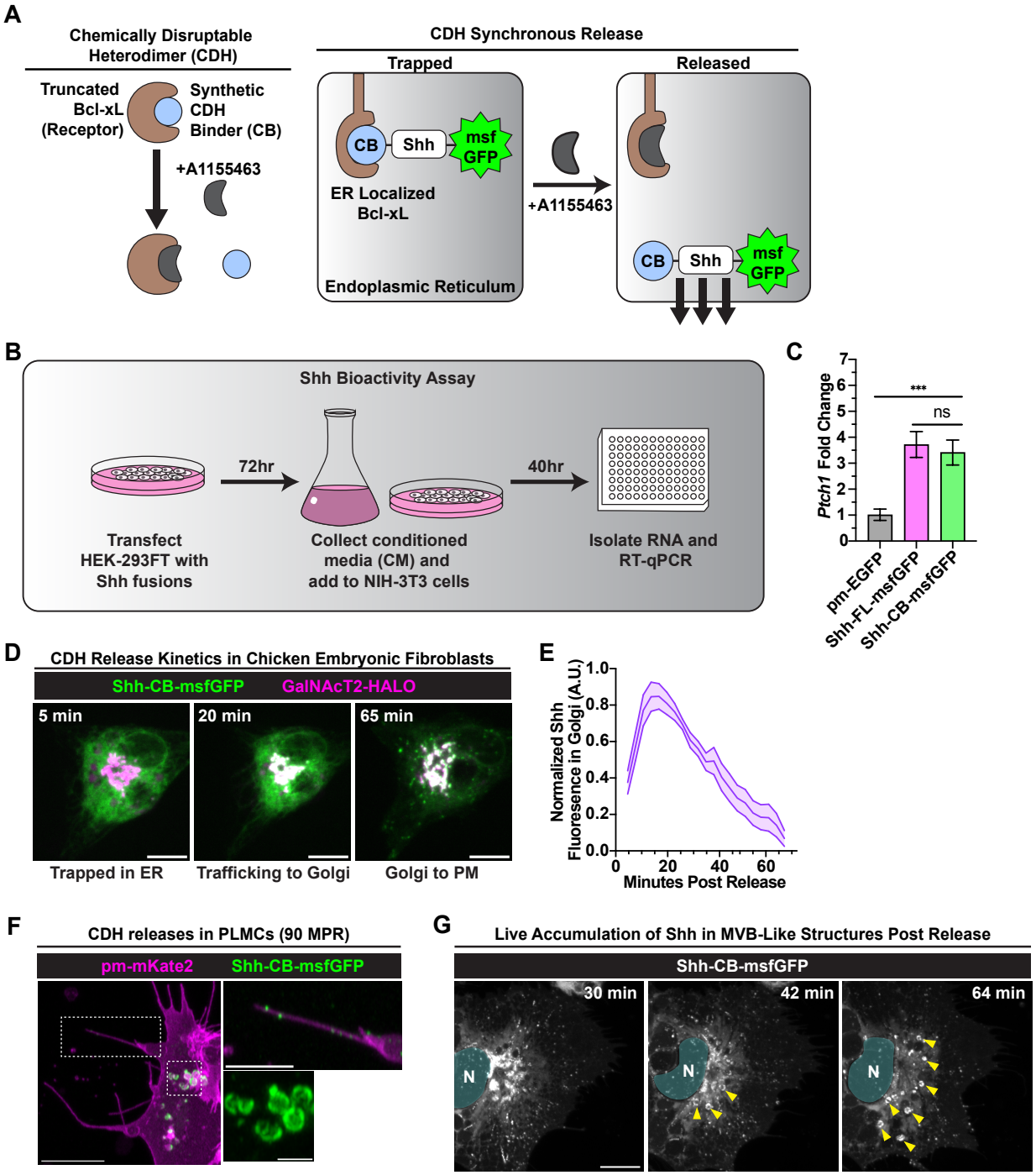


Figure 2.4: A CDH synchronous release system reveals that Shh rapidly accumulates in MVB-like structures after leaving the Golgi Apparatus.

(Figure 2.4 continued) (A) Overview of the Chemically Disruptable Heterodimer (CDH) protein switch and its use to trap and release cargo from the ER. (B) Overview of the bioactivity assay. (C) RT-qPCR of Ptch1 expression after conditioned media treatment ($n = 3$ biological replicates, ± SD). (D) Stills from Video S3 showing distribution of Shh-CB-msfGFP after release from the ER in Chicken Embryonic Fibroblasts (CEFs). GalNAcT2-HaloTag (magenta) was co-expressed to mark the Golgi apparatus. (E) Time series measurement of normalized Shh-CB-msfGFP fluorescence in the Golgi after release ($n = 12$ cells/releases, data pooled from 2 independent experiments, Mean trace ± SEM). (F) Airyscan Super Resolution micrograph of Shh-CB-msfGFP in PLMC 90 minutes post release. Top white box shows magnified and brightened view of Shh-CB-msfGFP localized to a cytoneme. Bottom white box shows magnified view of Shh-positive MVB-like structures. (G) Distribution of Shh in PLMCs at indicated timepoints after induction of release from Video S4. Yellow arrowheads mark Shh localized to MVB-like structures. Nucleus, N, pseudo colored cyan. Scale Bars in (D, F left panel, G) = 10 μm, (F) top right panel = 5 μm, (F) bottom right panel = 2 μm. Significance testing was performed using one-way ANOVA with Tukey's Multiple Comparisons.

while moving throughout the cell (Figure 2.4G; Video S4, white arrowheads). We observed similarly rapid accumulation of Shh-CB-msfGFP puncta along cytonemes (Video S4, white arrows).

Shh-positive MVB-like structures are bona fide multivesicular bodies

MVBs are characterized by their endocytosis-dependent generation and by their enrichment of specific markers such as the tetraspanin CD63.(Mathieu et al., 2021; Xu et al., 2023) To test whether the formation of Shh-positive MVB-like structures require endocytosis, we released Shh-CB-msfGFP in PLMCs expressing a dominant negative form of the GTPase Rab5a (Rab5a-DN(S34N)), that is known to inhibit endocytosis and prevent formation of MVBs (Figure 2.5A)(Barbieri et al., 2004; Dinneen and Ceresa, 2004). In control cells, Shh-CB-msfGFP accumulates heavily in MVB-like structures from 60-90 minutes post-release (Figure 2.6B, left panels, inset). However, in cells expressing Rab5a-DN(S34N), Shh oligomers were highly enriched on the plasma membrane, compared to control cells, and Shh-CB-msfGFP containing MVB-like structures were absent (seen in max intensity projected images in Figure 2.6B, right panels, inset). To determine whether Shh-positive MVB-like

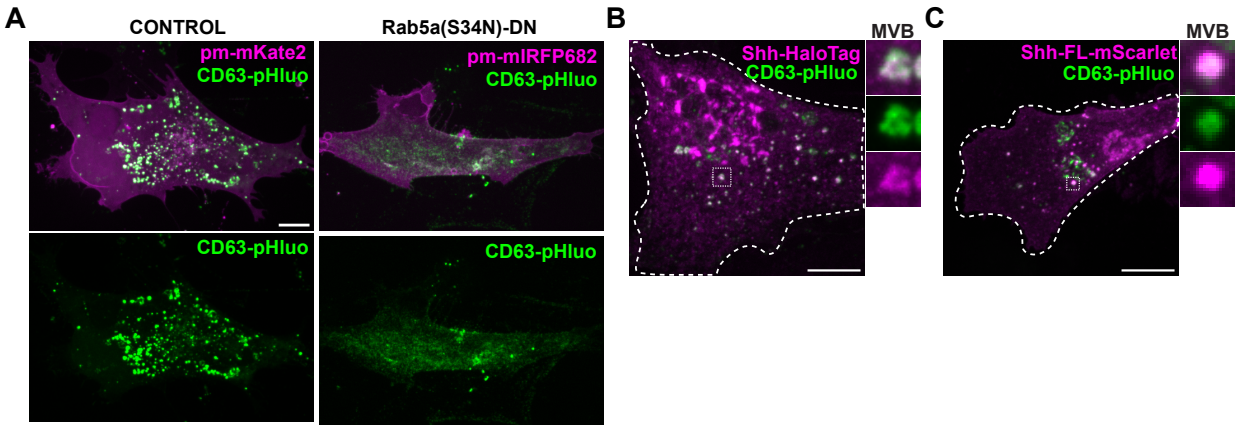


Figure 2.5: Shh fusion proteins colocalize in endocytosis-derived CD63-positive MVBs. (A) Micrographs of fixed PLMCs expressing CD63-pHluo and pm-mKate2 with or without co-expression ofRab5a(S34N)-DN. B) Fixed PLMC co-expressing a Shh-HaloTag (Janelia Fluor JFX650) and CD63-pHluo. C) PLMC co-expressing Shh-FL-mScarlet and CD63-pHluo. A-B) Cell outlines are marked with wavy dashed lines; white dashed boxes highlight colocalization of Shh and CD63 in MVB-like organelles Scale Bars = 10 μm.

structures are enriched in CD63, we fixed and immunostained cells co-expressing untagged Shh and CD63 tagged with a pH-sensitive pHluorin (pHluo) fluorescent protein(Sung et al., 2020), which fluoresces at neutral pH in both live and fixed cells (Figure 2.6C). We observed strong co-enrichment of untagged Shh (detected by immunostaining) and CD63-pHluo signal in MVB-like structures (Figure 2.6D), and similar co-enrichment of Shh-HaloTag and of Shh-FL-mScarlet with CD63-pHluo in MVB-like organelles (Figure 2.5B-C). We conclude that the Shh-positive MVB-like structures we observe are *bona fide* MVBs.

MVBs secrete Shh-containing exosomes

MVBs can fuse to the plasma membrane, resulting in exosome secretion, or they can fuse to lysosomes, resulting in degradation (Figure 2.6A). To test whether PLMCs use MVBs as an intermediate to secrete Shh-positive exosomes into the extracellular space, we co-expressed Shh-FL-mScarlet and CD63-pHluo in PLMCs and combined live multicolor spinning disk confocal microscopy with automated feature detection to identify mScarlet- and pHluo-labelled puncta in the extracellular space around individual PLMCs (Figure 2.6E; see Methods). Over 40% of extracellular Shh-FL-mScarlet puncta were also positive for CD63-

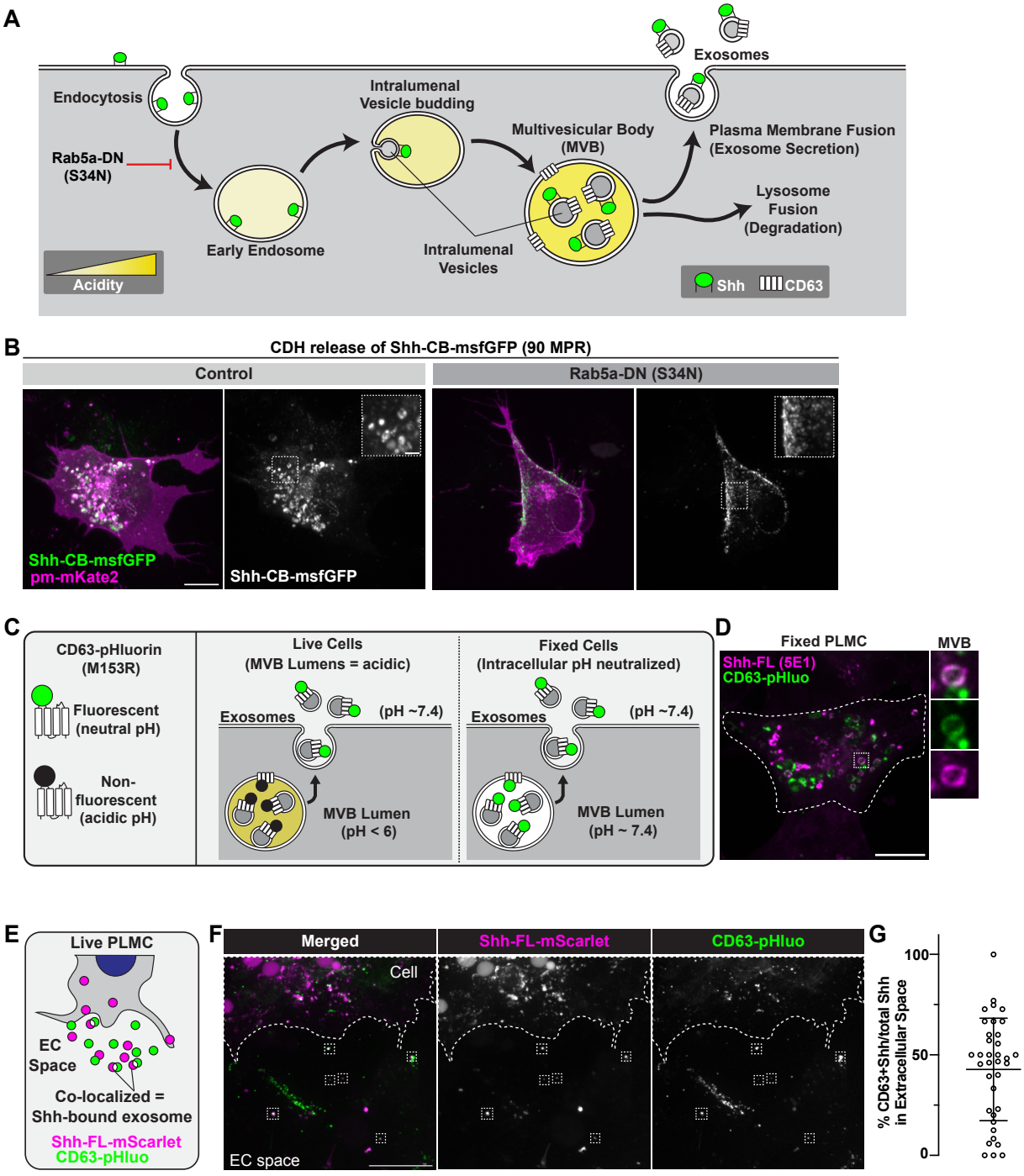


Figure 2.6: Shh-positive endosomal structures are bona fide multivesicular bodies (MVBs) that fuse to the plasma membrane to release Shh-bound exosomes.

(Figure 2.6 continued) (A) Overview of exosome biogenesis. (B) Maximum intensity projections of Shh-CB-msfGFP localization 90 minutes post release in control PLMCs or PLMCs expressing Rab5a-DN(S34N) after fidelis fixation. Insets show Shh enrichment in MVB-like structures in control cells and on the cell perimeter in Rab5a-DN(S34N). (C) Use of CD63-pHluo(M153R) as a pH sensitive marker in live and fixed cells. (D) IF staining of Shh (5E1) in an anterior limb bud derived PLMC expressing CD63-pHluo and full length Shh (Shh-FL). Curved dashed white line highlights outline of PLMC cell body. Thin dashed white box highlights an individual MVB; magnified views of individual and merged channels on the right illustrate colocalization of the two signals within the MVB. (E) Experimental strategy for detecting colocalization of Shh-FL-mScarlet with CD63-pHluo. (F) A PLMC co-expressing Shh-FL-mScarlet and CD63-pHluo. Dashed white boxes highlight colocalization of signal in extracellular space. (G) Quantification of colocalization of Shh-FL-mScarlet with CD63-pHluo in extracellular space ($n = 36$ cells, data pooled from 3 independent experiments, $\pm$ SD). Scale Bars = 10 μm.

pHluo (Figure 2.6F-G, white dashed boxes) suggesting that a large fraction of secreted Shh is associated with putative exosomes. Notably, since not all exosomes are CD63-positive (Coulter et al., 2018; Mathieu et al., 2021), the fraction of Shh-FL-mScarlet puncta that are bound to exosomes may be substantially larger than 40%.

To test whether the putative Shh-bound exosomes arise from fusion of MVBs, we used Total Internal Reflection Fluorescence (TIRF) microscopy to image PLMCs expressing CD63-pHluo, exploiting the fact that in living cells, CD63-pHluo is quenched in the acidic lumen of MVBs, but fluoresces when exposed to extracellular space upon MVB fusion with the plasma membrane (Figure 2.6C)(Sung et al., 2020; Verweij et al., 2018). Using fast timelapse acquisition, we observed many transient, localized bursts of CD63-pHluo fluorescence with spatial extents, amplitudes, and decay kinetics resembling those of well-characterized MVB-plasma membrane fusion events (Figure 2.7A-B, Video S5)(Bebelman et al., 2020; Verweij et al., 2018). We observed MVB fusion events throughout the cell body, including near the base of cytonemes, but not along cytonemes or at their tips (Figure 2.7C). Similarly, the GTPase Rab27a, which localizes to MVBs and mediates their fusion with the plasma membrane, was also broadly distributed within MVBs in PLMC cell bodies, but not along cytonemes, when visualized by immunostaining (Figure 2.7D)(Ostrowski et al., 2010). To confirm that the

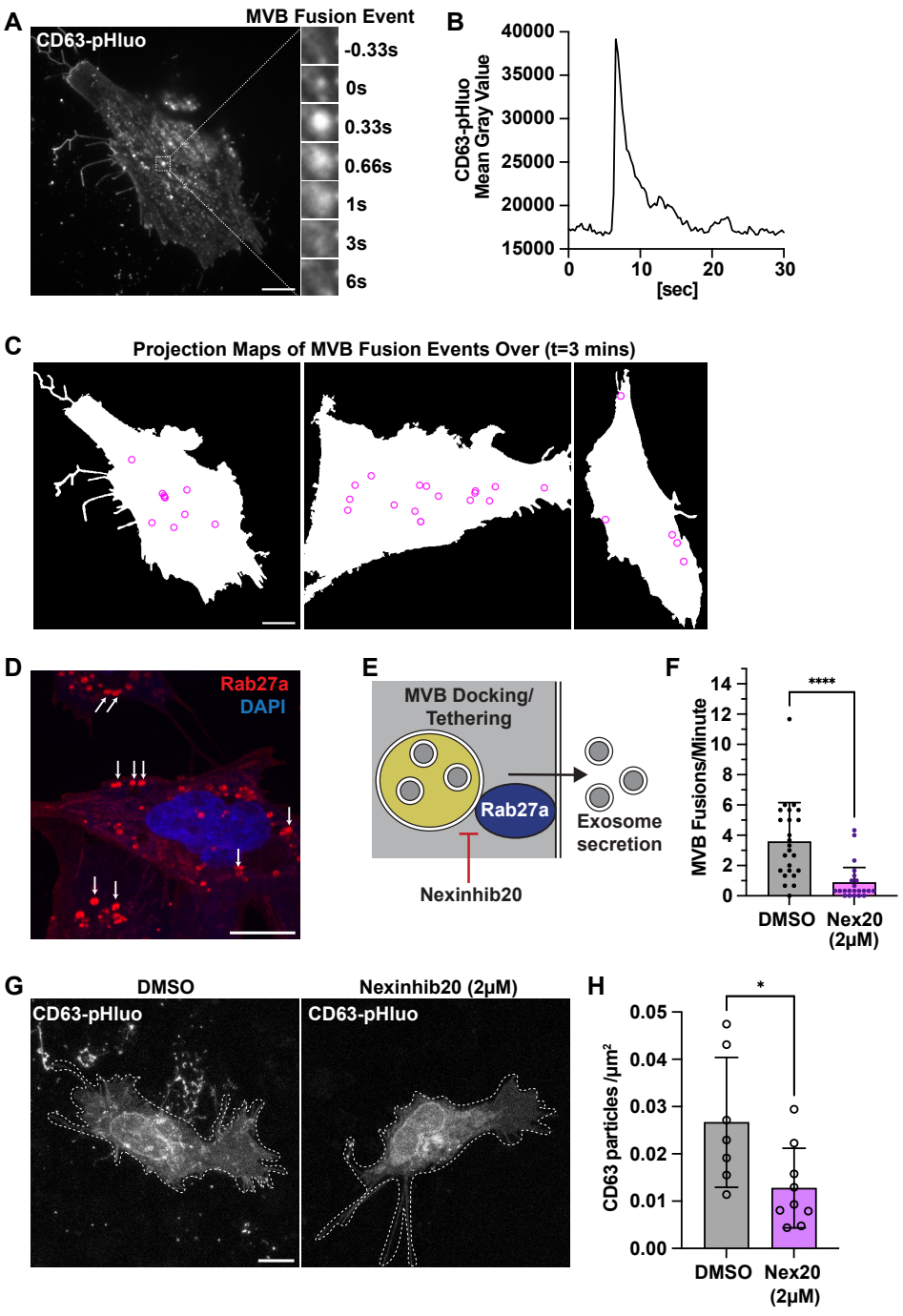


Figure 2.7: MVB-plasma membrane fusion events in PLMC cell bodies generate extracellular CD63-pHluo labeled exosomes

(Figure 2.7 continued) (A) Total Internal Reflection Fluorescence (TIRF) micrograph of a PLMC expressing CD63-pHluo. Magnified views to the right highlight an individual burst of CD63-pHluo fluorescence reflecting the fusion of an MVB with the plasma membrane (B) Average fluorescence intensity trace for the MVB-plasma membrane fusion event highlighted in (A). (C) Spatial distribution of MVB-plasma membrane fusion events over a 3-minute interval for three representative cells D) Immunofluorescence staining of endogenous Rab27a GTPase in a PLMC. White arrows highlight individual MVBs. (E) Site of action of the small molecule inhibitor Nexinhib20. (F) Quantification of MVB-plasma membrane fusion events in PLMCs incubated with either DMSO or Nex20 (2 μM) for 24 hours. Quantification was performed using the Analyzer of MVB Exocytosis (AMvBE) FIJI macro (n = 24 DMSO cells, n = 22 Nexinhib20 cells, pooled from 3 independent experiments, ± SD). (G) Max projected confocal micrographs of PLMCs treated with either DMSO or Nexinhib20 (2 μM) for 24 hours. (H) Quantification of CD63-pHluo puncta in the extracellular space surrounding PLMCs (n = 7 DMSO treated cells, 9 Nexinhib20 treated cells, one experimental replicate). Mann-Whitney U test performed for statistical comparison in (F, H). Scale Bars = 10 μm.

observed pHluo bursts represent MVB fusions, we treated PLMCs expressing CD63-pHluo with Nexinhib20 - a pharmacological inhibitor of Rab27a (Gustafson et al., 2022; Johnson et al., 2016). Treatment with 2 µM Nexinhib20 produced a sharp reduction in the number of CD63-pHluo bursts (Figure 2.7E-F, Video S5) and a corresponding reduction in the number of extracellular CD63-pHluo puncta (Figure 2.7G-H), relative to vehicle-treated controls, confirming that these puncta are *bona fide* exosomes derived from MVB-plasma membrane fusion. In summary, we find that a substantial fraction of newly secreted Shh is rapidly endocytosed from the plasma membrane, packaged into MVBs, and then re-secreted into the extracellular space bound to diffusible exosomes.

Exosome-bound Shh binds to and is transported along the external surface of cytonemes

Previous studies have proposed at least four distinct mechanisms for localization of Shh to cytonemes (Figure 2.8a). Shh could travel inside cytonemes in (1a) secretory vesicles or (2a) small MVBs(Gradilla et al., 2014; Hall et al., 2021). Alternatively, Shh could travel along the outer surfaces of cytonemes as membrane-tethered oligomers (1b) or bound to extracellular vesicles/exosomes (2b)(Gradilla et al., 2014; Sanders et al., 2013).

To determine whether Shh travels inside cytonemes or on their outer surfaces, we immunostained Shh in non-permeabilized PLMCs expressing Shh-FL-msfGFP to selectively label Shh exposed to the extracellular media (Figure 2.8B). In contrast to results reported for NIH-3T3 fibroblasts(Hall et al., 2021), the vast majority (roughly 70%) of Shh-FL-msfGFP on cytonemes was labeled by this method (Figure 2.8C white arrowheads, 2.8D). The absence of fluorescent signal associated with cytoplasmic MVBs confirmed the specificity of extracellular labeling (Figure 2.8C, white arrows). These results are consistent with a previous study, which used split-GFP to detect association of Shh with the external surfaces of cytonemes in the limb bud mesenchyme *in vivo* (Sanders et al., 2013). Thus, in PLMCs, the majority of Shh associated with cytonemes is exposed directly to extracellular space.

To determine whether secreted Shh travels along the outer surfaces of cytonemes as "naked" oligomers or on MVB-derived exosomes, we performed CDH release experiments to visualize the association of newly secreted Shh with cytonemes in living PLMCs. We occasionally observed Shh-containing structures (yellow arrowheads), with the size and shape of MVBs, that travelled to the base of a cytoneme and then broke apart into smaller Shh-containing puncta that undergo directed movements along the cytoneme towards its distal tip (yellow arrows) (Figure 2.8E, Video S6). We hypothesized that these puncta represent newly secreted Shh-positive exosomes that are transported along the external surface of the cytonemes. To test this hypothesis further, we co-expressed Shh-FL-mScarlet and CD63-pHluo with a plasma membrane marker (pm-mIRFP682) to visualize the association of Shh-positive exosomes with cytonemes in living PLMCs. Like the broader pool of extracellular Shh puncta (Figure 2.6F-G), roughly 40% of cytonemal Shh-FL-mScarlet puncta colocalized with CD63-pHluo (Figure 2.8F, white boxes), indicating that they are secreted exosomes. Interestingly, timelapse imaging of PLMCs expressing Shh-FL-mScarlet, CD63-pHluo, and pm-mIRFP682 revealed transient binding of Shh-positive exosomes to cytonemes, as well as directed transport, suggesting that once secreted from the cell body, Shh-containing exosomes

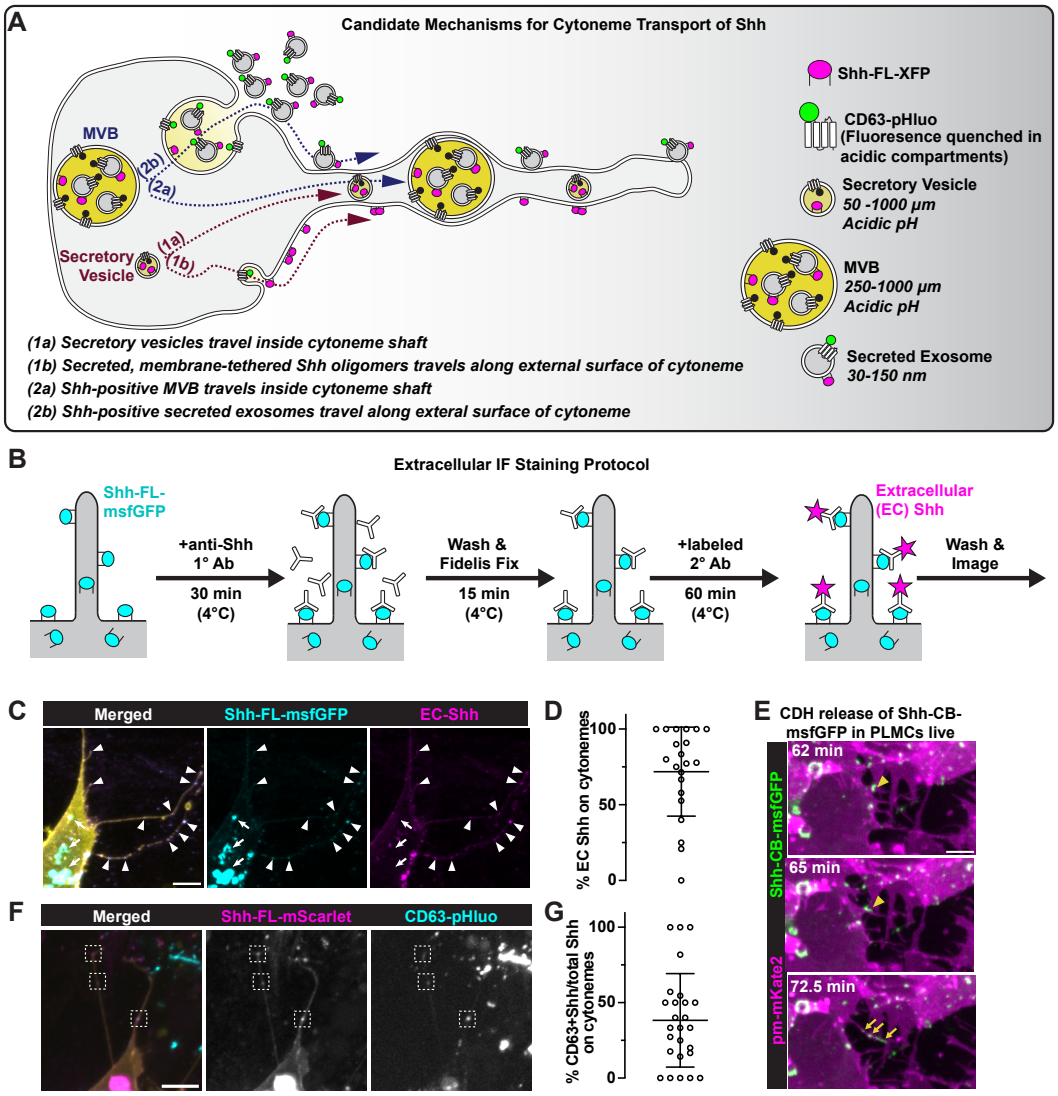


Figure 2.8: Shh-bound secreted exosomes associate with and travel along cytonemes. A) Possible modes of cytoneme localization and transport of Shh. B) Protocol for extracellular IF staining. C) Visualization of total (Shh-FL-msfGFP) and extracellular (EC-Shh) Shh on cytonemes (white arrowheads). Note that internal Shh-enriched structures are unlabeled (white arrows). D) Colocalization of Shh-FL-msfGFP (Total) and EC-labeled Shh on cytonemes per cell ($n = 21$ cells, pooled from 2 independent experiments, ± SD). E) Frames from Video S6 – Shh-CB-msfGFP in PLMC at indicated times starting 62 min post release. Yellow arrowheads mark Shh-positive MVB-like structure. Yellow arrows mark small Shh puncta along cytoneme. F) PLMC co-expressing Shh-FL-mScarlet, CD63-pHluo, and pm-mIRFP682 (yellow). White boxes highlight Shh puncta co-localized with CD63-pHluo. G) Quantification of the fraction of overlapping CD63-pHluo/Shh-FL-mScarlet puncta over total Shh-FL-mScarlet puncta along cytonemes per cell ($n = 26$ cells, pooled from 3 independent experiments, ± SD). Scale Bars = 10 μm.

can switch between diffusive and directed modes of transport (Video S7, red arrowhead and white arrows, respectively).

To examine how exosome secretion regulates the localization of Shh to cytonemes, we quantified the number and distribution of Shh-CB-msfGFP puncta along cytonemes at 90 minutes post release in cells co-expressing Rab5a-DN (S34N) to inhibit endocytosis or treated with Nexinhib20 to block MVB fusion and release (Figure 2.9A). In control cells, Shh puncta are present on a subset of cytonemes, with slight enrichment near their tips. This pattern of accumulation was unaffected in cells expressing Rab5a-DN (S34N) (Figure 2.9B-F), presumably reflecting the overall enrichment of "naked" Shh oligomers on the outer leaflets of cell membranes (Figure 2.9B). However, Nexinhib20 treatment reduced the number of Shh-positive cytonemes per cell, the number of Shh puncta per cytoneme, and the enrichment of Shh at cytoneme tips, compared to DMSO treated control cells, suggesting that exosome secretion contributes to the accumulation and tip enrichment of Shh on cytonemes (Figure 2.9G-K).

Exosome secretion is required for 2D Shh signaling gradient formation

Our results suggest that exosome packaging and secretion may play a key role in Shh dispersal and the formation of Shh signaling gradients in the limb bud mesenchyme. To test this idea further, we adapted a recently published assay to reconstitute and measure Shh signaling gradients *in vitro* (Li et al., 2018; Schlissel et al., 2024). In the original assay, NIH-3T3 fibroblast "sender cells" expressing Shh are seeded at low density onto a confluent layer of "receiver" NIH-3T3 fibroblasts expressing a fluorescent Shh activity reporter composed of an array of Gli-binding sites driving nuclear mCitrine expression. Over time, a radial signaling gradient of Shh reporter activity is formed around the sender cell. We modified this assay to replace fibroblast sender cells with PLMCs derived from anterior limb bud cells, which do not express endogenous Shh (Figure 2.10A)(Riddle et al., 1993). We used a bidirectional promotor to produce highly correlated co-expression of Shh-FL-msfGFP and

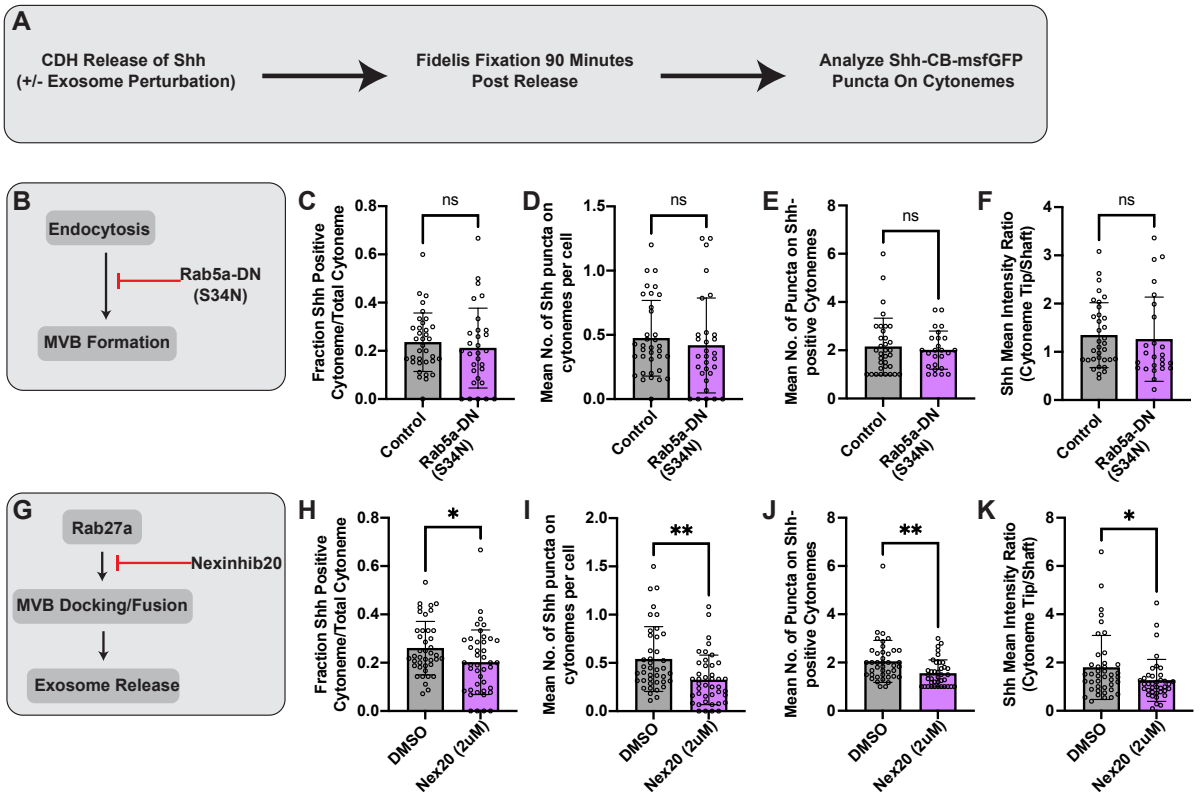


Figure 2.9: Exosome secretion contributes to Shh association along cytonemes. (A) Experimental workflow.(B) Site of action of Rab5a-DN (S34N). (C–F) Quantification of cytoneme associated CDH released Shh-CB-msfGFP in PLMCs with or without expression of Rab5a(S34N)-DN ($n = 34$ control cells and $n = 30$ Rab5a-DN cells, pooled from 3 independent experiments). (C) Fraction of Shh-positive cytonemes/total cytonemes per cell (± SD). (D) Mean number of Shh puncta per cytoneme per cell (± SD). (E) Quantification of the mean number of Shh puncta per Shh-positive cytonemes per cell ($n = 34/34$ control cells and $n = 25/30$ Rab5a-DN cells, ± SD). (F) Ratio of Shh-CB-msfGFP fluorescence in the cytoneme tip (last 1 μm) versus cytoneme shaft (1 μm from tip to base) per cell from data subset in (K). (G) Nexinhib20 site of action. (H–K) Quantifications of cytoneme associated CDH released Shh-CB-msfGFP in PLMCs treated with DMSO (vehicle) or 2 μM Nexinhib20 ($n = 41$ DMSO cells, $n = 42$ Nexinhib20 cells, pooled from 3 independent experiments). (H) Fraction of Shh-positive cytonemes/total cytonemes per cell (± SD). I) Mean number of Shh puncta per cytoneme per cell (± SD). (J) Mean number of Shh puncta per Shh-positive cytonemes per cell ($n = 41/41$ DMSO treated cells, $n = 38/41$ Nexinhib20 treated cells, ± SD). (K) Ratio of Shh-CB-msfGFP fluorescence in the cytoneme tip (last 1 μm) versus cytoneme shaft (1 μm from tip to base) per cell from data shown in (J). Significance testing was performed using two tailed Mann-Whitney U-test.

a membrane marker (palmitoylated mKate2) in PLMC sender cells (Figure 2.11A-B) and used the intensity of the membrane signal as a proxy for Shh expression level to normalize the signaling response gradients measured for individual cells. PLMC sender cells expressing Shh-FL-msfGFP induced response gradients with a spatial decay length of ~ 100 µm, which is comparable to gradients induced by PLMCs expressing untagged Shh (Figure 2.11C-D) and to those induced by NIH-3T3 cells expressing untagged or Halo-Tagged Shh (Schlissel et al., 2024).

To test a specific role for exosomes in gradient formation, we analyzed signaling gradients in co-cultures continuously exposed to Nexinhib20 to inhibit MVB fusion/exosome secretion or formed by PLMCs co-expressing Rab5a-DN(S34N) to inhibit endocytosis. Nexinhib20 treatment induced a strong reduction in the intensity of Shh signaling gradients, compared to DMSO-treated controls (Figure 2.10B-C), confirming that exosome release is essential for normal signaling gradients. Notably, inhibiting endocytosis in sender cells produced a sharp reduction in signal gradient intensity, relative to controls (Figure 2.10D-E), even though Shh remains highly enriched on sender cell membranes and cytonemes (Figure 2.6B, Figure 2.9B-F), suggesting that primary secretion and enrichment of membrane-tethered Shh is insufficient to form short-range signaling gradients. Instead, our results demonstrate that primary secretion, followed by MVB biogenesis and exosome secretion is required for high-intensity, short-range ($\leq$100 µm) Shh dispersal that establishes signaling gradients in 2D mesenchymal tissues.

Latrunculin A treatment abolished cytonemes (Figure 2.11E-G) (Arthur et al., 2021; Fujiwara et al., 2018; Segal et al., 2016), but did not affect the Shh response gradient relative to vehicle treated controls (Figure 2.10F-G), as previously reported for fibroblast sender cells in the original, 2D gradient assays (Schlissel et al., 2024). The cytonemes produced by PLMCs and fibroblast cells are much shorter (2-10µm) than the decay length of the observed signaling gradients (~100µm). Thus, while Shh-containing exosomes accumulate

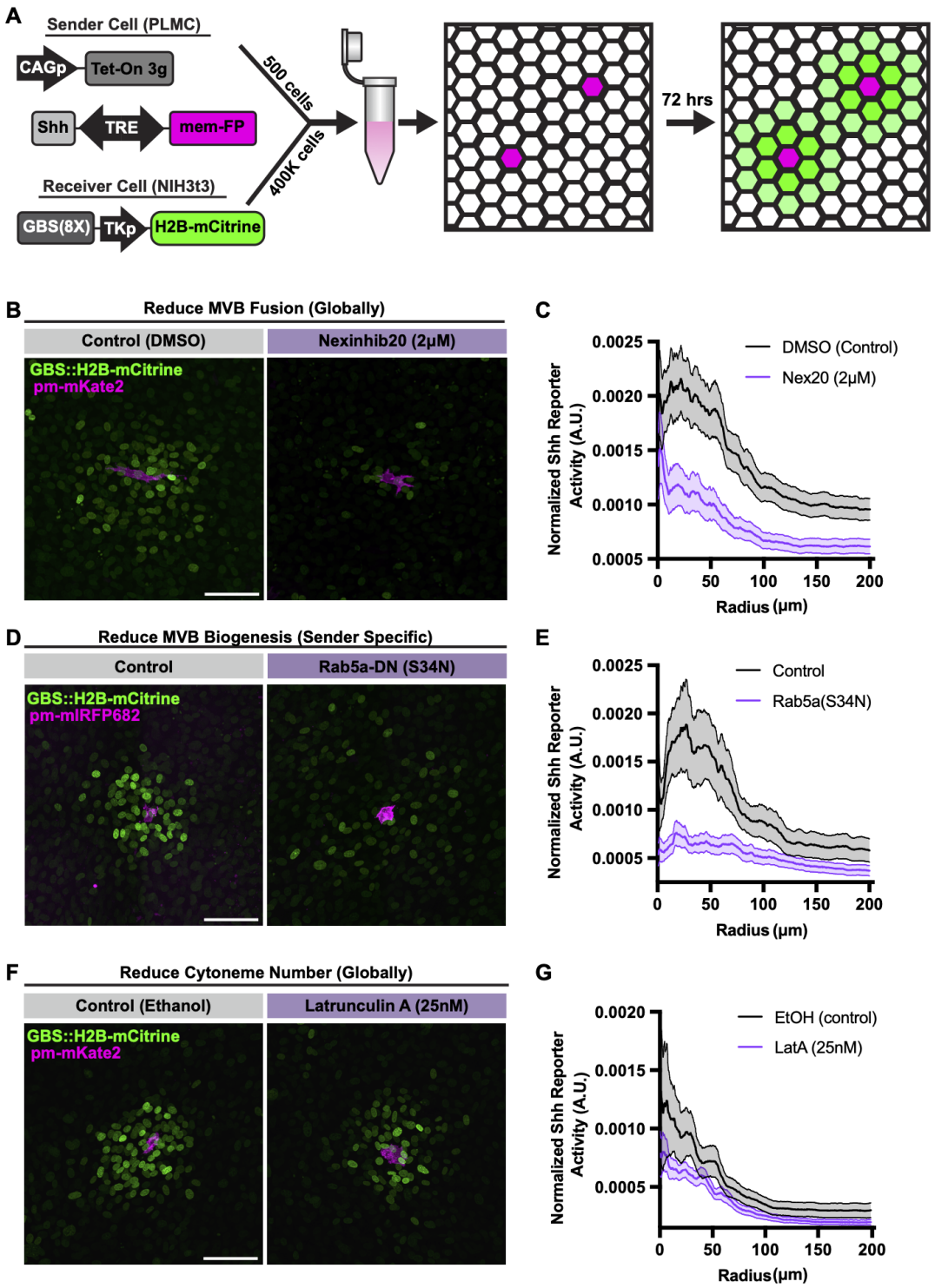


Figure 2.10: Exosome secretion is required for Shh dispersal and signal gradient formation.

(Figure 2.10 continued) (A) Overview of the reconstituted signaling gradient assay. (B–G) Representative images (B, D, F) and average gradients (C, E, G) for: (B–C) DMSO and Nexinhib20 treated cells ($n = 31$ DMSO gradients, $n = 30$ Nexinhib20 gradients, pooled from 2 independent experiments). (D–E) control and Rab5a-DN(S34N) expressing sender cells ($n = 17$ control gradients, $n = 15$ Rab5a-DN(S34N) gradients, pooled from 3 independent experiments). (F–G) Ethanol and Latrunculin A treated cells ($n = 24$ Ethanol gradients, $n = 27$ Latrunculin A gradients, pooled from 2 independent experiments). Measured gradients are plotted as a function of distance from the center of the gradient: solid curves and shaded regions indicate mean ± SEM. Scale Bars = 100 μm.

on and travel along PLMC cytonemes *in vitro*, the reduced lengths of these cytonemes may preclude a significant contribution to 2D gradient formation.

Secreted exosomes carrying Shh associate with and move along cytonemes made by limb bud mesenchymal cells in vivo

While cytonemes are not required for short range signaling gradients formed by PLMCs *in vitro*, limb bud mesenchymal cells *in vivo* project dynamic cytonemes with lengths far greater than those measured *in vitro* (Figure 2.12A-C, Video S8)(Sanders et al., 2013), suggesting that transport of Shh-bound exosomes along cytonemes may make a more significant contribution to shaping Shh signaling gradients *in vivo*.

To determine whether Shh-bound exosomes travel along cytonemes *in vivo*, we performed CDH-based trap and release of Shh-CB-msfGFP *in vivo,* followed by fixation and 3D confocal imaging. 60 minutes post release, Shh accumulates in MVB-like structures in the cell bodies (Figure 2.12D, arrows) and Shh puncta decorate the shafts of long cytonemes produced by limb bud mesenchyme cells (Figure 2.12D, arrowheads). We observed similar localization at 90 minutes post release (Video S9). With live imaging, we also observed co-localization of Shh-FL-mScarlet and CD63-pHluo along cytonemes *in vivo*, suggesting that, as *in vitro*, Shh-positive secreted exosomes travel along the external surface of cytonemes *in vivo* (Figure 2.12E). Consistent with this idea, scanning electron microscopy of ectoderm peeled limb buds revealed small (30-60 nm), spherical vesicles on the surfaces of a subset of cytonemes in the ZPA region (Figure 2.12F-G). These vesicles are similar in size and shape to cell surface-

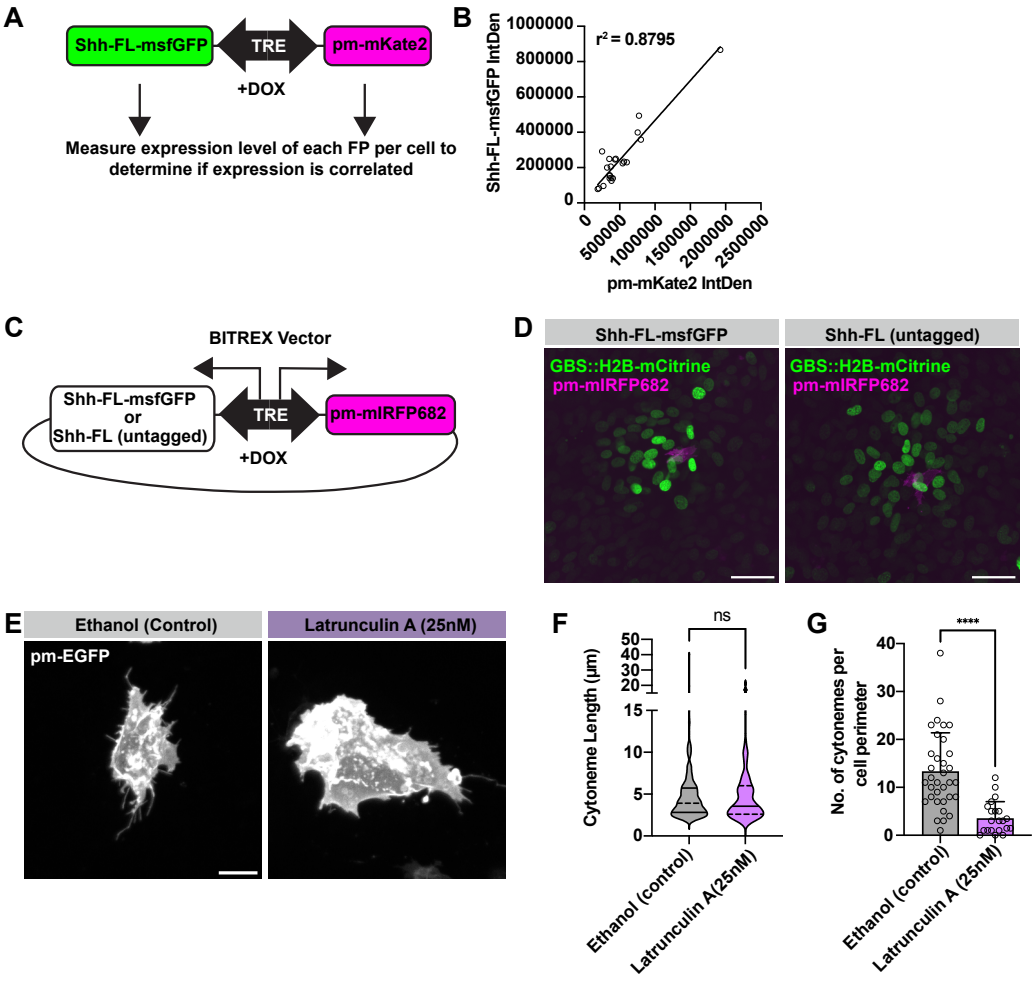


Figure 2.11: Controls related to Shh signaling gradients. (A) Map of BITREX vector and overview of assay to measure correlative expression of Shh-FL-msfGFP and pm-mKate2. To note, BITREX is a bidirectional Tet Response Element (TRE) promoter-based plasmid that drives expression of both Shh-FL-msfGFP and pm-mKate2. (B) Correlation of integrated density of Shh-FL-msfGFP and pm-mKate2 per cell ($n = 22$ cells, one independent experiment). Solid line indicates linear regression with $r^2 = 0.8795$. (C) Map of BITREX vector driving expression of either Shh-FL or Shh-FL-msfGFP and pm-mIRFP682. (D) Representative Shh Reporter Gradients formed by PLMCs expressing either untagged or msfGFP tagged Shh. (E) PLMCs expressing pm-EGFP and treated with Ethanol (vehicle) or Latrunculin A (25 nM) for 24 hours. (F–G) Quantification of cytonemes in ethanol or Latrunculin A treated PLMCs ($n = 34$ cells in Ethanol treatment, $n = 21$ cells in Latrunculin A treatment, 1 independent experiment). (F) Quantification of cytoneme lengths ($n = 452$ cytonemes in Ethanol treated cells, $n = 73$ cytonemes in Latrunculin A treated cells. (G) Quantification of average cytoneme number per cell perimeter. Scale Bar in (B) = 50 μm and in (E) = 10 μm. Significance testing was performed using a two-tailed Mann-Whitney U-test.

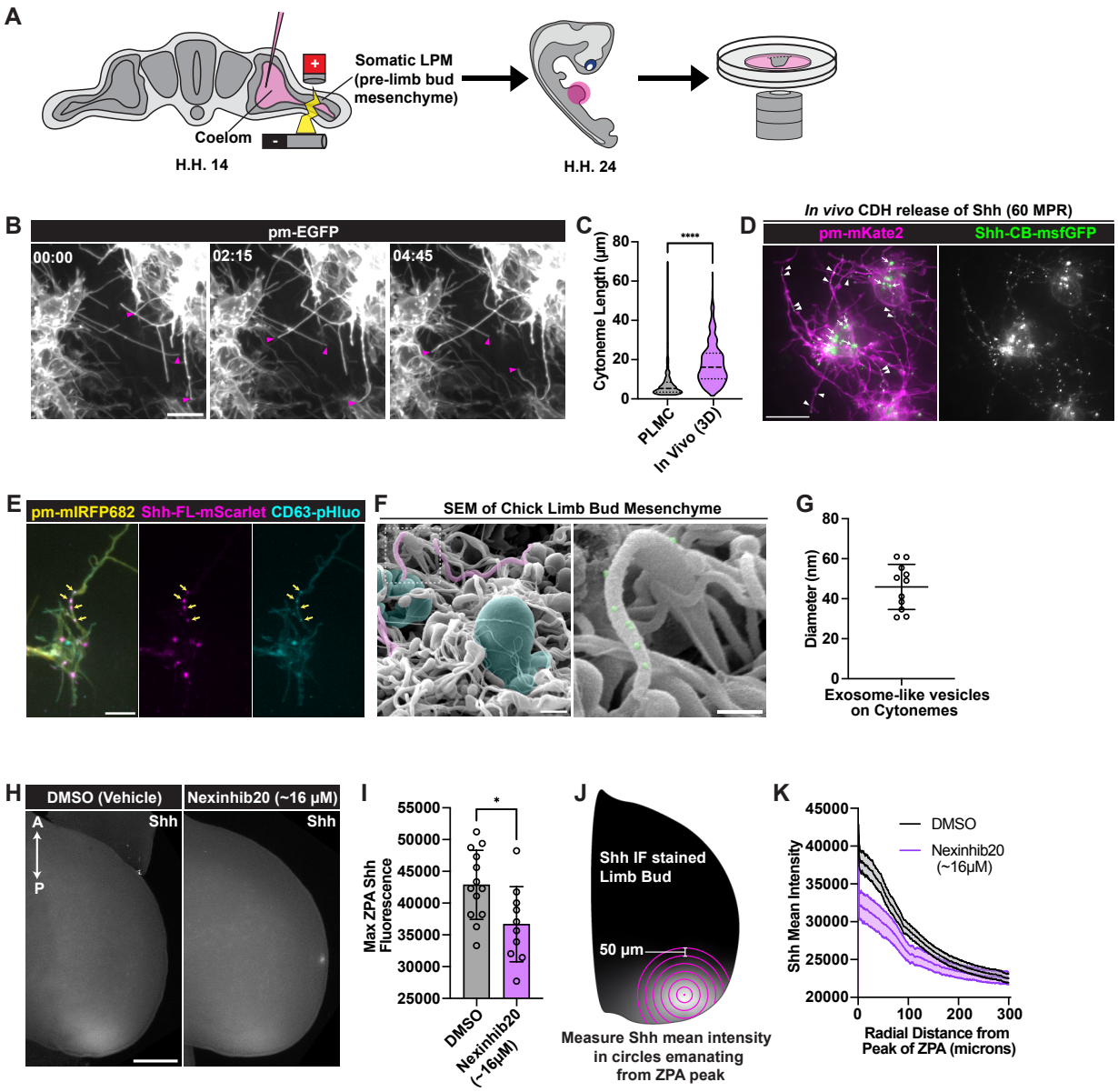


Figure 2.12: Exosomes are transported along the external surface of cytonemes and are required to establish Shh concentration gradients in vivo. (A) Scheme for *in ovo* electroporation of the chick limb bud mesenchyme. (B) Representative frames (minutes:seconds) from Video S8 (cropped) of limb bud mesenchymal cells *in ovo* electroporated with pm-EGFP. Magenta arrowheads label cytoneme tips extending and retracting. (C) Quantification of 2D PLMC cytoneme lengths (From Figure 1D/ Figure S1D) compared to 3D cytoneme lengths *in vivo* ($n = 490$ PLMC cytonemes, $n = 307$ *in vivo* cytonemes, pooled from 5 biologically independent forelimb buds). (D) Micrographs of Shh-CB-msfGFP in limb bud mesenchymal cells *in vivo* at 60 minutes post release. White arrows mark Shh-positive MVB-like structures and white arrowheads mark Shh puncta along cytonemes.

(Figure 2.12 continued) (E) Micrograph of limb bud mesenchymal cell expressing Shh-FL-mScarlet, CD63-pHluo, and pm-mIRFP682. Yellow arrows highlight colocalized Shh-FL-mScarlet and CD63-pHluo puncta along cytoneme. (F) Scanning electron micrograph of intact limb bud mesenchyme in the ZPA region at HH stage 22–23. Cyan masks mark mesenchymal cell bodies and magenta masks mark selected cytonemes. The white box highlighting one cytoneme in the left panel is magnified on the right panel. Green masks highlight spherical exosome-like structures decorating the external surface of the cytoneme. (G) Diameter measurements of exosome-like vesicles on cytonemes (n = 11 exosome-like vesicles, 2 independent limb bud ZPA SEM micrographs) (H) Max-projected micrographs of right forelimb buds derived from embryos treated with either DMSO or ∼16 μM Nexinhib20, fixed at HH stage 22 and immunostained for Shh. (I) Graph showing the peak fluorescence intensity within the ZPA (n = n = 13 DMSO limb buds, n = 10 Nexinhib20 limb buds, pooled from 2 independent experiments) (J) Diagram showing how radial average intensity plots of Shh fluorescence are measured. (K) Radial intensity profile plots (mean ± SEM) emanating from the peak of the ZPA from the same embryos treated with DMSO or ∼16 μM Nexinhib20. Scale Bars in (B, D) = 10 μm, (E) = 5 μm, (F) left panel = 1 μm, (F) right panel = 500 nm, (H) = 200 μm. Significance testing was performed using two tailed Mann-Whitney U-test.

associated exosomes previously observed by SEM (Edgar et al., 2016). Notably, the small diameters of cytonemes *in vivo* (˜150 nm; Figure 2.13) make transport of MVBs (250-1000 nm)(Altick et al., 2009; von Bartheld and Altick, 2011; Haigler et al., 1979) within cytonemes unlikely.

Finally, we sought to test whether exosome secretion is required to form Shh morphogen gradients *in vivo*. Genetic manipulations *in ovo* suffer from low and variable penetrance due to the inherently mosaic incorporation of electroporated DNA. As an alternative approach, we injected Nexinhib20 just beneath the embryo at HH stage 19/20 when Shh signaling in the limb bud begins. We adjusted concentration and volume of injectant to achieve an effective concentration (total amount of injected drug divided by egg volume) of 16-18 µM. We dissected and fixed right forelimb buds at 16 hours post-injection, performed wholemount immunofluorescence staining of Shh, followed by SeeDB2G-mediated tissue clearing, and confocal imaged each limb bud. In DMSO injected controls, we observed a radial gradient of endogenous Shh fluorescence with a peak near the center of the ZPA in the posterior limb

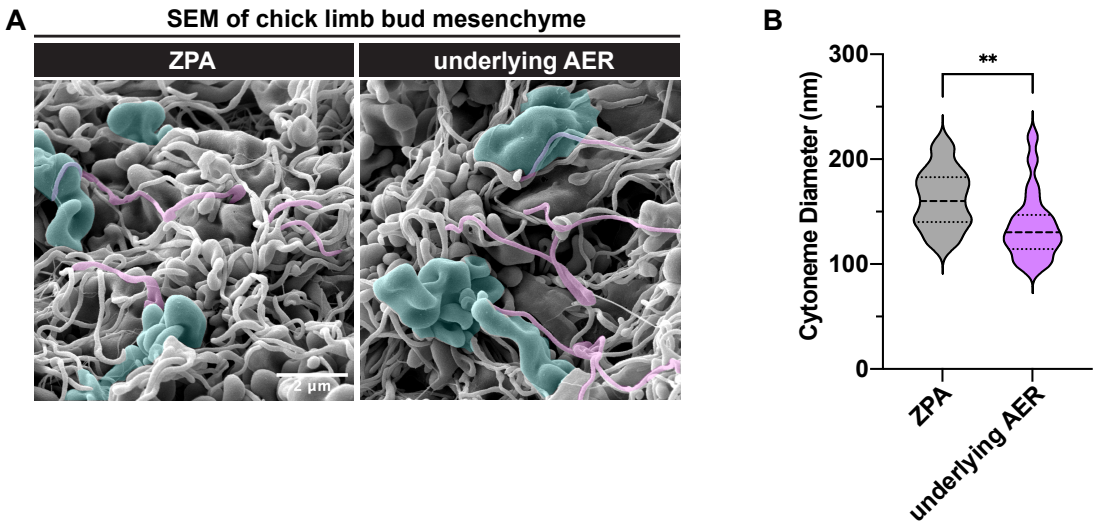


Figure 2.13: Ultrastructural views of limb bud mesenchymal cells in vivo highlight narrow cytoneme diameters. (A) Scanning electron micrographs of the surface of limb bud mesenchyme (ectoderm removed) from HH stage 22-24 chick embryos. Left panel is a representative micrograph of the ZPA, while the right is a representative micrograph of the mesenchyme underlying the AER region at the distal tip of the limb bud. Note globular cell bodies (cyan masks) and complex network of cytonemes (magenta masks). (B) Graph shows the composite (average) diameter of cytonemes in the ZPA and AER (n = 20 cytonemes, pooled from 2 biologically independent forelimb buds). Significance testing was performed using a two-tailed Mann-Whitney U-test.

bud (Figure 2.12H, left panel). In Nexinhib20 injected embryos, we observed a significant reduction in the peak Shh fluorescence intensity near the ZPA (Figure 2.12H, right panel, 2.12I), and in the amplitude of the Shh protein gradient over the first 100 microns from the ZPA peak (Figure 2.12J-K). Although we could not directly monitor the effects of Nexinhib20 on MVB fusion or exosome release *in vivo*, we verified that injection of Nexinhib20, to an effective concentration of 16-18µM, produced no changes in limb bud cell morphology or death, compared to DMSO-injected controls, after 16 hours of incubation (Figure 2.14). This suggests that the observed effects on Shh protein distribution are caused by Nexinhib20-mediated inhibition of MVB fusion and exosome secretion, and that secretion of Shh-containing exosomes is also required for normal spatial distributions of Shh in intact limb buds.

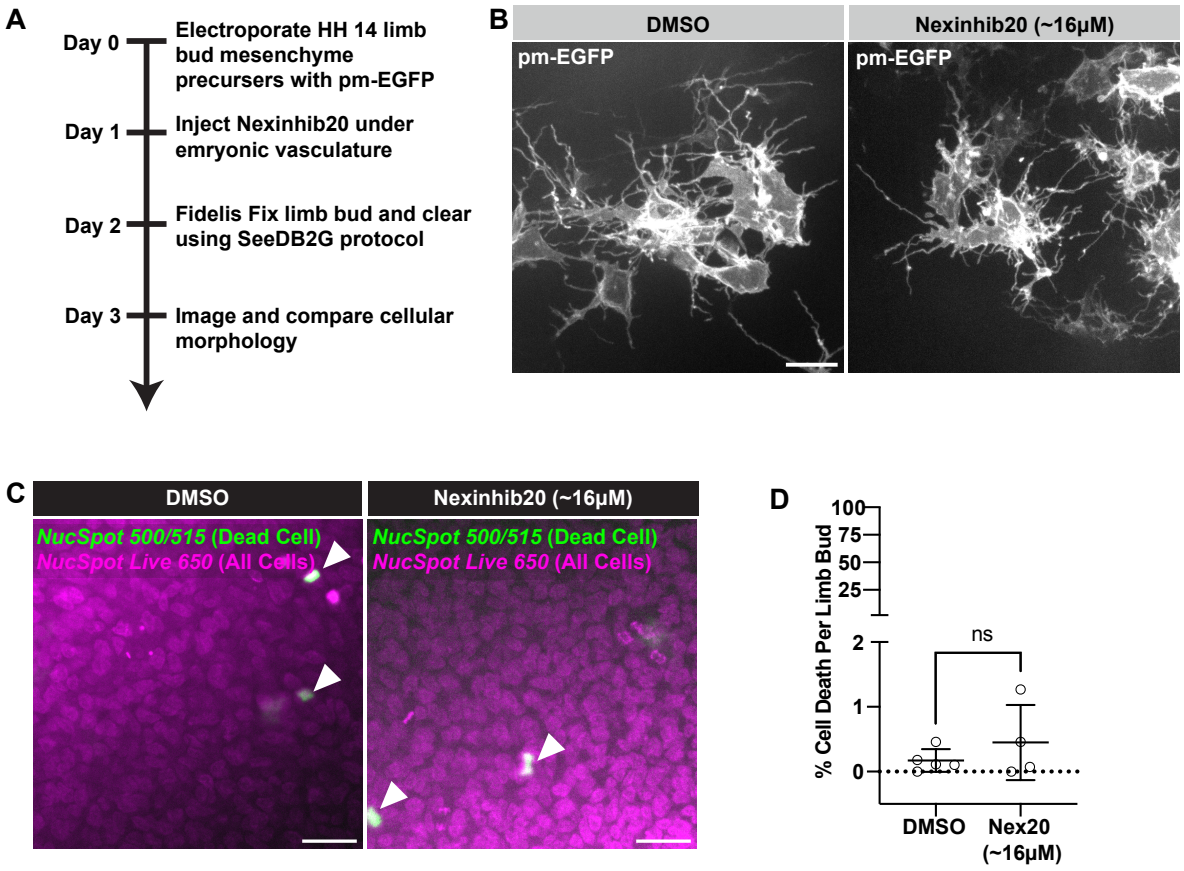


Figure 2.14: Embryonic injection of Nexinhib20 in vivo does not affect cell morphology or cell death in the limb bud mesenchyme. (A) Overview of the cell morphology assay. (B) Representative micrographs of limb bud mesenchymal cells electroporated with pm-EGFP and treated with either DMSO or Nexinhib20 ($\sim$16 μM) in vivo. (C) Limb bud mesenchyme incubated with membrane permeable NucSpot650Live and membrane impermeable NucSpot500/515 after treatment with either DMSO or Nexinhib20. White arrowheads point to dying/dead cells with compromised membrane integrity detected by NucSpot 500/515 staining. (D) Quantification of cell death as measured by the fraction of NucSpot500/515-positive cells/NucSpot650live-positive cells in the limb bud mesenchyme after treatment with DMSO or Nexinhib20 (n = 5 forelimbs treated with DMSO, 4 forelimbs treated with Nexinhib20, in each limb bud 3 zones were imaged and averaged). Scale Bars in (B) = 50 μm, (C) = 10 μm. Significance testing was performed using a two-tailed Mann-Whitney U-test.

2.3 Discussion

Here, we identify a fundamental role for exosome secretion in Shh dispersal and signaling gradient formation in the chick limb bud.

Endocytic recycling and secondary secretion on extracellular vesicles has emerged as a widely-used strategy for morphogen dispersal, although intracellular trafficking routes, and modes of extracellular transport, vary across different organisms and tissue types (Gradilla et al., 2018; Gradilla and Guerrero, 2022; Matusek et al., 2020). In Drosophila wing discs, where morphogen secretion and transport have been most intensively studied *in vivo*, recycled Hh is sorted into two distinct pathways. One pool is routed to the apical surface and packaged into microvilli-derived ectosomes for extracellular diffusion (D'Angelo et al., 2015; Hurbain et al., 2022), and a second pool is packaged into MVBs, routed to the basolateral surface and secreted on CD63-positive exosomes that travel along basal cytonemes (Gradilla et al., 2014). In mouse embryos, Shh produced by notochord and floorplate cells is also routed towards basolateral domains and transported along cytonemes towards target cells in the neural tube, although the nature of the vesicle carrier is less clear (Hall et al., 2024). Our data suggest that limb bud mesenchymal cells use a pathway for endocytic recycling and secondary secretion of Shh that resembles the basolateral pathways used in wing discs and mouse neural tubes. PLMCs lack apicobasal polarity but still use this pathway to produce a pool of exosomes that can either diffuse through extracellular space or travel along cytonemes.

How is secondary secretion of Shh coordinated with cytoneme-based transport? One possibility, supported by studies in immortalized cell culture lines overexpressing Shh (Hall et al., 2021), is that MVBs or other endosomal compartments containing recycled Hh are transported inside of cytonemes and fuse with the membrane along cytoneme shafts or at their tips (Daly et al., 2022; Gradilla et al., 2018). An alternative possibility is that exosomes released near the cell body associate with and travel along the outside surfaces of cytonemes. Our data strongly support this latter possibility: First, MVB release events

occur on the cell body or near the bases of cytonemes, but not along their lengths or at their tips. Second, antibody staining of non-permeabilized PLMCs reveals that ~70 % of Shh along cytonemes is exposed to extracellular space (Figure 2.8B-D), consistent with the conclusions of a previous *in vivo* analysis using different methods (Sanders et al., 2013). Finally, much of the externally transported Shh is bound to CD63-positive exosomes both in PLMCs and *in vivo* (Figure 2.8F-G, Figure 2.12E). Previous studies in Drosophila wing discs reached the similar conclusion that Hh can travel on CD63-positive EVs along the outer surfaces of basolateral cytonemes (Gradilla et al., 2014), suggesting that wing disc epithelial cells and limb bud mesenchymal cells may use very similar mechanisms to package recycled Hh onto exosomes for external transport along cytonemes. Whether cells use specific mechanisms to target MVB fusion and exosome release to the bases of cytonemes, or simply rely on secondary capture of secreted exosomes, remains unclear in either system.

It is likely that other mechanistic features are shared across these different contexts. For example, in both wing discs and mouse neural tubes, the transmembrane protein Dispatched is required for the endocytosis of secreted Hh and its delivery to cytonemes (D'Angelo et al., 2015; Gradilla et al., 2014; Hall et al., 2021). Thus, Dispatched may play similar roles in mediating the endocytic recycling and re-secretion of Shh in chick limb buds. A growing body of work suggests that vertebrate cells use Myosin-10 as a molecular motor both to control cytoneme growth and for anterograde transport of Hh, and other morphogens, along cytonemes (Daly et al., 2022; Hall et al., 2021, 2024). Notably, Shh puncta are transported along cytonemes in the chick limb bud mesenchyme within the range of velocities measured for Myosin-10 (Sanders et al., 2013; Shangguan and Rock, 2024). Also, the tail of Myosin-10 contains a MyTH4-FERM domain that can bind to and transport surface receptors and integrins that may interact with numerous glypicans, receptors, and integrins present on exosomal membranes (Liu et al., 2012; Zhang et al., 2004; Buzás et al., 2018). Thus, it seems likely that limb bud mesenchymal cells use Myosin-10 to transport Shh-containing

exosomes along the outer surfaces of cytonemes. More generally, palmitoylated Wnt/Wg morphogens also undergo endocytosis, re-packaging, and secretion on MVB-derived exosomes (Beckett et al., 2013; Gross et al., 2012; Yamazaki et al., 2016), and undergo Myosin-10-dependent transport along cytonemes (Hu et al., 2021; Huang and Kornberg, 2015; Mattes et al., 2018; Rogers et al., 2023), suggesting that exosome-based transport may represent broadly a conserved strategy for dispersal of lipid-modified morphogens.

The use of EVs as morphogen carriers likely conveys additional biological advantages beyond providing a natural way to shield hydrophobic lipid modifications. Combining primary secretion with endocytosis, sorting, and secondary secretion could confer an additional layer of signaling regulation by concentrating morphogens with other key signaling machinery such as co-receptors, chaperones/transporters, regulatory cargo such as luminal RNAs/proteins, and membrane tethered ECM molecules into a single, condensed signaling package. For example, Hh-bound exosomes are also enriched in Dispatched, the co-receptor Ihog, the glypican Dally-like protein, and various miRNAs (Gradilla et al., 2014; Vyas et al., 2014). Similarly, packaging morphogens and other factors into secreted EVs, whose membranes are topologically equivalent to the plasma membrane, may facilitate the more flexible use of different modes of dispersal such as extracellular diffusion, interaction with other secreted transporters and ECM, and directed transport along cytonemes, as seen in this work and in Gradilla et al., to modify the effective range, duration, or direction of signaling (Gradilla et al., 2014). Thus, secreted exosomes may provide a highly versatile biological strategy for integrating diverse modes of dispersal with modulation of signal presentation and reception to tune morphogen gradients across a wide range of tissues.

Recent work suggests that PI3K signaling gradients control distinct modes of Shh transport in proximal and distal compartments to pattern Shh signaling in mouse limb buds (Wang et al., 2022). In particular, it was proposed that free diffusion of small exosome-like particles in the distal compartment promote long-range transport, while local trapping of

larger Shh-containing structures (referred to as punctata) on cytonemes limits Shh transport within proximal compartments. Our data suggest that, in the chick limb bud, Shh-containing exosomes released by ZPA cells can either diffuse freely through extracellular space or bind to and travel along cytonemes. The apparent restriction of exosome release to cell bodies (Figure 2.7C), the large fraction of Shh on cytonemes that is exosome-associated (Figure 2.8F-G), the tip enrichment of Shh-containing exosomes on PLMCs *in vitro* (Figure 2.9F and 2.9K), and its dependence on MVB fusion and exosome release (Figure 2.9G-K) suggest that Shh-containing exosomes are efficiently loaded onto the surface of cytonemes and transported towards cytoneme tips *in vitro*. Our *in vivo* observations suggest that Shh is similarly packaged into exosomes and transported towards the tips of much longer cytonemes made by ZPA cells in intact limb buds. The Shh-containing and CD63-positive puncta observed on cytonemes in intact chick limb buds by light microscopy *in vivo* (Figure 2.12D-E)(Sanders et al., 2013) and the vesicles we observed on cytonemes by SEM *in vivo* (Figure 2.12F-G), are comparable in size to exosomes, rather than the much larger Shh "punctata" associated with cytonemes in mouse limb buds (Wang et al., 2022). Thus, we currently favor a model in which a mixture of local diffusion and cytonemal transport of exosome carriers, within the same compartments, pattern Shh signaling in the chick limb bud: with diffusion of exosomes through extracellular space mediating short-range, high-intensity Shh signaling, and with cytonemal transport of exosomes promoting longer-range or sustained signaling during patterning. Ultimately, these models must be tested by selective inhibition of these different modes of transport *in vivo*.

LIMITATIONS OF THE STUDY

Our study relies largely on primary limb mesenchyme cell cultures as a tractable and developmentally relevant model system. PLMCs cannot be passaged and naturally begin to differentiate within days of culture precluding the use of clonally derived cell lines for uniform expression of transgenes or CRISPR mediated endogenous protein tagging. Thus, we

relied on overexpression of fluorescently tagged proteins for the majority of our experiments. Additionally, the low and variable penetrance of genetic manipulations in chick embryos, while suitable for live imaging, precludes robust tissue scale manipulations, limiting our ability to test functional relevance of exosome diffusion and cytoneme transport *in vivo*.

RESOURCE AVAILABILITY

Lead contact

Further information and requests for resources and reagents should be directed to the lead contact, Ed Munro (emunro@uchicago.edu).

Materials availability

Many of the plasmids generated in this study have been deposited at Addgene and can be made available upon request.

Data and code availability

- All data reported in this paper will be shared be the lead contact upon request.
- All original code (ImageJ/FIJI macro script) has been deposited at Zenodo and are publicly available at https://doi.org/10.5281/zenodo.22804959.
- Any additional information required to reanalyze the data reported in this paper is available from the lead contact upon request.

ACKNOWLEDGEMENTS

We would like to thank Pulin Li, Alissa Weaver, Benjamin Glick, and Miriam Domowicz for genetic constructs, cell lines, and general reagents. We would like to thank Bruno Correia and Sailan Shui for DNA constructs and general advice about using CDH protein switches. We would like to thank Christine Labno (Director of the Integrated Light Microscopy Core) and Fernando Valbuena (Laboratory of Benjamin Glick) for creating a core section of an ImageJ macro script that was utilized for analysis. Light microscopy was performed in the Integrated Light Microscopy Core at University of Chicago, which receives financial

support from the Cancer Center Support Grant (2P30CA014599) and RRID: SCR_019197. Additionally, this work made use of instruments in the Electron Microscopy Core of UIC's Research Resources Center. This work was funded by NIH R01 GM 143576 and NIH T32 HD055164 training grant.

DECLARATION OF INTERESTS

The authors declare no competing interests.

DECLARATION OF GENERATIVE AI AND AI-ASSISTED TECHNOLOGIES

The authors declare no use of generative AI and AI-assisted technologies.

2.4 Materials and Methods

Table 2.1: Key Resource Table

REAGENT or RESOURCE	SOURCE	IDENTIFIER
Antibodies		
Mouse monoclonal anti-Shh (concentrate)	Developmental Studies Hybridoma Bank	RRID:AB_528466
Rabbit polyclonal anti-Rab27a	Thermo Fisher Scientific	Cat#PA5-110257; RRID:AB_2855668
FluoTag-X2 anti-mouse IgG1 Abberior Star 580	NanoTag Biotechnologies	Cat#N2002 (Specific conjugation no longer sold)
FluoTag-X4 anti-rabbit IgG Abberior Star 580	NanoTag Biotechnologies	Cat#N2404 (Specific conjugation no longer sold)
Bacterial and virus strains		

(Table 2.1 continued)

REAGENT or RESOURCE	SOURCE	IDENTIFIER
Invitrogen™ One Shot™ ccdB Survival™ 2 T1R Competent Cells	Invitrogen	Cat#A10460
Mix & Go!™ Competent Cells - Strain Zymo 5α	Zymo Research	Cat#76020-668
Chemicals, peptides, and recombinant proteins		
IDTE pH 7.5 (1X TE Solution)	IDT	Cat#11-05-01-15
Q5® High-Fidelity DNA Polymerase	NEB	Cat#M0491S
SapphireAmp® Fast PCR Master Mix	Takara	Cat#RR350A
UltraPure Agarose	Invitrogen	Cat#16-500-100
DMEM/F12 with GlutaMAXTM supplement	Gibco	Cat#10565018
DMEM, high glucose, GlutaMAX™ Supplement	Gibco	Cat#10566016
Opti-MEM™ I Reduced Serum Medium	Gibco	Cat#31985070
FoundationTM Fetal Bovine Serum	Gemini Bio	Cat#900-108-500
Penicillin-Streptomycin (10,000 U/mL)	Gibco	Cat#15140122
Chicken Serum	Gibco	Cat#16110082
HEPES (1M)	Gibco	Cat#15630080

(Table 2.1 continued)

REAGENT or RESOURCE	SOURCE	IDENTIFIER
DPBS, no calcium, no magnesium	Gibco	Cat#14190144
TRI-Reagent	Zymo Research	Cat#R2050-1-50
Hanks' Balanced Salt Solution	Sigma Aldrich	Cat#H6648-1L
PHEM Buffer, 0.2M	Electron Microscopy Sciences	Cat#11164
Paraformaldehyde 16% Aqueous Solution, EM grade	Electron Microscopy Sciences	Cat#157-8-100
Aqueous Glutaraldehyde EM solution 25%	Electron Microscopy Sciences	Cat#16220
Dimethyl Sulfoxide Hybri-MaxTM	Sigma Aldrich	Cat#D26650-100ml
SuperBlock Blocking Buffer	Thermo Fisher Scientific	Cat#37580
Nexinhib20	MedChemExpress	Cat#HY-125792
Latrunculin A	Cayman Chemical	Cat#10010630
Doxycycline	MP Biomedicals	Cat#198955
A1155463	MedChemExpress	Cat#HY-19725
Omnipaque (iohexol) injection 350	GE Healthcare	Cat#00407141493
Dispase in DMEM-F12	STEMCELL Technologies	Cat#07923
Saponin Practical Grade	MP Biomedicals	Cat#02102855-CF
Triton-X100	Sigma Aldrich	Cat#X100-5ml
NucSpot Live 650	Biotium	Cat#40082-T

(Table 2.1 continued)

REAGENT or RESOURCE	SOURCE	IDENTIFIER
NucSpot 500/515	Biotium	Cat#41040-T
Critical commercial assays		
DNA Clean & Concentrator-5	Zymo Research	Cat#D4003
ZymocleanTM Gel DNA Recovery Kit	Zymo Research	Cat#D4002
Zyppy Plasmid Miniprep Kit	Zymo Research	Cat#D4020
ZymoPURE II Plasmid Midiprep Kit	Zymo Research	Cat#D4201
Anza™ 10-Pack Starter Kit	Invitrogen	Cat#IVGN3006
Direct-zol RNA Microprep Kit	Zymo Research	Cat#R2060
ZymoScript RT PreMix Kit	Zymo Research	Cat#R3012
DreamFect Gold	OZ Biosciences	Cat#DG80500
Applied Biosystems™ SYBR™ Green Universal Master Mix	Applied Biosystems	Cat#4309155
Experimental models: Cell lines		
Human: HEK-293FT	Gift from Miriam Domowicz	N/A
Chicken: Primary Embryonic Fibroblasts	This paper	N/A
Chicken: Primary Limb Bud Mesenchymal Cells	This paper	N/A
Mouse: NIH-3T3	Gift from Miriam Domowicz	N/A

(Table 2.1 continued)

REAGENT or RESOURCE	SOURCE	IDENTIFIER
Mouse: NIH-3T3 8X-GBS-miniCMV-H2B-mCitrine	Schlissel et al.	N/A
Experimental models: Organisms/strains		
Fertilized Chicken (White Leghorn) eggs	University of Illinois	N/A
Oligonucleotides		
Mouse GAPDH RT-qPCR Forward Primer: CGTCCCGTAGACAAAATGGT	This paper	N/A
Mouse GAPDH RT-qPCR Reverse Primer: GAGGTCAATGAAGGGGTCG	This paper	N/A
Mouse Ptch1 RT-qPCR Forward Primer: TGTTCCAGTTAATGACTCCC	This paper	N/A
Mouse Ptch1 RT-qPCR Reverse Primer ACACTCTGATGAACCACCTC	This paper	N/A
Recombinant DNA		
CDV-hyPBase	Yusa et al.; Sanders et al.	N/A
APX1	Dady et al.	N/A
APX1-pm-EGFP	Dady et al.	Addgene ID: 245520
APX1-pm-mKate2	Dady et al.	Addgene ID: 245521

(Table 2.1 continued)

REAGENT or RESOURCE	SOURCE	IDENTIFIER
pLS434-sec-Bclxl-KDEL	A gift from Bruno Correia	N/A
pLS428-sec-LD3-nluc	A gift from Bruno Correia	N/A
pEF-GalNAcT2-HaloTag(C262V)	A gift from Benjamin Glick	N/A
pEntr/D-TOPO pHluo_M153R-CD63	Sung et al. (A gift from Alissa Weaver)	N/A
BITREX-pm-mKate2	Gift from Maria Barna	N/A
APX2	This paper	N/A
BITREX-pm-mIRFP682	This paper	Addgene ID: 257788
APX3	This paper	Addgene ID: 257787
APX4	This paper	Addgene ID: 257789
APX1-UCHD-mIRFP682	This paper	Addgene ID: 257790
APX1-pm-mScarlet	This paper	Addgene ID: 257807
APX1-Myosin10(HMM)-msfGFP	This paper	Addgene ID: 257791
BITREX-Shh-FL-msfGFP-pm-mKate2	This paper	Addgene ID: 257792
APX1-TetOn-3g	This paper	Addgene ID: 257793
APX3-BclxL-KDEL	This paper	Addgene ID: 257794
APX2-Shh-LD3(D138a)-msfGFP	This paper	Addgene ID: 257795
BITREX-Shh-LD3(D138A)-msfGFP-pm-mKate2	This paper	Addgene ID: 257796

(Table 2.1 continued)

REAGENT or RESOURCE	SOURCE	IDENTIFIER
BITREX-Shh-LD3(D138A)-msfGFP-pm-mIRFP682	This paper	Addgene ID: 257797
APX1-Shh-LD3(D138A)-msfGFP	This paper	Addgene ID: 257799
APX1-Shh-FL-msfGFP	This paper	Addgene ID: 257800
APX4- Rab5a(S34N)-mKate2	This paper	Addgene ID: 257803
APX2-CD63-pHluo(M153R)	This paper	N/A
BITREX-CD63-pHluo(M153R)-pm-mIRFP682	This paper	N/A
APX2-Shh-HaloTag	This paper	N/A
APX4-Shh	This paper	Addgene ID: 257806
APX3-Str-KDEL	This paper	Addgene ID: 257804
APX1-Shh-SBP-msfGFP2	This paper	Addgene ID: 257805
Software and algorithms		
Fiji: an open-source platform for biological-image analysis	Shindelin et al.	`https://imagej.net/software/fiji/downloads`
StarDist	Schmidt et al.	`https://github.com/stardist/stardist-imagej`
Analyzer of MVB Exocytosis (AMvBE)	Bebelman et al.	
ComDet v.05.5 plugin for ImageJ		`https://github.com/UU-cellbiology/ComDet`

(Table 2.1 continued)

REAGENT or RESOURCE	SOURCE	IDENTIFIER
Radial Angle Profile	Paul Baggethun	https://imagej.net/ij/plugins/radial-profile.html
Prism v11.01(99)	Graph Pad	https://www.graphpad.com/
Python v3.12.4	Python Software Foundation	https://www.python.org
Imaris v9.1.2	Oxford Instruments	https://imaris.oxinst.com/versions/9
Corcoran_et_al_2026_Cell Reports (Custom Written ImageJ Macros) v1.0.1	This paper (deposited on Zenodo)	https://doi.org/10.5281/zenodo.22804959
Other		
Super Electroporator NEPA21 Type II	NepaGene	
Electroporation Cuvettes 2mm gap	Bulldog Bio	Cat#12358-346
1mm platinum disk electrode on tip of stick	Bulldog Bio	Cat#CUY700P1L
Platinum chopstick electrodes, 7mm bend, 2mm tip length	Bulldog Bio	Cat#CUY611P7-2
4 inch thin wall glass capillaries with filament	World Precision Instruments	Cat#TW100F-4
35 mm Glass bottom dishes	Cellvis	Cat#D35-10-1.5-N

(Table 2.1 continued)

REAGENT or RESOURCE	SOURCE	IDENTIFIER
m-Plate 24 well ibiTreat	Ibidi	82426
18-well chambered cover Glass with #1.5 high performance cover glass	Cellvis	C18SB-1.5H
Pneumatic PicoPump	World Precision Instruments	PV820

EXPERIMENTAL MODEL AND STUDY PARTICIPANT DETAILS

Chicken Embryos

We purchased fertilized White Leghorn chicken eggs (*G. gallus*) from the University of Illinois, Urbana-Champaign and stored them at 15°C until incubation. We incubated eggs in a non-rotary incubator at 37.5°C with approximately 45-55%-humidity until they reached the desired stage according to Hamburger and Hamilton (HH)(Hamburger and Hamilton, 1951). Sex of chicken embryos cannot be morphologically determined until after embryonic day 6.5 (> HH29)(Luo et al., 2023) which is beyond the stages utilized for experiments in this study. So, we assume an equal percentage of male and female chicken embryos used in all experiments. All Animal Experiments were performed before late gestation in accordance with the guidelines of The University of Chicago IACUC.

Generation of Primary Limb bud Mesenchymal Cells (PLMCs)

To generate PLMCs for each experiment, we modified a micromass culture approach (Barna and Niswander, 2007; Bobick et al., 2014; Solursh et al., 1981). First, we incubated white

leghorn chicken (*G. gallus*) eggs until they reached HH 22 (∼E3.5). We transferred embryos to room temperature Hanks' Balanced Salt Solution (Sigma) supplemented with penicillin/streptomycin (Gibco) and dissected out a minimum of 20 limb buds from at least 5 embryos using ethanol sterilized forceps and Vannas scissors. We transferred all the limb buds to a microcentrifuge tube containing 1mL of Tryp-LE (Gibco) and incubated the tube for 20 minutes at 37°C. We then replaced Tryp-LE with DMEM-F12 (Gibco) supplemented with penicillin/streptomycin, 10% FBS (Gemini Bio), GlutaMAX (Gibco), and 25 mM HEPES (Gibco). We used repeated passage through a 21G needle to fully dissociate limb buds into single cells. We then passed the dissociated cells through a 40 μm cell strainer, spun the cells down for 3 minutes at $200 \times g$, resuspended in fresh DMEM-F12 and then seeded roughly 1×10^5 PLMCs into each well of a glass-bottom 18-well chamber slide (CellVis). We incubated these cells at 37°C with 5% CO_2. For some experiments, we introduced plasmids by electroporation before seeding (see *In vitro* Electroporation). Cell passaging is not possible as PLMCs can undergo chondrogenesis starting within three days of culture (Barna and Niswander, 2007), so every experiment using PLMCs requires this generation protocol to be done anew. As sex determination of embryos at the stage of harvesting was not possible, we cannot determine the sex of PLMCs used so we assume an equal percentage of male and female. Thus, biological sex remains a potential variable.

Generation of Chicken Embryonic Fibroblast (CEF):

We prepared cultures of Chick Embryo Fibroblasts (CEFs) from White Leghorn chickens (G. gallus) similar to previous reports (Fekete and Cepko, 1993). Briefly, we used sterile forceps to extract at embryonic day 10 (HH 36), removed the head, limbs and viscera, and used a razor blade to mince 4 - 6 embryos in a glass petri dish, before adding 10 mL of Tryp-LE (Gibco). We used a wide-mouthed pipet to transfer the minced embryos in Tryp-LE to a sterile 250 ml flask, stirred gently for 15 minutes, allowed them to settle for 5 minutes, and

then transferred the supernatant to a 50 mL conical tube. After vigorously pipetting the supernatant to dissociate any remaining tissue, we added an equal volume of 100% FBS and mixed by inversion to inactivate Tryp-LE. We allowed the solution to settle for 5 minutes and transferred the supernatant to a fresh 50 mL conical tube, centrifuged for 5 minutes at $200 \times g$, removed the supernatant, and then resuspended in 10 mL of 100% FBS (Gemini Bio). After a second round of centrifugation (5 minutes at $200 \times g$) and removal of supernatant, we resuspended the pelleted cells in 5 mL of CEF media (DMEM high glucose, GlutaMAX (Gibco) supplemented with 10% FBS (Gemini Bio), 2% heat inactivated chicken serum (Gibco), and penicillin/streptomycin (Gibco). We then plated cells at various concentrations (between 10^5 and 10^6 cells) in 10 mL CEF media on 10 cm plates and incubated them at 37°C with 5% CO2. We passaged cells every 2-3 days and selected the healthiest cultures for further use and subsequent freezing. Upon thawing, CEFs were maintained in culture and used for experiments up to passage 10. Sex of embryos that CEFs were derived from were not determined, so biological sex remains a potential variable.

Immortalized Cell Lines

Wild type immortalized human embryonic kidney cells (HEK-293FT) were gifted from Miriam Domowicz and were routinely cultured in DMEM high-glucose supplemented with GlutaMAX (Gibco), 10% FBS (Gemini Bio), and penicillin/streptomycin (Gibco) at 37°C with 5% CO_2 according to standard procedures. Cells were maintained in culture and used for experiments up to passage 10. Cells were not independently authenticated upon being received, so biological sex of cells was not determined and remains a potential variable.

Two immortalized mouse fibroblasts (NIH-3T3) cell lines were utilized. Wild type murine NIH-3T3 cells were gifted from Miriam Domowicz. Pulin Li gifted us a NIH-3T3 cell line that was stably edited to express the fluorescent transcriptional reporter (8X-GBS-miniCMV-H2B-mCitrine). The details regarding its creation can be found in (Schlissel et al., 2024)

Both NIH-3T3 cell lines were routinely cultured in DMEM high-glucose supplemented with GlutaMAX (Gibco), 10% FBS (Gemini Bio), and penicillin/streptomycin (Gibco) at 37°C with 5% CO_2 according to standard procedures. Cells were maintained in culture and used for experiments up to passage 10. Both NIH-3T3 cell lines were not independently authenticated upon being received, so biological sex of cells was not determined and remains a potential variable.

METHOD DETAILS

Plasmids

We used the piggyBac transposition system to genetically integrate DNA constructs for extended expression in cell culture and during chicken embryogenesis. We co-expressed the hyperactive piggyBac transposase using the CDV-hyPBase plasmid in all transfection and electroporation-based experiments to stably integrate expression vectors (Yusa et al., 2011).

General cloning strategy

All subcellular localized fluorescent protein fusion and release system DNA constructs were created either through overlap extension PCR or direct gene block synthesis (IDT/Twist Bioscience) and were subcloned into the Gateway Entry/Donor Vectors pENTR/DTOPO or pDONR221 (Invitrogen) using standard methods. Gateway Entry Clones were then subsequently recombined into one of the Gateway Destination Vectors listed below to produce unique expression vectors for transfection or electroporation.

Destination Vectors used and created for Gateway Cloning

All destination vectors used and created were engineered to harbor improved PiggyBac ITRs. For stable, constitutive expression of various constructs, we used the APX1 backbone (Dady et al., 2025). This allowed for convenient Gateway mediated generation of numerous piggyBac compatible expression vectors with a strong, constitutively active cytomegalovirus (CMV) enhancer/chicken β-actin (CAG) promoter. To create a destination vector for doxy-

cycline inducible expression, we replaced the CAG promoter of APX1 with the TRE3G promoter (Clontech/Takara) through restriction cloning to generate the APX2 vector. For bidirectional doxycycline inducible expression, we used the BITREX-pm-mKate2 vector (a gift from Maria Barna) which uses a bidirectional TRE3G promoter (Clontech/Takara) to drive dual expression of palmitoylated (pm) mKate2 (the first 20-amino acid palmitoylation sequence of rat GAP-43 MLCCMRRTKQVEKNDEDQKI fused to the N terminus of mKate2) and an RfA Gateway cassette (Invitrogen) for Gateway LR Clonase II mediated recombination. We additionally modified BITREX-pm-mKate2, by replacing the pm-mKate2 with a similarly palmitoylated mIRFP682 (Matlashov et al., 2020) through restriction cloning to generate BITREX-pm-mIRFP682 (Deposited in Addgene, Plasmid #257788).

For dual expression of TetOn-3G and a gene of interest, we created two novel destination vectors. We first created the APX3 destination vector by inserting and a construct encoding an IRES2 element and TetOn-3G (Clontech/Takara) immediately downstream of the RfA Gateway Recombination cassette of the APX1 backbone using restriction cloning (Deposited in Addgene, Plasmid #257787). Second, we created a bidirectional backbone, APX4 (Deposited in Addgene, Plasmid #257789), by inserting a construct encoding a SV40 polyA signal, TetON-3G (Clontech/Takara), and the Ubiquitin C (UBC) promoter into the multiple cloning site (MCS) upstream the CAG promoter of APX1 backbone by restriction cloning.

Subcellular and Organelle Markers

To visualize cellular and cytonemal plasma membrane, we used various palmitoylated fluorescent protein constructs. We used overlap extension PCR to fuse the first 20 amino acid palmitoylation sequence of rat GAP-43 (MLCCMRRTKQVEKNDEDQKI) to the N-terminus of either EGFP, mKate2, mScarlet, or mIRFP682. To visualize F-actin, we used overlap extension PCR to fuse mIRFP682 to the N-terminus of first 261 amino acids of human Utrophin (gift from Dyche Mullins) to create Utrophin Calponin Homology Do-

main (UCHD)-mIRFP682. To visualize myosin10, we used overlap extension PCR to fuse msfGFP to the N-terminus of *Bos taurus* Myosin10-heavy meromyosin (HMM) (gift from Richard Cheney).(Bohil et al., 2006) For expression of the Rab5a(S34N) dominant negative mutant, we replaced the mCherry sequence from the mCherry-Rab5DN(S34N) plasmid (Addgene ID: #35139) with mKate2 and directly synthesized a pTwistENTR Kozak (Twist Bioscience) with the mKate2-human Rab5a(S34N) insert. Corresponding expression vectors are deposited to Addgene.

To visualize CD63 in live and fixed settings, we used the pEntr/D-TOPO pHluo_M153R-CD63 plasmid (Gift from Alissa Weaver) that inserts superecliptic pHluorin(M153R) into the first extracellular loop of human CD63 (Sung et al., 2020). To visualize the Golgi apparatus, we directly used pEF-GalNAcT2-HaloTag(C262V) (Gift from Benjamin Glick) for constitutive expression of human GalNAcT2 with a C-terminal HaloTag (C262V).

Sonic Hedgehog Fusion Proteins

To generate full length, dual lipidated Shh Fluorescent Protein fusion constructs (Shh-FL-XFP), we inserted a DNA cassette comprised of a GGGS (2×) flexible linker, either msfGFP or mScarlet, and an additional Serine between Serine196 and Glycine 197 of murine Shh. This internal insertion maintains the critical autoprocessing amino acid motif (SGGCF) after the insertion that is required for autocatalytic cleavage and the resulting cholesterol modification (Chamberlain et al., 2008; Sanders et al., 2013; Vincent et al., 2003).

Additionally, we synthesized a pTwistENTR Kozak (Twist Bioscience) vector containing a codon-optimized Shh-HaloTag insert. The Shh-HaloTag insert was previously designed by inserting a gly-HiBit-gly-ser-Halo-gly-ser-HA-gly cassette in the murine Shh coding sequence after E130 (non-codon optimized sequence was a kind gift from Pulin Li)(Petrov et al., 2020; Schlissel et al., 2024).

Genetic Constructs of Chemically Disruptable Heterodimer (CDH) Synchronous Release System

To create the endoplasmic reticulum (ER) localized Bcl-xL trap portion of the CDH synchronous release system, we first cloned the sequence encoding a truncated human Bcl-xL (amino acids 45-84 corresponding to an unstructured flexible loop region and amino acids after R209 corresponding to the mitochondrial transmembrane region were deleted) from pLS434-sec-Bclxl-KDEL (a kind gift from Bruno Correia). Then we used overlap extension PCR, to insert the first 38 amino acids (including the signal peptide) from the human STIM1L gene at the 5' end of the truncated Bcl-xL sequence and the nucleotides encoding a KDEL amino acid sequence at the 3' end of Bcl-xL.

To create Shh-CB-msfGFP, we inserted a DNA cassette containing a GGGS (2×) flexible linker, the LD3 sequence (gift from Bruno Correia) with a D138A point mutation, msfGFP, and an additional Serine between Serine 196 and Glycine 197 of murine Shh CDS following the same logic as our Shh-FL-msfGFP and Shh-FL-mScarlet constructs.

Corresponding expression vectors are deposited to Addgene.

Genetic Constructs of Retention Using Selective Hooks (RUSH) System

To create the luminal endoplasmic reticulum (ER) localized streptavidin trap portion of the RUSH system, we synthesized a gene block using the Str-KDEL sequence from Str-KDEL_TNF-SBP-mCherry plasmid (Addgene # 65279) and flanked the sequence with attB sites for subsequent recombination into Gateway vectors.

To create Shh-SBP-msfGFP, we inserted a DNA cassette containing a GGGS (x2) flexible linker, Streptavidin-Binding-Protein (SBP), msfGFP2, and an additional Serine between Serine196 and Glycine 197 of murine Shh CDS following the same logic as our Shh-FL-msfGFP and Shh-FL-mScarlet constructs.

Corresponding expression vectors are deposited to Addgene.

Confocal Microscopy

We acquired super-resolution confocal images using two microscopy systems. (1) Images were captured with a 3i Marianas Super-resolution through Optical Reassignment (SoRa) Yokogawa-type spinning disk confocal microscope (Intelligent Imaging Innovations, Denver, CO) with dual Prime 95B Illuminated Scientific CMOS (Teledyne Photometrics Vision Solutions, Tucson, AZ) run by Slidebook software (Intelligent Imaging Innovations, Denver, CO). For SoRa acquisitions, we used 100×/1.3 NA, Plan NeoFluar oil, 63×/1.4NA Plan Apochromat oil, 40×/1.3NA Plan NeoFluar oil, and 20×/ 0.5 NA Plan NeoFluar Ph2 dry objective lenses (Zeiss). (2) images were captured with a Zeiss LSM 980 Laser-scanning confocal equipped with Airyscan 2. For LSM 980 acquisitions, we used a 63× /1.4NA Plan Apochromat oil lens (Zeiss) and acquired images in Airyscan 2 SR mode.

We acquired non-super-resolution confocal images using two microscopy systems. (1) Images were captured with a Nikon Ti-E inverted microscope equipped with a Yokogawa CSU-X1 spinning disk scan head, and a Ti-ND6-PFS Perfect Focus Unit. A laser merge module (Spectral Applied Research) controlled tunable delivery of 481-nm and 561-nm laser excitation from 50 mW solid-state lasers (Coherent Technology) All image acquisition was controlled by VisiView software. We collected images using a 60X Nikon Plan Apo 1.2NA water immersion objective onto an Andor iXon3 897 EMCCD camera. (2) Images were captured with a Zeiss LSM 880 inverted microscope. All image acquisition was controlled by Zen Black software. We collected images using a 10×/0.3NA EC Plan-Neofluar M27 objective (Zeiss).

Total Internal Reflection Fluorescence (TIRF) Microscopy

We performed TIRF microscopy on a Nikon Ti2-E inverted microscope equipped with a LunF XL laser combiner housing solid state 488nm, 561nm and 640nm lasers and feeding three separate TIRF illumination arms, a Ti2 N-ND-P Perfect Focus unit, and a CFI APO

100X 1.49NA TIRF (Nikon) objective. We acquired images on an Andor IXON Life 897 EM-CCD camera to achieve a pixel size of ∼160 nm. Image acquisition was controlled by Nikon Elements software.

Scanning Electron Microscopy (SEM) of Chicken Limb Buds

We dissected limb buds from HH 22-24 chicken embryos, incubated the limb buds in Dispase/DMEM-F12 solution for 60 minutes at 37 °C, and used forceps to gently remove the outer sheath of ectoderm. We then immediately fixed the ectoderm-peeled limb buds using the cytoneme-preserving Fidelis Fix protocol (See Below). To ensure tissue rigidity for EM processing, we then double fixed the limb bud mesenchyme in 2% paraformaldehyde and 2.5% glutaraldehyde in PHEM buffer for 1 hour on ice. We then dehydrated the tissue in a series of ethanol solutions and transferred the tissue to the University of Illinois, Chicago EM staff. They fully dehydrated the limb buds using HMDS, mounted the limb buds onto an SEM pin with conductive tape, and sputter coated the tissue with 10 nm of platinum. We then imaged the limb bud mesenchyme at 5.0 kV using the Secondary Electron Detector on a JEOLJSM-IT500HR SEM.

Image Analysis and Visualization

We used ImageJ/FIJI software to process all image data for analysis and display. We used standard maximum intensity projections to produce single projected views from confocal Z-stacks, cropped the images to highlight features or regions of interest. For multichannel imaging, brightness and contrast was often adjusted before saving final images in RGB format. Background subtraction was used sparingly for image analysis of immunofluorescence staining of PLMCs and specifically mentioned in figure legends when used.

In vitro Electroporation

For *in vitro* electroporation, we suspended 1×10^6 cells (PLMCs or CEFs) in 2mm gap cuvettes containing 10 μg of plasmid DNA in 100 μL of a modified Sucrose Electroporation Buffer (68 mM Sucrose, 250 μM $MgCl_2$, Opti-mem)(Bobick et al., 2014). We placed the cuvettes on ice for 5 minutes and then electroporated using a Nepa21 type II electroporator using a square wave pulse train of 5 poring pulses (275 V, 0.1 msec Pulse Length, 100 msec Pulse Interval, 10% Decay Rate, + Polarity) and 5 transfer pulses (20 V, 50 msec Pulse Length, 50 msec Pulse Interval, 40% Decay Rate, +/− Polarity). We then allowed incubated cells to recover on ice for 5 minutes before seeding onto glass bottom 18 well chamber slides or tissue culture treated dishes.

Chicken Embryo Microinjection and in ovo Electroporation

We incubated fertilized chicken eggs at 37.5 °C for 50-52 hours until HH 13-14. To access embryos, we used an 18-gauge needle to remove 3 ml of thin albumin to "drop" embryos, opened windows in the eggshell, added HBSS, and then gently dissected the vitelline membrane above the limb field. We used a Leica Stereoscope equipped with a 470/40 nm bandwidth emission filter to provide the necessary contrast against the background yolk for injection. We prepared plasmids for injection by dilution to 2-5 μg/μL in endotoxin free water, supplemented with 0.1M phenol red to enable visualization of injections. We loaded the plasmid solution into 1mm diameter glass capillary needles and then microinjected, using a Pneumatic PicoPump, into the embryonic coelom of the forelimb field. To electroporate plasmids into the somatic lateral plate mesoderm, we positioned a 2mm tip platinum chopstick negative electrode ∼1 mm below the embryo's forelimb field and a 1mm platinum disk on a stick positive electrode 1-2 mm above the embryo's forelimb field. We then used a Nepa21 electroporator to deliver a square wave pulse train of one 8V pulse (50 msec pulse length) followed by two 6V pulses (50msec pulse length, 1 sec interval), then removed the electrodes and pipetted

500 μL of HBSS onto the embryo. Following microinjection or electroporation, we taped the egg window using packaging tape and transferred the egg to a 37.5°C incubator until embryos reached HH 21-23. We then dissected right forelimb buds and transferred them to tubes of either DMEM-F12 supplemented with 10% FBS and 20mM HEPES (if live) or PBS (if fixed). We gently transferred the limb buds to a glass coverslip bottom 35mm dish and immobilized the limb buds by sandwiching them between the glass bottom cover slip and a 12 mm circular coverslip using a thin ring of petroleum jelly as a spacer. We performed all live imaging in 37°C imaging chambers. This procedure was modified from Sanders et al.(Sanders et al., 2013)

Stable Integration and Doxycycline Regulated Gene Expression

Stable Integration of DNA constructs

For all microinjection/electroporation experiments, we added the piggyBac transposase plasmid (CDV-hyPBase) to the plasmid solution as a 0.1-0.5 molar fraction of the expression plasmids to mediate stable genomic integration and high expression over time.

In vitro Gene Expression

For all standard cell culture experiments involving doxycycline induced expression of TRE3G-driven constructs, we introduced doxycycline (1-2 μg/mL) to the culture medium 24 hours post-electroporation/transfection.

In ovo Gene Expression

For all experiments involving doxycycline induced expression of TRE3G-driven constructs, we removed windowed eggs from incubation 24 hours after electroporation and injected 500 μL of doxycycline solution in HBSS (200 μg/mL) beneath the vasculature using a 27-gauge needle. We then incubated eggs for an additional day before further analysis.

Fixation

Fixation of cultured cells

To preserve cytonemes, we used a fixative cocktail, Fidelis Fix, containing 5 ml of 0.2M PHEM buffer, 1.25 ml of 16% paraformaldehyde, 80 μl of 25% glutaraldehyde, and 3.67 ml of Milli-Q H20. We rinsed cells once with ice cold 0.1M PHEM buffer, incubated them in Fidelis Fix for 15 minutes on ice, rinsed them once with ice cold 0.1M PHEM buffer and then washed three times for 5 minutes each with PBS before further analysis.

To preserve cytonemes in dissected limb bud tissue, we pre-incubated limb buds in ice cold 0.1M PHEM buffer supplemented with 60 mM sucrose (S-PHEM) for 5 minutes. We then incubated limb buds in Fidelis Fix supplemented with 120 mM sucrose and on ice for 1 hour, washed once with S-PHEM buffer for 10 minutes, then washed three times with PBS for 15 minutes each before further analysis.

For all other cell experiments, we rinsed cells briefly with ice cold DPBS without calcium or magnesium and then fixed them using 4% paraformaldehyde in PBS on ice for 15 minutes, followed by three washes with PBS for 5 minutes each.

Antibodies, HaloTag Ligands and Staining Reagents

To immunostain Shh, we used a mouse anti-Shh (5E1) primary antibody (1:50; Developmental Studies Hybridoma Bank). To immunostain Rab27a, we used rabbit polyclonal anti-Rab27a primary antibody (1:50; Thermo Fisher Scientific). For secondary antibody staining, we used either FluoTag-X2 anti-mouse IgG1 Abberior Star 580 (1:500; NanoTag Biotechnologies) or FluoTag-X4 anti-rabbit IgG Abberior Star 580 (1:500; NanoTag Biotechnologies). Nuclear counter staining was performed using DAPI (1 μg/ml working concentration).

Cells expressing HaloTag fusion proteins were incubated in their respective their cell media supplemented with 500 nM Janelia Fluor JFX650 overnight. We then washed cells with fresh media prior to live or fixed imaging.

Immunofluorescence Staining

After fixation protocols listed above were performed, we permeabilized cells by with 0.1% Triton-X100 in PBS at room temperature for five minutes followed by three 10-minute washes with PBS on ice. We then blocked the cells using SuperBlock Blocking Buffer on ice for one hour. Cells were stained overnight with primary antibodies diluted in PBS supplemented with 20% SuperBlock at 4 °C. The next day, we performed two 5-minute rinses followed by four 15-minute washes with PBS supplemented with 5% SuperBlock on ice. We then incubated cells with secondary antibodies diluted in PBS supplemented with 20% SuperBlock (and optional DAPI) for 1-hour at room temperature followed by four 15-minute washes in PBS.

Extracellular Shh Immunofluorescence Staining

We generated PLMCs as described from the anterior half of limb buds (to ensure no endogenous Shh expression) and electroporated them with APX1-TetOn-3g and BITREX-Shh-FL-msfGFP-pm-mIRFP682 plasmids. 48 hours post electroporation, we incubated cells in a primary staining solution comprised of 5E1 anti-Shh primary antibody (1:50) in DPBS supplemented with 10% SuperBlock Blocking Buffer on ice for 30 minutes to prevent endocytosis. We rinsed cells three times with ice cold DPBS and then incubated them with Fidelis Fix on ice for 15 minutes, followed by three wahes with ice cold DPBS (5 mins each). We then incubated cells with FluoTag-X2 anti-Mouse IgG1 secondary antibody conjugated to Abberior STAR 580 dye (1:500, NanoTag Biotechnologies) in a 20% SuperBlock PBS solution for one hour at room temperature, followed by four 15-minute washes with ice cold PBS.

We acquired maximum intensity projected Z-stacks from EC immuno-stained cells using a 100× objective on the Marianas SoRa spinning disk confocal. To correct for non-specific background, we measured the average fluorescence intensity of control cells lacking primary

antibody staining and subtracted this background value from all images before analysis. We traced all individual cytonemes using the pm-mIRFP682 signal to produce a composite ROI, performed spot-based colocalization using the ComDet v.05.5 plugin for ImageJ with the following parameters for both channels: Include larger particles: true, Segment larger particles: true, Approximate particle size: 9, Intensity threshold (in SD): 40 and Max distance between colocalized spots = 9. We then computed the fraction of extracellular Shh (Shh-FL-msfGFP-positive, Abberior STAR 580-positive) puncta divided by the total number of Shh-FL-msfGFP puncta for each cell.

Kinetic Analysis of Synchronously Released Shh

For synchronous release experiments, we co-electroporated CEFs with APX3-BclxL-KDEL, APX2-Shh-CB-msfGFP, and pEF-GalNAcT2-HaloTag(C262V). 24 hours after electroporation, we replaced the CEF media and supplemented it with 1μg/ml doxycycline to induce expression of Shh-CB-msfGFP. 48 hours after electroporation, we added media supplemented with 20μM A1155463 to the cell culture dishes to induce synchronous release of Shh. We then performed timelapse imaging using the Marianas SoRa spinning disk confocal, and a 63$\times$ objective. Starting 5 minutes post-release, we acquired Z-stacks through entire cells ($\sim$10 μm at 1 μm intervals in Z) every 3 minutes for one hour.

To analyze the kinetics of Shh release, we used ImageJ/FIJI to construct maximum intensity projections from the individual Z-stacks. We used a custom written FIJI macro to create ROIs of the Golgi apparatus at every time point and measure the integrated density of Shh-CB-msfGFP in each ROI. For comparison across cells, we performed min max normalization and plotted the normalized integrated density as a function of time.

Cytoneme Quantifications

To quantify cytoneme numbers and lengths in PLMCs expressing palmitoylated fluorescent proteins (pm-EGFP, pm-mKate2), we used the Marianas SoRA to acquire Z-stacks through entire cells ($\sim$10 μm at 0.5 μm intervals in Z). We produced maximum intensity projections and then measured cytoneme number and length using FIJI. To quantify cytoneme numbers and lengths for limb bud cells expressing palmitoylated fluorescent proteins (pm-EGFP, pm-mKate2) *in vivo*, we acquired Z-stack images of fields of cells then used the Neuroanatomy SNT plugin to measure and track cytonemes in 3D (Arshadi et al., 2021).In both cases, we considered all filopodia above 2 microns in length to be cytonemes.

To quantify the role of exosome secretion in localizing Shh to cytonemes, we performed CDH releases in PLMCs electroporated with APX3-BclxL-KDEL and BITREX-Shh-CB-msfGFP-pm-mKate2 using media supplemented with 20 μM A1155463 and either DMSO or 2μM Nexinhib20. 90 minutes post release, we fixed PLMCs with Fidelis Fix, and we acquired Z-stacks through entire cells (0.5 μm intervals in Z) using the Nikon Ti-E spinning disk confocal microscope. We produced maximum intensity projections and then created cytoneme ROIs by manually tracing cytonemes from tip to base. We manually counted the numbers of Shh-CB-msfGFP puncta along each cytoneme. To determine the relative tip/shaft enrichment of Shh along cytonemes, we first used the profile plot function in ImageJ to generate Shh intensity plots along the length of cytonemes containing Shh-puncta. For each cell, we averaged the Shh fluorescence intensity for every pixel distance in the last micron (tip) and in the remaining length (shaft) of these cytonemes and divided the mean tip/shaft fluorescence values to create the Mean Shh Intensity Ratio (Cytoneme Tip/Shaft) reported in Figure 5. We repeated this analysis in PLMCs electroporated with APX3-BclxL-KDEL, BITREX-Shh-CB-msfGFP-pm-mIRFP682 with or without expression of APX2-Rab5a(S34N)-DN to quantify the role of endocytosis on localizing Shh to cytonemes.

To quantify cytoneme diameter in SEM images of the limb bud mesenchyme *in vivo*, we

measured cytoneme width in three locations per cytoneme using FIJI and then averaged the measurements to create a composite diameter measurement.

Colocalization Analysis of Shh and CD63-pHluo

To analyze what fraction of Shh colocalizes with secreted exosomes, we electroporated PLMCs with APX1-TetOn-3g, BITREX-CD63-pHluo-pm-mIRFP682, and APX2-Shh-FL-mScarlet plasmids. 24 hours after electroporation, we replaced the media and with fresh media supplemented with 1μg/ml doxycycline to induce expression of CD63-pHluo, pm-mIRFP682, and Shh-FL-mScarlet. 24 hours after doxycycline addition, we imaged the PLMCs.

To examine colocalization in the extracellular space, we acquired Z-stacks using the Marianas SoRa spinning disk confocal with a 100× objective with additional 2.8× magnification. We constructed max intensity Z-projections and constructed a cell body mask by thresholding the pm-mIRFP682 membrane channel using FIJI's Triangle threshold and Fill Holes function and inverted this mask to create an ROI representing extracellular space. To detect and quantify colocalization between CD63-pHluo and Shh-FL-mScarlet puncta in the extracellular space ROI, we used the ComDet v.05.5 plugin for ImageJ with the following parameters for both channels: Include larger particles: true, Segment larger particles: true, Approximate particle size: 9, Intensity threshold (in SD): 40 and Max distance between colocalized spots = 9.

To examine colocalization along cytonemes, we acquired and projected Z-stacks as above, but without 2.8× additional magnification. We traced individual cytonemes visible within each projection manually to produce a composite ROI. We performed detection and colocalization of CD63-pHluo and Shh-FL-mScarlet puncta using the ComDet v.05.5 plugin the following parameters for both channels: Include larger particles: true, Segment larger particles: true, Approximate particle size: 3, Intensity threshold (in SD): 40 and Max dis-

tance between colocalized spots = 3.

For both extracellular and cytoneme-associated puncta, we computed and report the fraction of exosome-bound Shh (CD63-pHluo-positive, Shh-FL-mScarlet-positive) divided by the total number of Shh-FL-mScarlet-positive puncta.

Quantifying MVB Fusion Events in PLMCs

To determine the effect of Nexinhib20 incubation on MVB fusion/exosome secretion, we electroporated PLMCs with APX1-TetOn3g and APX2-CD63-pHluo plasmids, cultured them at 37°C for 24 hours, and then incubated the PLMCs with media containing both 1 μg/mL doxycycline and either 2 μM Nexinhib20 or DMSO for another 24 hours. We imaged MVB fusion events in PLMCs at room temperature ($\sim$22°C) across both conditions using TIRF microscopy for 3 minutes at 300ms intervals with identical TIRF angle, laser power, and exposure. To correct for bleaching of the CD63-pHluo signal, we performed bleach Correction (Simple Ratio) using FIJI.

To quantify the number of MVB-plasma membrane fusion events in each cell imaged, we used the published ImageJ macro Analyzer of MVB Exocytosis (AMvBE)(Bebelman et al., 2020) designed for detecting pH sensitive fusion events from TIRF microscopy timelapse imaging. Using 0.16 μm pixel size and 0.3s frame rate, we user defined the following AMvBE parameters: Time window for event correction (# of frames) = 6, Condition for fluorescence decrease after exocytosis (min. # of frames) = 3, Condition for fluorescence increase prior to exocytosis (max. # of frames) = 3, Minimum event size to be considered (micrometer) = 0.4, If the decay condition is not fulfilled, threshold value (N) for exocytosis event rescue such that Mean + N*Std. = 3, Manual threshold for vesicle movement fixed by users (unit in number of vesicle diameter) = 2. We displayed the data as number of MVB-plasma membrane fusion events per minute.

Bioactivity Assay:

Treating NIH 3T3 cells with conditioned media

We seeded 1×10^5 HEK293FT cells into wells of a 12 well tissue culture dish containing DMEM supplemented with 10% FBS (DMEM10), cultured them for 24 hours at 37°C, and then transfected each well with either APX1-pm-EGFP, APX1-Shh-FL-msfGFP, or APX1-Shh-CB-msfGFP using the DreamFect Gold kit according to the manufacturer's protocol. After culturing for an additional 24 hours, we dissociated transfected cells using Tryp-LE as described above, centrifuged for 3 minutes at $200 \times g$, resuspended with 5 mL of DMEM supplemented 2% FBS and transferred the dissociated cells to a 60mm tissue culture dish. After an additional 72 hours of culture at 37°C, we collected the conditioned media from each dish, centrifuged for 5 minutes at $200 \times g$, and then filtered through a 0.22 μm filter. We added 2ml of freshly collected conditioned media, combined with 2 mL of new DMEM10, to NIH-3T3 cells grown to 75% confluency on 6 well dishes. We then cultured the cells in conditioned media for 40 hours before RT-qPCR analysis.

RNA isolation, cDNA synthesis, and quantitative PCR

After 40 hours of culture in conditioned media, we performed RNA extraction using the Direct-zol RNA Microprep kit, followed by reverse transcription, using the ZymoScript RT PreMix Kit, to generate 50 ng/μL cDNA. We performed qPCR using PowerUp SYBER Green Master mix on a QuantStudio3 Real-Time PCR system (Applied Biosystems) for 40 cycles to amplify and measure murine *PTCH1* and *GAPDH* mRNA transcripts. We used the delta delta Ct ($\Delta\Delta C_t$) method to quantify changes in relative gene expression induced by conditioned medium (Livak and Schmittgen, 2001). Graphs display $2^{-\Delta\Delta C_t}$ fold change and we computed statistical significance using one-way ANOVA with Tukey's multiple comparisons test on ΔC_t values.

Reconstituted Shh Activity Gradient Formation and Analysis

To quantify how exosome and cytoneme perturbations affect Shh activity gradients in a tissue, we adapted a published 2D synthetic reconstitution approach using a confluent field of Shh-Reporter "Receiver" cells and sparsely seeded Shh-expressing "Sender" cells (Li et al., 2018; Schlissel et al., 2024). The "Receiver" cells were comprised of a clonally selected NIH-3T3 cell line stably expressing a Gli binding site array driving H2B-mCitrine (kind gift from Pulin Li) and were seeded on polymer coverslip bottom 24 well plate at a density of 4×10^5 to act as a confluent seed layer to represent a mesenchymal tissue. The "Sender" cells were PLMCs collected exclusively from the anterior half of limb buds (free of endogenous Shh expression), electroporated with APX1-TetOn3g and BITREX-Shh-FL-msfGFP-pm-(mKate2 or mIRFP682), and sparsely seeded (500 cells per well) on top of the "Receiver" tissue. We then incubated each co-culture tissue with cell media supplemented with 2 μg/mL doxycycline for 72 hours followed by fixation as previously described.

To image the Shh signaling gradients in each well, we used the SlideBook acquisition software to image the entire mCitrine reporter gradient surrounding a membrane labeled (pm-mKate2 or pm-mIRFP682) Shh expressing PLMC using a two-color montage acquisition comprised of four separate 20 μm z-stacks (step size = 1.2 μm) centering around the Sender cell. We used identical laser power, exposure time, and gain in each independent experiment to ensure quantitative comparison

For quantitative gradient analysis, we used FIJI software to open and create maximum intensity projections of all 4 z-stacks per gradient for both the Receiver cell (H2B-mCitrine) and the Sender cell membrane label (pm-mKate2 or pm-mIRFP682) channels. We stitched the 4 max projected images of each gradient, created a cell mask ROI around the membrane-labeled Sender cell, and measured the integrated density of the palmitoylated fluorescent protein membrane label (mKate2 or mIRFP682). As the palmitoylated fluorescent protein membrane label and Shh-FL-msfGFP are genetically coupled on the same plasmid, we used

the integrated density of the membrane label acted as a proxy to normalize for each Sender cell's level of Shh expression. Next, we used the StarDist 2D plugin in FIJI to segment and create nuclear ROIs in the H2B-mCitrine stitched image.(Schmidt et al., 2018) To find the center position of each gradient or "gradient centroid" position, we created a rectangle ROI that exclusively highlighted the visible H2B-mCitrine gradient, measured the center of mass, bounding rectangle, and mean fluorescence of all nuclear ROIs within this rectangle gradient ROI, and then calculated the center of mass using nuclear position and mean values as weights. Using FIJI, we then created a 200 μm radius circle ROI centered around the gradient centroid coordinates and used the Radial Profile Plot plugin (https://imagej.net/ij/plugins/radial-profile.html) to produce a profile plot of normalized integrated intensities in concentric circles emanating from the gradient centroid. Considering each PLMC sender cell had variable amounts of Shh expression, we normalized the H2B-mCitrine profile plot values by dividing by the integrated intensity of the PLMC membrane fluorescent protein.

SeeDB2G Limb Bud Tissue Clearing

We cleared fixed limb bud tissues using a modified SeeDB2G protocol (Ke and Imai, 2018). Fixed limb buds transferred to a microcentrifuge tube containing 1 ml of permeabilization buffer (100 μl of 20% Saponin + 900 μl of ddH20) and gently rocked at room temperature for 2 hours. The limb buds were then transferred to increasingly concentrated solutions of Omnipaque-350. First, the limb buds were transferred to a microcentrifuge tube containing 1 ml of clearing solution A (100 μl of 20% Saponin + 333 μl of Omnipaque-350 + 567 μl of ddH20) and gently rocked at room temperature for $\geq$ 2 hours. The limb buds were then transferred to a microcentrifuge tube containing 1ml of clearing solution B (100 μl of 20% Saponin + 500 μl of Omnipaque-350 + 400 μl of ddH20) and gently rocked at room temperature for $\geq$ 2 hours. As the last stage of clearing, the limb buds were transferred to a

microcentrifuge tube containing 1 ml of SeeDB2G clearing solution (100 μl of 20% Saponin + 900 μl of Omnipaque-350) and gently rocked at room temperature for $\geq$ 2 hours. Finally, we transferred the cleared limb buds to 100% Omnipaque-350 for immediate imaging or storage.

Wholemount Limb Bud Immunofluorescence Staining and Shh Protein Gradient Analysis in Embryonic Limb Buds In vivo

In ovo Drug Injection

We incubated fertilized chicken eggs at 37.5 °C with 45-55% humidity for 78 hours until embryos reach HH stage 19-20. To access embryos, we used an 18-gauge needle to remove 3 ml of thin albumin to "drop" embryos thus reducing the overall volume of egg yolk/albumin to 42 - 45 ml. We then opened a window in the eggshell and used a 27-gauge needle to inject 500ul of either DMSO or Nexinhib20 (1.5 mM) underneath the vasculature and embryo yielding an estimated final concentration $\leq$ 16 - 18 μM. We then sealed the window in the eggshell with packaging tape and returned the embryos to incubate at 37.5°C with 50-60% humidity for 16 hours before either wholemount limb bud immunofluorescence staining or cell viability assays.

Wholemount Limb Bud Immunofluorescence Staining:

In HBSS, we dissected the right forelimb/wing bud of every embryo and then fixed pools of limb buds in 4% PFA on ice for 2 hours followed by three 30-minute washes in PBS on ice. We then permeabilized the limb buds by incubating them in 0.1% Triton-X100 in PBS for 2 hours with gentle rocking at 4 °C. We then replaced the permeabilization solution with SuperBlock Blocking Solution supplemented with 0.1% Triton-X100 for 2 hours with gentle rocking at 4 °C. Next, we incubated the limb buds with our primary mouse anti-Shh (5E1, 1:50) antibody in PBS supplemented with 20% SuperBlock Blocking Solution for $\sim$ 40 hours with gentle rocking at 4 °C. The limb buds were then rinsed three times for 5 minutes each

and washed four times for 30 minutes each with PBS supplemented with 5% SuperBlock with gentle rocking at 4 °C. We then performed a rapid 30-minute incubation with SuperBlock followed by overnight incubation with secondary antibody solution comprised of FluoTag-X2 anti-Mouse IgG1 secondary antibody conjugated to Abberior STAR 580 dye (1:500, NanoTag Biotechnologies) and DAPI in a 20% SuperBlock PBS solution at 4 °C with gentle rocking. Limb buds were subsequently rinsed three times for 5 minutes each and washed four times for 30 minutes with PBS. Immunostained limb buds were then cleared using SeeDB2G method described above and entire limb bud z-stacks were imaged using the 10× objective with 0.7× zoom on Zeiss LSM 880 confocal microscope.

Radial Average Intensity Gradient Measurements

First, we performed maximum intensity projections on Shh-Stained limb bud z-stacks and manually drew ROIs around the ZPA region of the limb bud. Using a custom written FIJI macro, we duplicated our Shh-stained limb bud max projected image, performed median filtering (radius = 4 pixels), created a limb bud mask ROI using manual Huang thresholding and saved both the median filtered image and the limb bud mask ROI. Using the median filtered image and ZPA ROI, we found the maximum fluorescence intensity value within the ZPA and found its XY coordinates. Now using our original Shh-stained limb bud max projected image, our limb bud mask ROI, we performed radial profile measurements within the boundaries of limb bud. Specifically, we used the ZPA peak coordinate as the center of a circle, and created concentric circles sweeping outward from the ZPA center with 1-micron radial steps until a circle with a radius of 300 microns is reached. Every pixel along each circle that falls within the boundary of the limb bud mask was counted and its fluorescence value was measured. For each radial circle, the mean intensity is calculated by dividing the sum intensity by number of pixels within our boundary. We then plotted the mean intensity values as a function of radial distance from ZPA peak to generate radial intensity gradients of Shh protein in the limb bud.

Cell Morphology and Viability Measurements

To qualitatively compared cell morphology in DMSO and Nexinhib20 treated limb buds *in vivo*, we performed *in ovo* electroporation of limb buds as described above with APX1-pm-EGFP to label cell membranes. Roughly 28 hours after electroporation, when embryos reached HH stage 19-20, we performed similar *in ovo* drug injections with DMSO or Nexinhib20 as described above. 16 hours after drug injection, we dissected the right forelimb/wing bud in HBSS and fixed the limb buds using Fidelis Fix to preserve cytoneme structure, cleared the tissue using SeeDB2G protocol, and used the 40× objective with 2.8× digital zoom on the Marianas SoRa spinning disk microscope to acquire z-stack images of individual limb bud mesenchymal cells from both conditions.

To quantitatively measure cell death in the limb bud mesenchyme after *in ovo* injection of DMSO or Nexinhib20, we bisected the right forelimb/wing bud in HBSS and immediately transferred the wing buds into a plastic dish containing PLMC culture media supplemented with 100 μM verapamil and both membrane permeable 1X NucSpot Live 650 and membrane impermeable 1X NucSpot 500/515. After 1.5 hours of incubation at 37°C with 5% CO_2, we transferred the bisected limb buds to a glass bottom 35mm dish as described above and acquired z-stacks (3μm step size) of 3 unique fields of view in each limb bud using a 20× objective with 2.8× magnification on the Marianas Sora spinning disk confocal. Based on membrane permeability, all cell nuclei should be labeled with the NucSpot Live 650 dye and only dead or dying cells should be labeled with NucSpot 500/515. To quantitatively measure this fraction, we max projected 2 image z-stacks, used a gaussian blur pixel size = 1, used StarDist ImageJ plugin to segment and create nuclear ROIs in the NucSpot Live 650 channel, and then measured the mean fluorescence intensity of NucSpot 500/515 dye within each nuclear ROI. If the mean intensity was 20% above background in a nuclear ROI, that cell was counted as a dead cell. We averaged the dead cell fraction over the 3 fields of view per limb bud for display.

QUANTIFICATION AND STATISTICAL ANALYSIS

For PLMCs, independent experiments represent pooled PLMCs that were harvested from 5 to 10 individual embryos on a given day subjected to electroporation, induced release, manipulation, and then imaging or other analysis. For cultured cell lines, (e.g. Chick Embryo Fibroblasts, HEK-293FT and NIH 3T3 cells), independent experiments represent pooled cells on a given day subjected to transfection or electroporation, pharmacological treatment, incubation and then imaging or other analysis.

We performed all statistical analysis using GraphPad Prism. Significance for comparisons between two experimental groups was determined with the Mann-Whitney U-test (2-tailed). Significance for comparison between more than two groups was determined by One-Way ANOVA with Tukey's multiple comparison tests. The asterisks in figure graphs correspond to the following p-values: n.s. $= p > 0.05$, $* = p \leq 0.05$; $** = p \leq 0.01$; $*** = p \leq 0.001$, $**** = p \leq 0.0001$. Figure legends describe sample size, n, replicates, independent experiments, statistical tests used, and how error is displayed.

CHAPTER 3

CONCLUSION AND FUTURE DIRECTIONS

3.1 Preface

Although the first morphogen was discovered over four decades ago, developmental biologists are still pondering fundamental questions about how morphogen mediated tissue patterning is regulated. Despite serving as a classic example of morphogen function, the regulation of Shh dispersal across tissues remains unclear. In this chapter, I will highlight key conclusions from my dissertation work on exosome-mediated Shh dispersal and gradient formation in the developing limb bud. Here, I will compare these conclusions to current views of Shh signaling and limb development, propose future directions, and discuss shared design principles of EV-mediated secretion in broad contexts.

3.2 MVB packaging and exosome release represents a central Shh secretion pathway

A central finding of this thesis is that Shh secretion is primarily mediated through exosomal packaging and release in the limb bud mesenchyme.

My initial findings in PLMCs not only demonstrate that Shh localizes to cytonemes, as previously described *in vivo* (Sanders et al., 2013), but also reveal that Shh accumulates in spherical endosomal organelles that are secreted to the extracellular space in punctate form. Morphological characterization via super resolution microscopy and colocalization with the tetraspanin CD63 clarified that the Shh-enriched endosomal organelles were MVBs and that a large fraction of the secreted Shh puncta were EVs, likely exosomes.

Similar observations are well-characterized in other tissue and cell models. For example, in the *Drosophila* wing disc, immuno-electron microscopy showed Hh ligands localized within

MVB intralumenal vesicles and bound to CD63-positive exosomes in the nearby extracellular space (Gradilla et al., 2014; Parchure et al., 2015). Similarly, Shh has been found on secreted CD63-positive exosomes from human cell lines and primary chicken notochordal cells (Vyas et al., 2014) (Vyas et al., 2014).

However, MVB localization and colocalization with CD63, does not necessarily prove that Hh-bound EVs are truly exosomes. While CD63 is primarily enriched in MVBs and exosomes, it can also localize to plasma membrane-derived ectosomes (Mathieu et al., 2021). Furthermore, studies in the wing disc and cell culture found that manipulation of endocytosis and endosomal sorting machinery (e.g., Rab5, dynamin, ESCRTI-III components) reduced EV secretion and perturbed Hh signaling gradients, yet these manipulations still do not definitively demonstrate that Hh is secreted on bona fide exosomes (Gradilla et al., 2014; Matusek et al., 2014; D'Angelo et al., 2015; Vyas et al., 2014). Many of these manipulated factors also regulate non-EV endocytic trafficking and ectosomal budding and fission (Cocucci and Meldolesi, 2015). Therefore, establishing a direct link between MVB-plasma membrane fusion and secreted EVs is required to be certain of their exosomal identity.

My work substantiates a link between MVB-plasma membrane fusion and secreted Shh-bound exosomes. Unlike the non-specific manipulations of endocytic and ESCRT machinery, manipulating the MVB-associated GTPase, Rab27a specifically inhibits the docking and fusion of MVBs to the plasma membrane. I found that treating PLMCs with Nexinhib20, a pharmacological inhibitor of Rab27a, greatly reduced the number of MVB-plasma membrane fusion events. Consequently, this same treatment also considerably reduced the number of CD63-pHluo vesicles in the extracellular space. From these results, I conclude that the Shh-CD63 colocalized vesicles in the extracellular space are indeed exosomes derived from MVB-plasma membrane fusion.

Although distinguishing whether Shh-positive EVs are exosomes or ectosomes may seem like a minor detail, the differences in the biogenesis could represent significant differences in

function. As a result, future work should focus on characterizing the biogenesis of Hh-EVs to specifically delineate how exosomes vs. ectosomes function in signaling.

3.3 A complex Shh trafficking route is shared between mesenchymal and epithelial tissues

By using the CDH synchronous release tool developed in this work to carefully dissect secretory trafficking, I found that Shh undergoes a complex secretory route that leads to MVB packaging. In particular, inhibiting endocytosis in this assay led to the accumulation of Shh at the plasma membrane and precluded packaging within MVBs. This suggests that Shh must first be secreted to the plasma membrane and subsequently get internalized and sorted to MVBs, as opposed to trafficking directly to endosomes/MVBs from the Golgi apparatus.

Interestingly, these findings show that limb bud mesenchymal cells that lack apico-basal polarity utilize Shh trafficking routes traditionally characterized within polarized epithelial cells. Work in the mouse neural tube, *Drosophila* wing disc, and immortalized Madin-Darby canine kidney cells demonstrates that Hh ligands are initially secreted to the apical plasma membrane, internalized in a Dispatched-dependent manner, and transcytosed to the basolateral domain (Callejo et al., 2011; Hall et al., 2024; Sandoval et al., 2022). Once transcytosed to the opposing domain, Hh ligands can be secreted on exosomes, transferred to extracellular carriers for diffusion, or transported along cytonemes. However, there is also evidence in the *Drosophila* wing disc that a pool of Shh that is apically secreted and internalized does not undergo transcytosis to the basolateral domain, but is resecreted apically for microvilli-derived ectosome release (D'Angelo et al., 2015; Hurbain et al., 2022). The shared secretory route suggests that this complex secretion, internalization, and resecretion pathway may be a universal way of priming long-range dispersal of Hh ligands.

Due to the shared secretory route, other molecular regulators of Shh trafficking seen in polarized epithelial cells might also function in the limb bud mesenchyme. In all previously

described examples where Hh ligands undergo this secretory route, Dispatched proteins are required to promote the internalization after primary secretion. Additionally, Dispatched colocalizes with Hh in basolateral MVBs and to secreted exosomes in the *Drosophila* wing disc, suggesting that the primary secretion and internalization can concentrate Hh ligands with other key signaling machinery (Gradilla et al., 2014). Further work is needed to determine if Dispatched is required for Shh internalization in limb bud cells and if Dispatched colocalizes or co-purifies with Shh-bound exosomes secreted by limb bud cells.

3.4 Exosome secretion is required for mesenchymal cells to establish Shh gradients

Studies in the *Drosophila* wing disc and mouse neural tube have demonstrated that exosomes play important roles in Hh-mediated patterning and development of epithelial tissues, yet their roles in mesenchymal tissues remained unknown (Gradilla et al., 2014; Parchure et al., 2015; Walvekar et al., 2025). A principle conclusion of my thesis is that exosome secretion is required for Shh gradient formation in the limb bud mesenchyme.

Using reconstituted co-culture assays, I found that single PLMCs can generate a roughly 100 μm Shh signaling activity gradient over the course of a few days. Similar sized gradients could be generated by NIH-3T3 fibroblast cells (Schlissel et al., 2024). Inhibition of MVB biogenesis via Rab5a dominant negative expression or of MVB-plasma membrane fusion via Nexinhib20 treatment nearly abolished the signaling activity gradients formed by Shh expressing PLMCs.

This finding indicates that other carrier-assisted diffusion mechanisms, including transfer to HDL and Scube proteins, may not be centrally required for Shh dispersal and gradient formation in mesenchymal tissues. HDL is naturally present in the fetal bovine serum (FBS) used in cell culture media; however, HDL was insufficient to sustain Shh dispersal when exosome secretion was inhibited (Busatto et al., 2022; Ghebosu et al., 2025). As a result,

HDL is either not needed in Shh-mediated patterning of mesenchymal tissues or functions downstream of exosome secretion as potential modulator of effective diffusion or potency. This juxtaposes the role of Lpp, a *Drosophila* form of HDL, in long-range Hh signaling in the wing disc epithelium, highlighting potential tissue-specific functions (Panáková et al., 2005). Although limb bud mesenchymal cells endogenously express *Scube1* and *Scube3* (Lin et al., 2023), their contribution to Shh dispersal and signal gradient formation does not appear to be required. This finding could be explained by either low levels of Scube expression in PLMCs or by a similar role downstream of exosomes for modulating Shh dispersal. The latter explanation is supported by the findings of Schlissel et al. who showed that the addition of exogenous Scube proteins to the media expands the spatial extent of pre-existing signaling gradients (Schlissel et al., 2024). Overall, this work suggests that HDL and Scube proteins may play a more modulatory role in tuning the size and shape of Shh gradients.

Lastly, the Nexinhib20 Rab27a inhibitor has specific roles in perturbing exosome secretion, but does not alter ectosome secretion (Ostrowski et al., 2010; Bobick et al., 2014). Thus, ectosome secretion is not required for limb bud mesenchymal cells to establish Shh signaling gradients. The requirement of exosomes, but not ectosomes, in signal gradient establishment perfectly exemplifies why the characterization of EV biogenesis can promote deeper understanding of EV function.

While the biological relevance of my *in vitro* gradient assay may be limited due to the nature of a 2D signaling field, the finding that Nexinhib20 also perturbs Shh protein distribution in the limb bud *in vivo* confirms the importance of exosomes in dispersing Shh in 3D mesenchymal tissue.

Developmental Roles of Exosome-Mediated Signaling Remain Unknown

How exosome-mediated Shh dispersal regulates anterior-posterior digit specification and limb bud growth is yet to be determined. As highlighted in Chapter 1, Shh's role in digit specification, growth, and cell survival is regulated across distance and, importantly, time.

In chicken embryos, Shh-mediated patterning is assumed to follow a promotion model in which mesenchymal cells are progressively "promoted" to more posterior fates over prolonged exposure to Shh signaling (Towers et al., 2011). Additionally, Shh signaling in the chick limb expands the digit forming field by promoting proliferation through the expression of D-cyclin cell cycle regulators (Towers et al., 2008). Moreover, in mouse embryos, only an early transient burst of Shh signaling is required to specify the identity of the digits, while a later phase of Shh signaling acts long-range to promote cell survival (Zhu et al., 2008, 2022). In both limb bud models, timing is a key factor in how Shh signaling regulates development. Hence, more future work should address whether exosome-mediated dispersal is necessary throughout the entirety of Shh mediated signaling or selectively during certain temporal phases.

Similarly, Shh has known morphogenic and mitogenetic roles. It was recently revealed that there are two populations of Shh-bound EVs in the developing neural tube: one population promotes patterning, while the other promotes proliferation (Walvekar et al., 2025). Thus, another key future direction should aim to examine if Shh-bound exosomes in the limb function in a patterning role, a proliferative/cell survival role, or both. The idea of separating Shh functions brings up a seemingly basic, but inherently philosophical, question: what is a morphogen?

The role of Shh is often described in relation to true morphogen function or to mitogenic or cell survival functions; however, I believe this dichotomy highlights an outdated way of thinking. There are two key criteria that help define a morphogen: 1) the molecule must act directly at a distance, and 2) it must induce distinct outputs in a concentration-dependent manner (Vincent and Briscoe, 2001). Using these criteria, most studies have primarily focused on how morphogens can mediate distinct cell identities (e.g., digit identity or ventral neuronal identities) (Riddle et al., 1993; Briscoe et al., 2000).

Historically, the role of Shh in mediating proliferation or cell survival is attributed to

a secondary "non-morphogen" function. For example, Zhu et al. argued that Shh isn't a limb morphogen because digit specification is likely mediated through a relay of secondary signals; however, they also claim that Shh acts as a long-range cell survival signal in a later phase (Zhu et al., 2022). In this second phase of signaling, Shh satisfies the first criteria of acting long-range as evidenced by a physical gradient of Shh protein emanating away from the ZPA. During this phase, Shh also directly promotes the graded expression of *Ptch1/Gli1* target genes and directly controls an inverse gradient of Gli3R, which partially satisfies the secondary criteria of a morphogen. Although Shh may not function as the digit specifying morphogen, its identity as a morphogen should still be considered if it directly controls graded levels of "secondary" functions like proliferation and survival.

3.5 Transport along cytonemes provides an alternative mode of exosome-mediated Shh dispersal

Cytonemes provide a direct route for Hh transport allowing precise, synapse-like connections between cells (Sanders et al., 2013; Hall et al., 2024; Bischoff et al., 2013). Along cytonemes in the wing disc, Hh ligands colocalize with CD63, suggesting a form of cytoneme-based EV transport (Gradilla et al., 2014). However, the identity of these EVs and their method of transport along cytonemes remained ambiguous.

The findings from my work resolved these ambiguities. Through extracellular immunofluorescence staining assays I demonstrated that the majority of cytoneme-associated Shh faced the extracellular space. Through CDH release experiments and multicolor live imaging, I revealed that a significant fraction of this Shh was a pool of secreted Shh-bound exosomes that bind to and transport along the extracellular surface of cytonemes. This suggests that the same secreted Shh-bound exosomes can be dispersed either by diffusion through the extracellular space or by directed transport along cytonemes. Multicolor live imaging and scanning electron microscopy further supported the observation that secreted exosomes travel along

the extracellular surfaces of cytonemes in the limb bud mesenchyme *in vivo*.

This mechanism of transport shifts the standard view of how cytonemes mediate Shh dispersal. A couple of key questions arise from this finding.

What are the biological roles of cytonemes in the limb bud mesenchyme?

In epithelial tissue contexts, cytonemes have essential roles in dispersing Hh ligands and other morphogens across tissues (Zhang and Scholpp, 2019). Both in the mouse neural tube and *Drosophila* wing disc and abdominal epithelia, cytoneme perturbations greatly reduce the length scale of Hh signaling gradients (Bischoff et al., 2013; Hall et al., 2024).

Inhibiting cytoneme formation in PLMCs had no effect on Shh signaling activity in 2D reconstituted mesenchymal co-culture assays, which corroborated previous results (Schlissel et al., 2024). However, the small size of cytonemes *in vitro* precludes any meaningful role in long-range signaling. *In vivo*, my work and previous findings established that cytonemes extend incredible lengths (Sanders et al., 2013). The long lengths and directional synapse-like connections of cytonemes *in vivo* may provide a way to extend the distance of signaling or modify the intensity or direction. Whether cytonemes are required for Shh dispersal in the vertebrate limb bud, and whether cytonemes function in coordination with or orthogonally to exosomes, have yet to be answered.

Considerable work will be required to determine the specific roles of cytonemes. First, the use of filipodia-specific manipulation is needed as many current cytoneme-inhibition methods necessitate the gross manipulation of F-actin regulators and the actin cytoskeleton itself which have pleiotropic effects. A synthetic tool to manipulate filopodia formation specifically was recently developed (Zhang et al., 2021), and I will further discuss its preliminary use in the limb bud in Appendix A. To probe the roles of cytonemes in Shh-mediated patterning in the limb bud, the spatial extent and intensity of key Shh target genes, including *Ptch1*, *Gli1,* *Grem1*, must be measured after cytoneme inhibition and compared to both exosome and dual exosome cytoneme inhibition. Similar manipulations would need to be performed with

readouts of apoptosis and proliferation to determine if exosomes and cytonemes represent functional differences in tissue patterning, proliferation, and survival.

How are exosomes transported along the external surface of cytonemes?

The question of how exosomes are transported along cytonemes can be broken down further. How do secreted exosomes bind to cytoneme surfaces, and why do they? Once bound, how do exosomes get actively transported along cytonemes? The mechanisms mediating exosome-cytoneme binding and transport remain unaddressed, but below I highlight potential candidates based on an extensive literature review.

Based on known Shh-specific interactions, one potential mechanism is that Shh-bound exosomes interact with Shh-receptors enriched on cytoneme membranes. Dispatched, the transmembrane protein, required for Shh release from the membrane localizes to cytonemes in NIH-3T3 fibroblasts (Hall et al., 2021) and in PLMCs (my unpublished work). Similarly, co-receptors, Ihog/Boi in *Drosophila* and Cdo/Boc in vertebrates, co-localize with Hh ligands along cytonemes in the wing disc and NIH-3T3 cells, respectively.

More generally, there are key insights from how exosomes bind to cells for reception that provide likely candidates for exosome-cytoneme interaction. Exosomes engage with receiving cells through a few key mechanisms: 1) direct membrane fusion, 2) endocytic internalization (clathrin/caveolin-mediated, macropinocytosis, phagocytosis), 3) ligand-receptor interactions at the membrane (Rahgoshay et al., 2025). All mechanisms rely on the interactions between surface proteins on exosome membranes and plasma membranes (Gonda et al., 2019).

Lectins are a class of soluble, membrane-bound receptors found on both cell membranes and exosome membranes that are known to interact with glycan moieties. There are multiple reports showing that perturbing lectin function, via blocking antibodies, can prevent exosome uptake (Yuan et al., 2017; Hao et al., 2007). Relatedly, glycans, including N-linked and O-linked glycoproteins, Sialic acid, and glycolipids, are abundantly expressed on exosome

and cell-membranes, thereby providing ample receptor-ligand binding pairs (Escrevente et al., 2013). Heparan sulfate proteoglycans (HSPGs), a commonly expressed glycoprotein family, have known roles in regulating Hh signaling by mediating oligomerization, Scube/HDL recruitment, and cytoneme guidance (Vyas et al., 2008; Jakobs et al., 2016; Puschmann et al., 2026; Bischoff et al., 2013). Moreover, cellular membrane-associated HSPGs also have been demonstrated to promote exosome binding and internalization (Mulcahy et al., 2014). Thus, the interactions of lectins and glycans, likely HSPGs, provide a key pair that might mediate the interactions of Shh-bound exosomes with cytonemes.

Integrins are highly diverse, broadly expressed cell-surface adhesion molecules that may promote exosome-cytoneme binding. Integrins bind primarily to extracellular matrix molecules, such as laminin, collagen, fibronectin, and HSPGs, but also interact with other cell-adhesion molecules, like ICAMs and VCAMs (Pan et al., 2016). Integrins are present on most exosome membranes and have key roles in selective exosome-homing to the proper receiving cell type (Shimaoka et al., 2019). In addition, filopodial membranes are enriched with selective integrins (He et al., 2017; Yang et al., 2022).

Transmembrane Integrins and netrin receptors are transported to the tips of filopodia through the filopodial actin motor, Myosin-10 (Zhang et al., 2004; Hirano et al., 2011). This implies that the Myosin-10 motor involved in anterograde active transport in cytonemes can form direct connections to the external surface through binding integrins and other potential receptors. Since integrins, ECM, and other cell-adhesion proteins are enriched on exosome membranes, this form of integrin-Myosin10 binding may act as the mechanism that transports Shh-bound exosomes along cytonemes. This hypothesis is further supported by reports showing that Shh travels along cytonemes in the limb bud at the same rate as Myosin-10 movement (Sanders et al., 2013), and that Shh-accumulation in NIH-3T3 filopodia is greatly inhibited by Myosin-10 perturbation (Hall et al., 2021).

To conclude, cytonemes may be enriched in selective ECM, integrins, and other surface

receptors that may provide a sticky substrate for Shh-bound exosomes. Once bound, active transport by Myosin-10 may transport externally bound Shh-positive exosomes through transmembrane connections (e.g., integrins). However, this is all speculation, and future work is needed to dissect the molecular composition of both exosomes and cytonemes to better understand specific candidates that mediate this binding and transport. This work will require advanced spatial proteomics and high-throughput screening of individual transmembrane proteins or ECM components.

Exosomes may interact with other extracellular transporters to modulate their signaling capability

Exosomes, and extracellular vesicles as a whole, are not the only methods posed to increase the diffusion of Hh ligands across the extracellular space. Dispatched can release Hh ligands from the plasma membrane and mediate the transfer to extracellular carriers, such as Scube proteins and HDL particles (Panáková et al., 2005; Tukachinsky et al., 2012; Wierbowski et al., 2020).

One key aspect of both mechanisms is that Dispatched is necessary for initial transfer to either extracellular carrier. Notably, Dispatched is also reportedly required for Hh ligand internalization and packaging into MVBs and is present on secreted exosomes (Gradilla et al., 2014). Thus, I argue that exosomes carrying both Shh and Dispatched can likely interact with Scube proteins and HDL at a distance from the Shh producing cell. As discussed above, previous reports illustrated that Scube acted as a tuning agent and was not necessary for 2D gradient formation (Schlissel et al., 2024), while my work showed that exosome secretion perturbed 2D gradient formation despite the presence of HDL. Therefore, transferring Shh from exosome membranes to HDL or Scube may confer additional diffusion range or mobility. Additionally, Scube2-Shh signaling complexes have been reported to undergo a relay to mediate reception and pathway activation: Scube2 transfers Shh to Cdo/Boc co-receptors, Cdo/Boc transfer Shh to Gas1, Gas1 transfers Shh to Ptch1 for pathway activation (Wier-

bowski et al., 2020). Another possibility is that Scube or HDL carriers in the extracellular space may increase the transfer of Shh from Dispatched-positive exosomes to reception machinery on receiving cells. Future work will be needed to determine if and what fraction of Shh-bound exosomes also carry Dispatched proteins and if these Shh-positive, Dispatched-positive exosomes confer differential signaling intensity or increased signaling range.

Overall, exosome release may act as a central secretion strategy for Shh-mediated tissue patterning by integrating other modes of transport, such as cytonemes or other extracellular carriers, to modulate the distance, intensity, or reception of signaling.

3.6 Extracellular vesicles serve as broad mediators of cell-cell signaling in both development and disease

Broad roles of EV packaging and secretion during developmental signaling

Many morphogens and developmental signaling molecules are hydrophilic (e.g., Bmp and Fgf) and disperse across a tissue using either simple diffusion or internal cytoneme transport (Pomreinke et al., 2017; Yu et al., 2009). Hence, the role of EVs may seem limited during development. However, a growing body of work suggests EVs may be a primary method of transporting membrane-associated signals long-range.

Similar to Hh, Wnts are posttranslationally modified by the covalent attachment of palmitoleic acid which confer a high degree of membrane tethering and hydrophobicity (Takada et al., 2006). Therefore, Wnt and Hh ligands share similar biophysical challenges in forming long-range gradients during tissue patterning. Accordingly, Wnt ligands have been reported to be dispersed by both carrier-assisted diffusion and cytoneme transport mechanisms. At the plasma membrane transmembrane, Wnt-less proteins promote release and transfer of Wnt ligands to extracellular carrier proteins sFRZ and WIF1, or serum factors (lipoproteins or Afamin), for diffusion across the hydrophilic extracellular space (de Almeida Magalhaes et al., 2024; Panáková et al., 2005; Neumann et al., 2009). This is highly analogous to

transmembrane Dispatched proteins handing off Hh ligands to Scube proteins or HDL for extracellular diffusion. Wnt ligands also have been reported to be transported along cytonemes across invertebrates and vertebrates alike Huang and Kornberg; Stanganello et al.. Lastly, Wnt ligands are secreted on exosomes in both human cells and in the *Drosophila* wing disc, often alongside Wntless (Gross et al., 2012; Działo et al., 2019). As Wnt signal dispersal reportedly uses the same diffusive and direct transport mechanisms as Hh signaling, I argue that exosome secretion may equally serve as a central secretion mechanism that fluctuates between extracellular diffusion and cytoneme transport to modulate signaling distance.

Notch signaling is another key signaling pathway that promotes cell fate decisions in development. Unlike classical morphogens, both Notch receptors and Notch ligands, such as Delta, Serrate, Lag2, and Jagged are transmembrane proteins, so the manner of their signaling has been assumed to occur exclusively through juxtacrine signaling in adjacent cells. For example, Notch receptor- Notch ligand interaction between adjacent cells can drive differential cell fates through a process called lateral inhibition (Bray, 2016). However, there is growing evidence that long-range Notch signaling exists. First, it was demonstrated that Notch receptors and ligands can localize to cytonemes that can mediate signaling across multiple cell diameters (Cohen et al., 2010; Huang and Kornberg, 2015). Second, recent reports have also shown that both Notch receptors and ligands are found localized to the membranes of extracellular vesicles (Giannandrea et al., 2022; Sheldon et al., 2010). Future work should look at the differential signaling ranges of cytoneme-mediated and EV-mediated Notch signaling.

Although my thesis work investigated the mechanisms of exosomes and cytonemes in Shh signaling, many of my conclusions can likely extend to any membrane-associated signaling molecule during development.

Roles of EV packaging and secretion during homeostasis and disease

Beyond embryogenesis, EVs are widely used to mediate cell-cell signaling during inflam-

mation, obesity and cancer (Kalluri and McAndrews, 2023). Cytokines represent a broad class of signaling proteins, including interleukins, interferons, TNFa, and chemokines, that are secreted by immune and non-immune cells to regulate inflammation. For instance, M1-type macrophages secrete EVs loaded with TNF-α, CXCL9 and CXCL10 that induce inflammatory responses in melanoma cells (Mäki-Mantila et al., 2026). Cytokines include standard hydrophilic signaling proteins (e.g., IL-6, IL-2), leaderless or cytosolic proteins (e.g., IL-1β, IL-18), and transmembrane proteins (e.g., TNF-α), all of which can be secreted on EVs. This suggests that EVs are used in much broader contexts beyond just membrane-associated signaling molecules.

Similar to organizing centers in tissue patterning, cancer cells have to modulate signaling across different length scales and across tissue types. Specifically, cancer cells use autocrine signaling to promote self-proliferation and survival and use paracrine signaling to manipulate the tumor microenvironment and drive metastasis(Yang et al., 2023; Li et al., 2025). Cancer-derived EVs mediate signaling in all of these steps. Cancer-derived EVs package miRNAs, cytokines, and re-purposed morphogens (Chideriotis et al., 2025). For example, in hepatocellular carcinoma (HCC), the most common form of primary liver cancer, Shh is secreted on EVs that directly promote tumorigenesis (Li et al., 2021). Additionally, numerous studies have described the roles of cytonemes and other F-actin cellular protrusions (e.g., tunneling nanotubes) in facilitating signaling between tumor cells and between tumor cells and the tumor microenvironment (Mahdi and Hall, 2026). Thus, my findings which describe the roles of Shh-bound exosomes diffusion and cytoneme transport may provide significant insights in how cancer cells modulate the range of signal dispersal.

EVs based secretion can provide key advantages over traditional secretion.

Through my work and the arguments posed in this chapter, exosomes, and extracellular vesicles as a whole, appear to be essential in mediating many forms of cell communication. EVs provide a couple advantages over conventional secretion.

First, packaging of signaling molecules in EVs provides additional protection against degradation. This is supported by evidence showing that freely soluble cytokines secreted by placental cells were degraded at a much higher rate than cytokines encapsulated in secreted EVs from the same cells (Fitzgerald et al., 2018). In the context of developmental patterning, increasing the stability of morphogens, through protection from degradation, could also have dramatic effects on shaping the size of morphogen gradients.

Second, both exosomal and ectosomal biogenesis can concentrate the primary signal, associated membrane proteins, and cytosolic factors to create a concentrated and modular form of signaling. In terms of signaling potency, EVs can act as discrete packets of variable amounts of ligand. Notably, synthetically packaging ligands in engineered EVs can increase the signaling potential 100 fold compared with soluble monomeric ligands (Staufer et al., 2022). Furthermore, EVs can selectively package regulatory RNAs that could either modulate the function of the primary signaling protein or provide an entirely separate signaling function. For instance, Shh-bound exosomes secreted in two distinct pools have different compositions of miRNAs which can alter whether Shh signaling promotes morphogenetic or mitogenic functions in the developing neural tube (Vyas et al., 2014; Walvekar et al., 2025).

Lastly, the composition of transmembrane proteins on EVs may have many modulatory effects on signaling. For example, the inclusion of Dispatched proteins on Hh-bound exosomes may increase the signaling distance, while integrins may promote cytoneme binding and transport. In addition, based on the composition of receptors and transmembrane proteins found on their surface, EVs have a natural tendency for specific cell type targeting (Turturici et al., 2015).

Due to their potential for stable, selective, and modulatory signaling capacity, engineering EVs with select protein signals and RNA species is rapidly growing as a potential delivery-based therapeutic avenue. Future work investigating the regulation of EV biogenesis, cargo sorting, and extracellular dispersal will provide invaluable biological and clinical insights.

APPENDIX A

SYNTHETIC CYTONEME MANIPULATION AND THE ROLE OF CYTONEMES IN SKELETAL PATTERNING OF THE LIMB

A.1 Preface

This appendix describes my preliminary work testing synthetic cytoneme manipulation tools with the aim of characterizing the contribution of cytonemes in Shh-mediated tissue patterning in the limb. A highly specific cytoneme perturbation method is required to precisely probe their function. Therefore, I tested the functionality of the recently developed Artificial Transport Vehicles (ATVs) in inhibiting cytoneme formation in primary limb bud mesenchymal cells, and I present preliminary findings on the effects of ATV-mediated cytoneme inhibition on skeletal patterning in the chicken limb.

Attributions

The cloning of the ATV- tool was performed by Timothy Sanders. The sequence of Myosin10-Tail was gifted from Richard Cheney.

A.2 Introduction

In metazoans, cell communication is essential to coordinate cellular behaviors over space and time including, proliferation, differentiation, migration, and morphogenesis. Morphogens are signaling molecules that disperse across tissues forming concentration gradients, and promote changes in cellular behavior based on concentration. Thus, morphogens are key regulators of tissue patterning. Although passive diffusion has served as the traditional model to explain how morphogens can disperse over a tissue to form a gradient, some morphogens have biophysical limitations in diffusion and, more generally, there are key concerns about the precision of diffusive mechanisms in patterning. A growing body of work shows that

cells can project specialized signaling filopodia, or cytonemes, to deliver morphogens directly through stable cell-cell connections (Kornberg, 2014).

In the limb bud, a small region in the posterior margin of the mesenchyme known as the Zone of Polarizing Activity (ZPA) acts as a signaling center that produces and disperses Sonic Hedgehog (Shh) across the limb bud to pattern the anterior-posterior axis of the limb and indirectly promote outgrowth along the proximal distal axis (Riddle et al., 1993; Niswander et al., 1994). Both Shh-expressing ZPA cells and Shh-receiving anterior limb bud cells, project long cytonemes that can form stable connections with each other (Sanders et al., 2013). Shh puncta are transported along cytonemes in the ZPA ,and the Shh co-receptors Cdo and Boc are enriched along cytonemes in the receiving cells. However, whether cytonemes are required for Shh-mediated patterning remains unknown.

Cytonemes are specialized filopodia comprised of unidirectional bundles of F-actin, and most methods used to test their function rely on gross manipulation of actin regulators or the actin cytoskeleton itself (Yamashita et al., 2018; Bischoff et al., 2013; Patel et al., 2022). However, the actin cytoskeleton plays numerous essential roles in the cell, including cell division and migration, so these manipulations can have unwanted pleiotropic effects on cell biology and development beyond cytoneme formation. Thus, probing the roles of cytonemes in Shh-mediated tissue patterning requires a filopodia-specific manipulation method.

A recent study engineered filopodial manipulation tools called Artificial Transport Vehicles or ATVs that use highly processive, tetramerically engineered myosin motors to shuttle actin regulators along filopodia (Zhang et al., 2021). ATVs are composed of a myosin head domain, a spectrin repeats, a tetramerization domain (GCN4-pLI coiled coil), and a GFP-Binding Protein (GBP) to bind any GFP-tagged cargo (Figure A.1A). Myosin-XI motor heads can transport GFP-tagged cargo towards the tips of filopodia (ATV+), whereas Myosin-XI motor heads can transport GFP-tagged cargo towards the cell body or depleting cargo from filopodia. Co-expressing plasmids encoding ATV- and a EGFP-tagged Myosin-

10 tail (EGFP-Myosin10-Tail), a filopodial motor domain that binds actin bundlers, can dramatically reduce filopodia formation. Thus, this synthetic tool can be used to probe the roles of cytonemes during tissue patterning.

Here, I tested whether ATV- can modulate cytoneme formation in the limb bud mesenchyme and used it to investigate the role of cytonemes in limb patterning and development. In primary limb bud mesenchymal cells (PLMCs) the ATV- tool could deplete Boc-EGFP from its standard localization in cytonemes. Additionally, co-expression of ATV- and EGFP-Myosin10-Tail in PLMCs significantly reduced the number of cytonemes per cell. In ovo electroporation of both constructs into the limb bud mesenchyme, produced a broad range of skeletal defects and a general, yet small, reduction in zeugopod and autopod element lengths at embryonic day 10. However, control limb buds electroporated with pm-mKate2 alone had cases of skeletal deformities, so the overall conclusions of these ATV-cytoneme perturbation experiments remain inconclusive.

A.3 Results and Discussion

A.3.1 ATV- can deplete GFP-tagged cargo from PLMC cytonemes

In previous reports, the ATV- tool was effectively used in C3H/10T1/2 fibroblasts, IPSC-derived neurons, and in regenerating axolotl limbs (Zhang et al., 2021). First, I tested whether ATV- could efficiently deplete GFP-tagged cargo from cytonemes in primary limb bud mesenchymal cells (PLMCs). Since the Shh coreceptor Boc is highly enriched along limb bud mesenchymal cytonemes (Sanders et al., 2013), I assumed it would serve as a convincing test of the ATV-. I first electroporated PLMCs with plasmids encoding palmitoylated mKate2 (pm-mKate2) to label the cell membrane including cytonemes and Boc-EGFP. Similar to what was observed in vivo, Boc-EGFP is highly enriched along PLMC cytonemes in punctate-like domains (Figure A.1B, top). However, Boc-EGFP was essentially absent

from cytonemes in PLMCs that coexpressed ATV- (Figure A.1B, bottom). This result demonstrated that the ATV- tool efficiently pulls GFP-tagged cargo away from cytonemes in PLMCs.

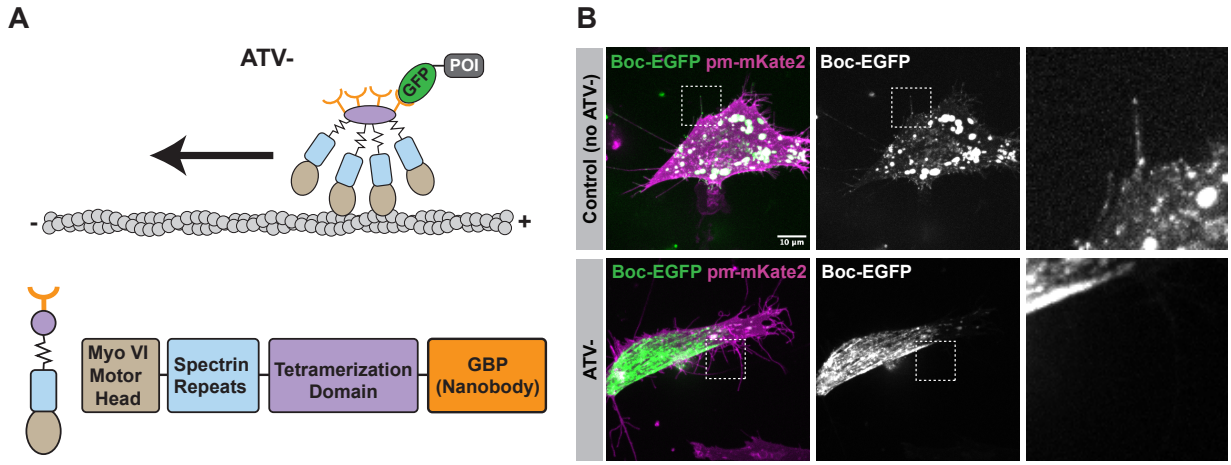


Figure A.1: ATV- can pull GFP-tagged cargo to the minus end of cytonemes. (A) Diagram of the ATV- tool. (B) Top panels depict micrographs of a PLMC expressing Boc-EGFP and pm-mKate2. The bottom panels depict micrographs of a PLMC expressing Boc-EGFP, pm-mKate2, and ATV-. The white dashed boxes highlight cytonemes for each condition and are magnified to the far right panel of each.

A.3.2 ATV- and EGFP-Myosin10-Tail coexpression can greatly reduce cytoneme formation in PLMCs

Next, I wanted to determine if the coexpression of ATV- and EGFP-Myosin10-Tail could inhibit cytoneme formation in PLMCs. So I electroporated PLMCs with plasmids encoding pm-mKate2, ATV-, and EGFP-Myosin10-Tail or just pm-mKate2 and ATV- alone as a negative control and quantified the number of cytonemes per cell (Figure A.2A). In the negative control condition, PLMCs projected roughly 25 cytonemes per cell on average, whereas the coexpression of ATV- and EGFP-Myosin10-Tail caused a dramatic reduction of cytonemes to roughly 10 per cell on average (Figure A.2B). Thus, coexpression of ATV- and EGFP-Myosin10-Tail provide a powerful synthetic approach to specifically reduce cytonemes

in limb bud mesenchymal cells.

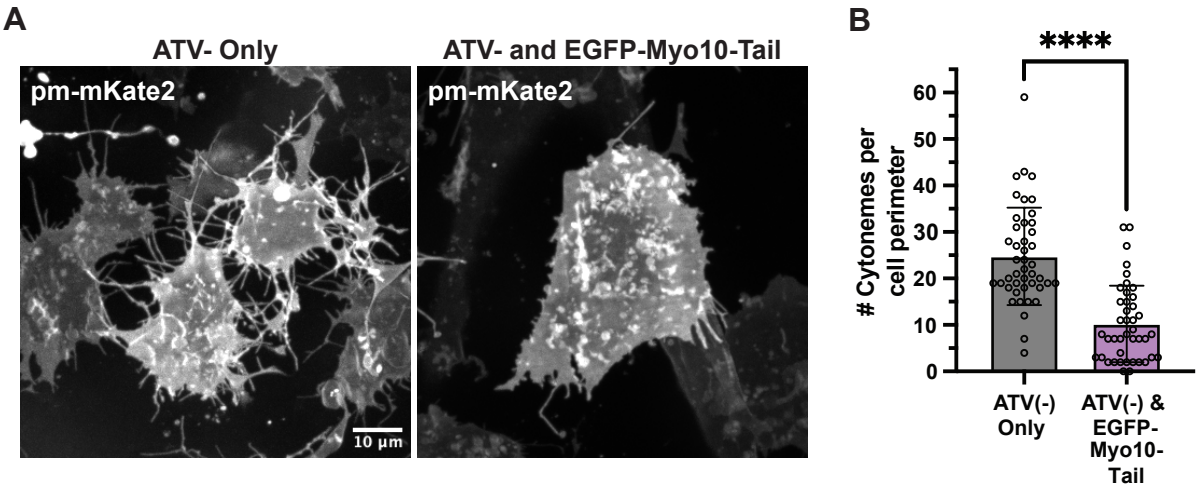


Figure A.2: ATV- and EGFP-Myosin10-Tail coexpression in PLMCs reduces cytoneme formation. (A) Representative micrographs of PLMCs expressing either pm-mKate2 and ATV- (left) or pm-mKate2, ATV-, and EGFP-Myosin10-Tail. (B) Quantification of the number of cytonemes per cell perimeter (n= 44 ATV- only control cells and n = 42 ATV- and EGFP-Myosin10-Tail cells, pooled from 2 independent experiments). Significance testing was performed using two tailed Mann-Whitney U-test with p-values represented by: n.s. = $p > 0.05$, $* = p \leq 0.05$; $** = p \leq 0.01$; $*** = p \leq 0.001$, $**** = p \leq 0.0001$.

A.3.3 Cytoneme loss of function in the limb bud in vivo causes variable skeletal defects

To test if cytonemes play a functional role in limb bud patterning, I electroporated the limb bud mesenchyme in ovo at hamburger hamilton stage 14 (roughly 50 hours of incubation) with either piggybac compatible plasmids encoding the ATV-, pm-mKate2, EGFP-Myosin10-Tail or just pm-mKate as a negative control. The following day I screened embryos by visually selecting limb buds with high pm-mKate2 expression as a proxy for electroporation efficiency. I then returned eggs to the incubator, and let the embryos develop until embryonic day 10. On day 10, I removed embryos, fixed, and performed alcian blue cartilage staining to label the cartilaginous elements of the limb skeleton.

As Shh-/- mice still possess a humerus (Chiang et al., 2001), I screened for defects in autopod and zeugopod skeletal elements, specifically losses of an element, in both conditions. Here, I found that 7/10 ATV- electroporated limb buds developed skeletal defects, while only 2/6 control electroporated limb buds developed defects (Figure A.3A). The skeletal defects in the ATV- electroporated limb buds ranged from loss of digit 1 to loss of a digit and either radius or ulna (Figure A.3B). The specificity of skeletal deformities were difficult to determine as the identity of each element was obscured by defects. However, for elements that remained intact with clear identity, I measured the lengths along the proximal distal axis and compared them with the unelectroporated contralateral wing elements. Here, I noticed that even in appropriately patterned skeletal elements, the lengths of each element were reduced compared to the unelectroporated control (Figure A.3C). This suggested that the cytoneme reductions in the limb bud not only caused defects in patterning, but likely reduced either cell proliferation or caused increased cell death.

Although ATV- limbs display skeletal defects, I am cautious about drawing biological conclusions for a few reasons. First, the cytoneme loss of function was constitutive from E2 through E10. Although the genetic manipulation was mosaic, constant inhibition of cytoneme production for such a prolonged period may affect multiple aspects of development outside of Shh-mediated signaling. Second, the broad variability of skeletal defects observed in the ATV- limbs does not point to a reproducible phenotype that can be accurately quantified. Third, although the control electroporation caused skeletal defects in a lower frequency, the defects seen suggest that electroporation alone can cause ill-effects such as cell death that can impact development. Fourth, skeletal development is affected by more than Shh signaling alone (Yang, 2009), thus it serves as a somewhat indirect readout on the role of cytonemes in Shh-mediated tissue patterning.

Future work will need to be directed at some of the issues listed above. Regardless of experimental setup, a larger sample size is needed to better determine trends in any

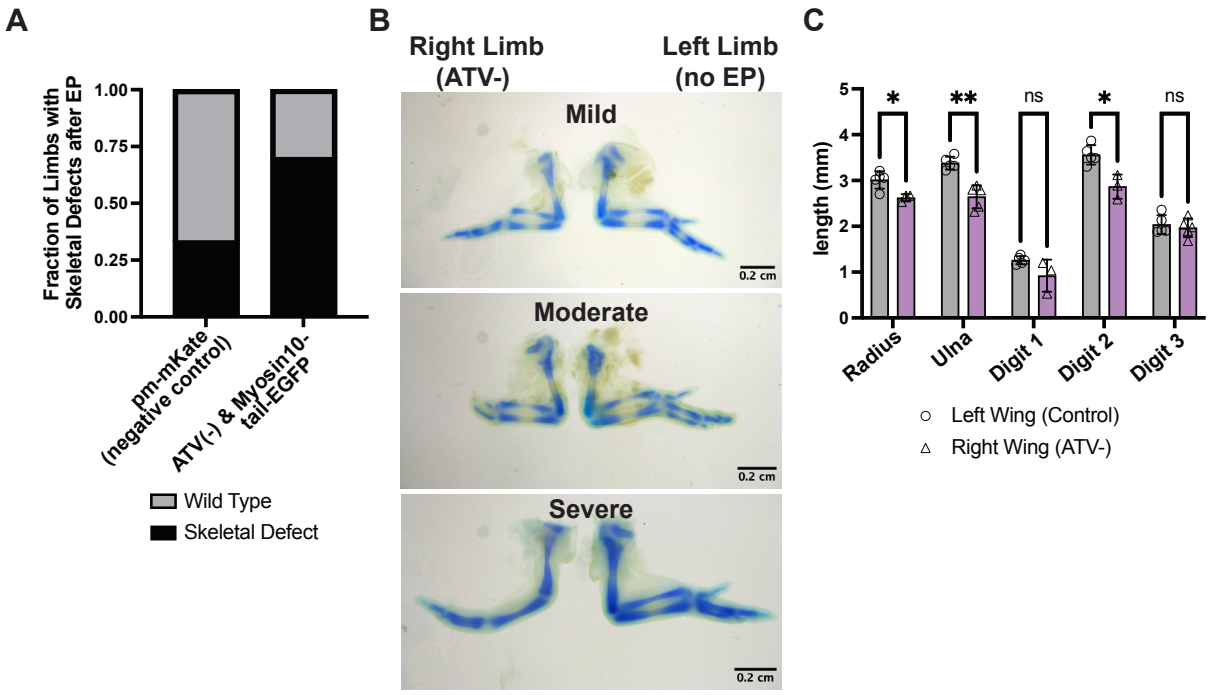


Figure A.3: ATV- mediated cytoneme inhibition causes variable skeletal defects in the limb. (A) Quantification of the fraction of limbs with skeletal elements (zeugopod and autopod) between control and cytoneme-loss of function electroporations (n = 6 pm-mKate2 negative control limbs, n = 10 ATV- and EGFP-Myosin10-Tail electroporated limbs, pooled from 2 independent experiments). (B) Representative micrographs of common skeletal defects in ATV-, EGFP-Myosin10-Tail electroporated limbs. In each image the leftmost limb represents the electroporated limb, while the rightmost represents the contralateral unelectroporated limb from the same embryo. (C) Quantification of identifiable skeletal element lengths between ATV- electroporated right limbs and unelectroporated left limb controls. Significance testing was performed using multiple unpaired T-tests with p-values represented by: n.s. = $p > 0.05$, $* = p \leq 0.05$; $** = p \leq 0.01$; $*** = p \leq 0.001$, $**** = p \leq 0.0001$.

phenotype observed. As the skeletal staining readout is somewhat indirect, biologically time consuming and highly variable, future phenotypical readouts should be designed to assay for changes in the intensity and expression pattern of key Shh target genes via hybridization chain reaction (HCR) or similar in situ hybridization methods. Lastly, more conservative electroporation parameters should be used to limit any unintentional cell death.

Overall, the use of ATVs in synthetically modifying cytonemes during tissue patterning and development is highly promising, yet considerable optimization will be required before

they can be used to accurately determine the role of cytonemes in Shh-mediated tissue patterning of the limb.

A.4 Materials and Methods

Experimental Models

Chicken embryos were obtained and cared for as described in Chapter 2. PLMCs were harvested and cultured as described in Chapter 2.

Plasmid and DNA Constructs

For genetic integration of DNA constructs for extended expression in cell culture and in limb buds in vivo, we utilized the piggyBac transposition system. Recombination Gateway cloning was used to create specific expression vectors. General cloning methods were performed as described in Chapter 2.

To label the plasma membrane and cytonemes in PMCs, we expressed a palmitoylated mKate2 fluorescent protein. For constitutive expression used in PLMCs, we used APX1-pm-mKate2 (Addgene # 245521). For doxycycline inducible expression used in vivo, we subcloned pm-mKate2 into the APX2 vector using Gateway recombination.

The ATV- construct was designed in reference to the original manuscript to include the MyoVI motor head, Spectrin repeats, a flexible linker, an engineered tetramerization domain from the coiled coil GCN4-pLI, a flexible linker, and a GFP nanobody sequence. This DNA construct was subcloned into a pENTR-D-TOPO vector for Gateway-mediated recombination into either APX3 (for use in vitro) or APX4 (for use in vivo).

The EGFP-Myosin10-Tail construct was gifted from Richard Cheney. The Myosin10-Tail is composed of the PH domains, MyTH4 domain, and FERM domain of Bos taurus Myosin10. EGFP was added to the N-terminus of the Myosin10-Tail and was subcloned into

APX1 using Gateway mediated recombination.

The Boc-EGFP construct was created by fusing EGFP-STOP cassette to the C-terminus of the coding sequence of murine Boc (STOP codon deleted). Boc-EGFP was subcloned into APX2 using Gateway mediated recombination.

In Vitro and In Ovo Electroporation of Genetic Constructs

The parameters and protocol of in vitro and in ovo electroporations were performed as described in Chapter 2.

Alcian Blue Cartilage Staining

Dissection and Fixation

I removed chicken embryos from incubation at embryonic day 10. I dissected the embryos in PBS (Sigma Aldrich) and removed the heads using sterilized dissection scissors. I rinsed the embryos twice in clean PBS and transferred them to a 50 ml conical tube of 4% paraformaldeyde in PBS (Electron Microscopy Sciences) to fix overnight at 4 °C. Embryos were washed three times in PBS for 30 minutes each and once overnight at 4 °C.

Dehydration and Alcian Blue Staining

I shifted the Chicken embryos to a dehydration series. I transferred the embryos to a 25% Ethanol solution for 4 hours, then transferred them to a 50% Ethanol solution for 4 hours and finally transferred them to a 70% Ethanol solution overnight at room temperature. I then transferred the embryos to an Acetic Ethanol solution made of 30% Glacial Acetic Acid (Sigma Aldrich) and 70% Ethanol for 4 hours at room temperature. Finally, I stained the embryos in an Alcian Blue Solution made of 40 mg Alcian Blue 8X powder (Sigma Aldrich) dissolved in 100 ml of Acetic Ethanol solution overnight at room temperature. To destain, I transferred the embryos to the Acetic Ethanol solution for overnight incubation.

Rehydration and Clearing

I then shifted the embryos into a rehydration series with 4 hour incubations in: 70% ethanol, 50% ethanol, and 25% ethanol. Then I transferred them to pure ddH20 and incubate overnight or until they sink. For clearing, I transferred the embryos to a solution of 2% KOH (Sigma Aldrich) in ddH20 for 4 hours. Then I shifted the embryos through 24 hour incubations in a series of 0.5% KOH to 80% glycerol solutions: 3 parts KOH to 1 part glycerol, 1 part KOH to 1 part glycerol, 1 part KOH to 3 parts glycerol, 1 part glycerol. Once this clearing process is complete, I imaged the embryos and limbs using brightfield imaging.

Microscopy

Confocal imaging was performed as described in Chapter 2. Brightfield images of Alcian blue stained limbs were captured using a Leica M205FA motorized fluorescence stereomicroscope with a Prior Metal Halide light source for the ability to visualize multiple fluorescent wavelengths and a Leica Color Camera coupled with Leica LAS software for documentation.

A.4.1 Image Analysis and Quantification

FIJI/ImageJ was used to process all image data for analysis and display. Brightness and contrast was adjusted as needed. Plot generation and significance testing were performed using GraphPad Prism.

To quantify cytoneme numbers for PLMCs expressing pm-mKate2, I performed maximum intensity projections on z-stacks and used the line segment and measure tool in FIJI to hand measure and count each filopodia along the perimeter of each cell. Significance testing was performed using a two-tailed Mann-Whitney U-test.

To screen for skeletal defects, I manually marked each missing zeugopod and autopod element and tried to assign which element was missing based on morphology when possible. For all clearly distinguishable skeletal elements, I used the line segment and measure tool in

FIJI to quantify the lengths of each element in the ATV- electroporated limb versus in its contralateral non-electroporated control limb. Significance testing for each skeletal element was performed using multiple unpaired T-tests.

The asterisks in each figure graph correspond to the following p-values: n.s. $= p > 0.05$, $* = p \leq 0.05$; $** = p \leq 0.01$; $*** = p \leq 0.001$, $**** = p \leq 0.0001$.

REFERENCES

A. L. Altick, L. M. Baryshnikova, T. Q. Vu, and C. S. von Bartheld. Quantitative analysis of multivesicular bodies (MVBs) in the hypoglossal nerve: Evidence that neurotrophic factors do not use MVBs for retrograde axonal transport. *Journal of Comparative Neurology*, 514 (6):641–657, 2009. doi:10.1002/cne.22047.

C. Arshadi, U. Günther, M. Eddison, K. I. S. Harrington, and T. A. Ferreira. SNT: a unifying toolbox for quantification of neuronal anatomy. *Nature Methods*, 18, 2021. doi:10.1038/s41592-021-01105-7.

A. L. Arthur, A. Crawford, A. Houdusse, and M. A. Titus. VASP-mediated actin dynamics activate and recruit a filopodia myosin. *eLife*, 10:e68082, 2021.

Verena A Bachmann, Johanna E Mayrhofer, Ronit Ilouz, Philipp Tschaikner, Philipp Raffeiner, Ruth Röck, Mathieu Courcelles, Federico Apelt, Tsan-Wen Lu, George S Baillie, Pierre Thibault, Pia Aanstad, Ulrich Stelzl, Susan S Taylor, and Eduard Stefan. Gpr161 anchoring of PKA consolidates GPCR and cAMP signaling. *Proceedings of the National Academy of Sciences*, 113(28):7786–7791, jul 2016. doi:10.1073/pnas.1608061113. URL `https://doi.org/10.1073/pnas.1608061113`.

Nikolaos Balaskas, Ana Ribeiro, Jasmina Panovska, Eric Dessaud, Noriaki Sasai, Karen M Page, James Briscoe, and Vanessa Ribes. Gene regulatory logic for reading the Sonic Hedgehog signaling gradient in the vertebrate neural tube. *Cell*, 148(1-2):273–284, jan 2012. ISSN 1097-4172 (Electronic). doi:10.1016/j.cell.2011.10.047.

Francesca Balordi and Gord Fishell. Hedgehog signaling in the subventricular zone is required for both the maintenance of stem cells and the migration of newborn neurons. *The Journal of neuroscience : the official journal of the Society for Neuroscience*, 27(22):5936–5947, may 2007. ISSN 1529-2401 (Electronic). doi:10.1523/JNEUROSCI.1040-07.2007.

Alejandro M. Barbieri, Sebastian Fernandez-Pol, Christine Hunker, Bruce H. Horazdovsky, and Philip D. Stahl. Role of Rab5 in EGF receptor-mediated signal transduction. *European Journal of Cell Biology*, 83(6):305–314, 2004.

M. Barna and L. Niswander. Visualization of cartilage formation: Insight into cellular properties of skeletal progenitors and chondrodysplasia syndromes. *Developmental Cell*, 12(6):931–941, 2007. doi:10.1016/j.devcel.2007.04.016.

K A Barth, Y Kishimoto, K B Rohr, C Seydler, S Schulte-Merker, and S W Wilson. Bmp activity establishes a gradient of positional information throughout the entire neural plate. *Development (Cambridge, England)*, 126(22):4977–4987, nov 1999. ISSN 0950-1991 (Print). doi:10.1242/dev.126.22.4977.

K Basler and G Struhl. Compartment boundaries and the control of Drosophila limb pattern by hedgehog protein. *Nature*, 368(6468):208–214, mar 1994. ISSN 0028-0836 (Print). doi:10.1038/368208a0.

M Albert Basson. Signaling in cell differentiation and morphogenesis. *Cold Spring Harbor perspectives in biology*, 4(6), jun 2012. ISSN 1943-0264 (Electronic). doi:10.1101/cshperspect.a008151.

M. P. Bebelman, P. Bun, S. Huveneers, G. van Niel, D. M. Pegtel, and F. J. Verweij. Real-time imaging of multivesicular body – plasma membrane fusion to quantify exosome release from single cells. *Nature Protocols*, 15, 2020. doi:10.1038/s41596-019-0245-4.

Karen Beckett, Solange Monier, Lucy Palmer, Cyrille Alexandre, Hannah Green, Eric Bonneil, Graca Raposo, Pierre Thibault, Roland Le Borgne, and Jean-Paul Vincent. Drosophila S2 cells secrete wingless on exosome-like vesicles but the wingless gradient forms independently of exosomes. *Traffic (Copenhagen, Denmark)*, 14(1):82–96, jan 2013. ISSN 1600-0854 (Electronic). doi:10.1111/tra.12016.

Soumaya Ben-Aicha, Lina Badimon, and Gemma Vilahur. Advances in HDL: Much More than Lipid Transporters. *International journal of molecular sciences*, 21(3), jan 2020. ISSN 1422-0067 (Electronic). doi:10.3390/ijms21030732.

Marcus Bischoff, Ana Citlali Gradilla, Irene Seijo, Germán Andrés, Carmen Rodríguez-Navas, Laura González-Méndez, and Isabel Guerrero. Cytonemes are required for the establishment of a normal Hedgehog morphogen gradient in Drosophila epithelia. *Nature Cell Biology*, 15(11):1269–1281, 2013. ISSN 14657392. doi:10.1038/ncb2856.

M J Bitgood, L Shen, and A P McMahon. Sertoli cell signaling by Desert hedgehog regulates the male germline. *Current biology : CB*, 6(3):298–304, mar 1996. ISSN 0960-9822 (Print). doi:10.1016/s0960-9822(02)00480-3.

B. E. Bobick, P. G. Alexander, and R. S. Tuan. High efficiency transfection of embryonic limb mesenchyme with plasmid DNA using square wave pulse electroporation and sucrose buffer. *BioTechniques*, 56(2):85–89, 2014. doi:10.2144/000114136.

G. Boncompain, S. Divoux, N. Gareil, H. De Forges, A. Lescure, L. Latreche, V. Mercanti, F. Jollivet, G. Raposo, and F. Perez. Synchronization of secretory protein traffic in populations of cells. *Nature Methods*, 9(5):493–498, 2012. doi:10.1038/nmeth.1928.

Caroline Bonnans, Jonathan Chou, and Zena Werb. Remodelling the extracellular matrix in development and disease. *Nature reviews. Molecular cell biology*, 15(12):786–801, dec 2014. ISSN 1471-0080 (Electronic). doi:10.1038/nrm3904.

Dimitris Bourikas, Vladimir Pekarik, Thomas Baeriswyl, Asa Grunditz, Rejina Sadhu, Michele Nardó, and Esther T Stoeckli. Sonic hedgehog guides commissural axons along the longitudinal axis of the spinal cord. *Nature neuroscience*, 8(3):297–304, mar 2005. ISSN 1097-6256 (Print). doi:10.1038/nn1396.

Sarah J Bray. Notch signalling in context. *Nature Reviews Molecular Cell Biology*, 17(11): 722–735, 2016. ISSN 1471-0080. doi:10.1038/nrm.2016.94. URL `https://doi.org/10.1038/nrm.2016.94`.

James Briscoe and Stephen Small. Morphogen rules: design principles of gradient-mediated embryo patterning. *Development*, 142(23):3996–4009, 2015. doi:10.1242/dev.129452. URL https://journals.biologists.com/dev/article/142/23/3996/47124/Morphogen-rules-design-principles-of-gradient.

James Briscoe, Alessandra Pierani, Thomas M Jessell, and Johan Ericson. A homeodomain protein code specifies progenitor cell identity and neuronal fate in the ventral neural tube. *Cell*, 101(4):435–445, 2000. ISSN 0092-8674. doi:https://doi.org/10.1016/S0092-8674(00)80853-3. URL https://www.sciencedirect.com/science/article/pii/S0092867400808533.

Richard Burke, Denise Nellen, Manolo Bellotto, Ernst Hafen, Kirsten-André Senti, Barry J. Dickson, and Konrad Basler. Dispatched, a novel sterol-sensing domain protein dedicated to the release of cholesterol-modified hedgehog from signaling cells. *Cell*, 99(7):803–815, 1999. ISSN 0092-8674. doi:https://doi.org/10.1016/S0092-8674(00)81677-3. URL https://www.sciencedirect.com/science/article/pii/S0092867400816773.

Sara Busatto, Yubo Yang, Dalila Iannotta, Irina Davidovich, Yeshayahu Talmon, and Joy Wolfram. Considerations for extracellular vesicle and lipoprotein interactions in cell culture assays., apr 2022. ISSN 2001-3078 (Electronic).

Edit I Buzás, Eszter Á Tóth, Barbara W Sódar, and Katalin É Szabó-Taylor. Molecular interactions at the surface of extracellular vesicles. *Seminars in immunopathology*, 40(5): 453–464, sep 2018. ISSN 1863-2300 (Electronic). doi:10.1007/s00281-018-0682-0.

Eva Cai, Jingyi Zhang, and Xuecai Ge. Control of the Hedgehog pathway by compartmentalized PKA in the primary cilium. *Science China. Life sciences*, 65(3):500–514, mar 2022. ISSN 1869-1889 (Electronic). doi:10.1007/s11427-021-1975-9.

Ainhoa Callejo, Aphrodite Bilioni, Emanuela Mollica, Nicole Gorfinkiel, Germán Andrés, Carmen Ibáñez, Carlos Torroja, Laura Doglio, Javier Sierra, and Isabel Guerrero. Dispatched mediates Hedgehog basolateral release to form the long-range morphogenetic gradient in the Drosophila wing disk epithelium. *Proceedings of the National Academy of Sciences of the United States of America*, 108(31):12591–12598, 2011. ISSN 00278424. doi:10.1073/pnas.1106881108.

Jordi Cayuso, Fausto Ulloa, Barny Cox, James Briscoe, and Elisa Martí. The Sonic hedgehog pathway independently controls the patterning,proliferation and survival of neuroepithelial cells by regulating Gli activity. *Development*, 133(3):517–528, feb 2006. ISSN 0950-1991. doi:10.1242/dev.02228. URL https://doi.org/10.1242/dev.02228.

C. E. Chamberlain, J. Jeong, C. Guo, B. L. Allen, and A. P. McMahon. Notochord-derived Shh concentrates in close association with the apically positioned basal body in neural target cells and forms a dynamic gradient during neural patterning. *Development*, 135(6): 1097–1106, 2008. doi:10.1242/dev.013086.

Frédéric Charron, Elke Stein, Juhee Jeong, Andrew P McMahon, and Marc Tessier-Lavigne. The morphogen sonic hedgehog is an axonal chemoattractant that collaborates with netrin-1 in midline axon guidance. *Cell*, 113(1):11–23, apr 2003. ISSN 0092-8674 (Print). doi:10.1016/s0092-8674(03)00199-5.

Yu Chen and Gary Struhl. Dual Roles for Patched in Sequestering and Transducing Hedgehog. *Cell*, 87(3):553–563, nov 1996. ISSN 0092-8674. doi:10.1016/S0092-8674(00)81374-4. URL https://doi.org/10.1016/S0092-8674(00)81374-4.

C Chiang, Y Litingtung, E Lee, K E Young, J L Corden, H Westphal, and P A Beachy. Cyclopia and defective axial patterning in mice lacking Sonic hedgehog gene function. *Nature*, 383(6599):407–413, oct 1996. ISSN 0028-0836 (Print). doi:10.1038/383407a0.

Chin Chiang, Ying Litingtung, Matthew P Harris, B.Kay Simandl, Yina Li, Philip A Beachy, and John F Fallon. Manifestation of the Limb Prepattern: Limb Development in the Absence of Sonic Hedgehog Function. *Developmental Biology*, 236(2):421–435, 2001. ISSN 0012-1606. doi:https://doi.org/10.1006/dbio.2001.0346. URL https://www.sciencedirect.com/science/article/pii/S001216060190346X.

Stavros Chideriotis, Alkmini T. Anastasiadi, Vassilis L. Tzounakas, Sotirios P. Fortis, Alexandros G. Kriebardis, and Serena Valsami. Morphogens and cell-derived structures (exosomes and cytonemes) as components of the communication between cells. *International Journal of Molecular Sciences*, 26(2):725, 2025. doi:10.3390/ijms26020725.

A M Clark, K K Garland, and L D Russell. Desert hedgehog (Dhh) gene is required in the mouse testis for formation of adult-type Leydig cells and normal development of peritubular cells and seminiferous tubules. *Biology of reproduction*, 63(6):1825–1838, dec 2000. ISSN 0006-3363 (Print). doi:10.1095/biolreprod63.6.1825.

Emanuele Cocucci and Jacopo Meldolesi. Ectosomes and exosomes: shedding the confusion between extracellular vesicles. *Trends in Cell Biology*, 25(6):364–372, jun 2015. ISSN 0962-8924. doi:10.1016/j.tcb.2015.01.004. URL https://doi.org/10.1016/j.tcb.2015.01.004.

Michael Cohen, Marios Georgiou, Nicola L Stevenson, Mark Miodownik, and Buzz Baum. Dynamic Filopodia Transmit Intermittent Delta-Notch Signaling to Drive Pattern Refinement during Lateral Inhibition. *Developmental Cell*, 19(1):78–89, jul 2010. ISSN 1534-5807. doi:10.1016/j.devcel.2010.06.006. URL https://doi.org/10.1016/j.devcel.2010.06.006.

Michael Cohen, Anna Kicheva, Ana Ribeiro, Robert Blassberg, Karen M Page, Chris P Barnes, and James Briscoe. Ptch1 and Gli regulate Shh signalling dynamics via multiple mechanisms. *Nature Communications*, 6(1):6709, 2015. ISSN 2041-1723. doi:10.1038/ncomms7709. URL https://doi.org/10.1038/ncomms7709.

Michael E Coulter, Cristina M Dorobantu, Gerrald A Lodewijk, François Delalande, Sarah Cianferani, Vijay S Ganesh, Richard S Smith, Elaine T Lim, C Shan Xu, Song Pang,

Eric T Wong, Hart G W Lidov, Monica L Calicchio, Edward Yang, Dilenny M Gonzalez, Thorsten M Schlaeger, Ganeshwaran H Mochida, Harald Hess, Wei-Chung Allen Lee, Maria K Lehtinen, Tomas Kirchhausen, David Haussler, Frank M J Jacobs, Raphael Gaudin, and Christopher A Walsh. The ESCRT-III Protein CHMP1A Mediates Secretion of Sonic Hedgehog on a Distinctive Subtype of Extracellular Vesicles. *Cell Reports*, 24 (4):973–986.e8, jul 2018. ISSN 2211-1247. doi:10.1016/j.celrep.2018.06.100. URL `https://doi.org/10.1016/j.celrep.2018.06.100`.

Francis Crick. Diffusion in Embryogenesis. *Nature*, 225(5231):420–422, 1970. ISSN 1476-4687. doi:10.1038/225420a0. URL `https://doi.org/10.1038/225420a0`.

P H Crossley, G Minowada, C A MacArthur, and G R Martin. Roles for FGF8 in the induction, initiation, and maintenance of chick limb development. *Cell*, 84(1):127–136, jan 1996. ISSN 0092-8674 (Print). doi:10.1016/s0092-8674(00)80999-x.

A. Dady, L. Davidson, N. Loyer, S. Rappich, G. M. Findlay, T. Sanders, J. Januschke, and K. G. Storey. Engineering fluorescent reporters in human pluripotent stem cells and strategies for live imaging human neurogenesis. *Development*, 152(21):dev205082, 2025. doi:10.1242/dev.205082.

Gabriel D Dakubo, Chantal Mazerolle, Marosh Furimsky, Chuan Yu, Benoit St-Jacques, Andrew P McMahon, and Valerie A Wallace. Indian hedgehog signaling from endothelial cells is required for sclera and retinal pigment epithelium development in the mouse eye. *Developmental biology*, 320(1):242–255, aug 2008. ISSN 1095-564X (Electronic). doi:10.1016/j.ydbio.2008.05.528.

Christina A Daly, Eric T Hall, and Stacey K Ogden. Regulatory mechanisms of cytoneme-based morphogen transport. *Cellular and molecular life sciences : CMLS*, 79(2):119, feb 2022. ISSN 1420-9071 (Electronic). doi:10.1007/s00018-022-04148-x.

G. D'Angelo, T. Matusek, S. Pizette, and P. P. Thérond. Endocytosis of Hedgehog through Dispatched regulates long-range signaling. *Developmental Cell*, 32(3):290–303, 2015. doi:10.1016/j.devcel.2014.12.004.

Taciani de Almeida Magalhaes, Jingjing Liu, Charlene Chan, Kleiton Silva Borges, Jiuchun Zhang, Andrew J Kane, Bradley M Wierbowski, Yunhui Ge, Zhiwen Liu, Prabhath Mannam, Daniel Zeve, Ron Weiss, David T Breault, Pengxiang Huang, and Adrian Salic. Extracellular carriers control lipid-dependent secretion, delivery, and activity of WNT morphogens. *Developmental Cell*, 59(2):244–261.e6, 2024. ISSN 1534-5807. doi:https://doi.org/10.1016/j.devcel.2023.11.027. URL `https://www.sciencedirect.com/science/article/pii/S1534580723006482`.

Andrés Dekanty and Marco Milán. The interplay between morphogens and tissue growth. *EMBO reports*, 12(10):1003–1010, sep 2011. ISSN 1469-3178 (Electronic). doi:10.1038/embor.2011.172.

A. M. DeLise, E. Stringa, W. A. Woodward, M. A. Mello, and R. S. Tuan. Embryonic limb mesenchyme micromass culture as an in vitro model for chondrogenesis and cartilage maturation. *Methods in molecular biology (Clifton, N.J.)*, 137:359–375, 2000. ISSN 10643745. doi:10.1385/1-59259-066-7:359.

Iman Dilower, Asef J Niloy, Vishnu Kumar, Ayushi Kothari, Eun Bee Lee, and M A Karim Rumi. Hedgehog Signaling in Gonadal Development and Function. *Cells*, 12(3), jan 2023. ISSN 2073-4409 (Electronic). doi:10.3390/cells12030358.

J. L. Dinneen and B. P. Ceresa. Expression of dominant negative Rab5 in HeLa cells regulates endocytic trafficking distal from the plasma membrane. *Experimental Cell Research*, 294: 509–522, 2004. doi:10.1016/j.yexcr.2003.12.006.

Hans Driesch. Entwicklungsmechanisiche Studien, I. Der Werth der beiden ersten FurchungszeHen in der Echino-dermentwicklung. Experimentelle Erzeugen von Theil-und Doppelbildung. *Zeitschr. wissenschaft. ZooL*, 53:160–184, 1891.

W Driever and C Nüsslein-Volhard. The bicoid protein determines position in the Drosophila embryo in a concentration-dependent manner. *Cell*, 54(1):95–104, jul 1988a. ISSN 0092-8674 (Print). doi:10.1016/0092-8674(88)90183-3.

W Driever, V Siegel, and C Nüsslein-Volhard. Autonomous determination of anterior structures in the early Drosophila embryo by the bicoid morphogen. *Development (Cambridge, England)*, 109(4):811–820, aug 1990. ISSN 0950-1991 (Print). doi:10.1242/dev.109.4.811.

Wolfgang Driever and Christiane Nüsslein-Volhard. A gradient of bicoid protein in Drosophila embryos. *Cell*, 54(1):83–93, 1988b. ISSN 00928674. doi:10.1016/0092-8674(88)90182-1.

Julien Dubrulle and Olivier Pourquié. fgf8 mrna decay establishes a gradient that couples axial elongation to patterning in the vertebrate embryo. *Nature*, 427(6973):419–422, 2004. doi:10.1038/nature02216. URL `https://www.nature.com/articles/nature02216`.

Michael A Dyer, Sarah M Farrington, Deanna Mohn, James R Munday, and Margaret H Baron. Indian hedgehog activates hematopoiesis and vasculogenesis and can respecify prospective neurectodermal cell fate in the mouse embryo. *Development*, 128(10):1717–1730, may 2001. ISSN 0950-1991. doi:10.1242/dev.128.10.1717. URL `https://doi.org/10.1242/dev.128.10.1717`.

Edyta Działo, Michał Rudnik, Roman I. Koning, Jakub Czepiel, Gariella Kania, Natalia Łabędźek, Zenon P. Czuba, Marek Sanak, and Przemysław Błyszczuk. Wnt3a and wnt5a transported by exosomes activate wnt signaling pathways in human cardiac fibroblasts. *International Journal of Molecular Sciences*, 20(6):1436, Mar 2019. doi:10.3390/ijms20061436. URL `https://doi.org`.

Y Echelard, D J Epstein, B St-Jacques, L Shen, J Mohler, J A McMahon, and A P McMahon. Sonic hedgehog, a member of a family of putative signaling molecules, is implicated in the

regulation of CNS polarity. *Cell*, 75(7):1417–1430, dec 1993. ISSN 0092-8674 (Print). doi:10.1016/0092-8674(93)90627-3.

James R Edgar, Paul T Manna, Shinichi Nishimura, George Banting, and Margaret S Robinson. Tetherin is an exosomal tether. *eLife*, 5:e17180, 2016. ISSN 2050-084X. doi:10.7554/eLife.17180. URL https://doi.org/10.7554/eLife.17180.

Holly R Eggington, Eoghan J Mulholland, and Simon J Leedham. Morphogen regulation of stem cell plasticity in intestinal regeneration and carcinogenesis. *Developmental Dynamics*, 251(1):61–74, jan 2022. ISSN 1058-8388. doi:https://doi.org/10.1002/dvdy.434. URL https://doi.org/10.1002/dvdy.434.

Erez Eitan, Ronald S Petralia, Ya-Xian Wang, Fred E Indig, Mark P Mattson, and Pamela J Yao. Probing extracellular Sonic hedgehog in neurons. *Biology Open*, 5(8):1086–1092, jul 2016. ISSN 2046-6390. doi:10.1242/bio.019422. URL https://doi.org/10.1242/bio.019422.

J. F. Fallon, A. Lopez, M. A. Ros, M. P. Savage, B. B. Olwin, and B. K. Simandl. Fgf-2: apical ectodermal ridge growth signal for chick limb development. *Science*, 264(5155):104–107, 1994. doi:10.1126/science.7908145. URL https://pubmed.ncbi.nlm.nih.gov/7908145/.

Pershang Farshi, Stefanie Ohlig, Ute Pickhinke, Susanne Höing, Katja Jochmann, Roger Lawrence, Rita Dreier, Tabea Dierker, and Kay Grobe. Dual roles of the Cardin-Weintraub motif in multimeric Sonic hedgehog. *The Journal of biological chemistry*, 286(26):23608–23619, jul 2011. ISSN 1083-351X (Electronic). doi:10.1074/jbc.M110.206474.

D. M. Fekete and C. L. Cepko. Replication-competent retroviral vectors encoding alkaline phosphatase reveal spatial restriction of viral gene expression / transduction in the chick embryo. *Molecular and Cellular Biology*, 13(4):2604–2613, 1993.

M Fernandez-Teran, M E Piedra, I S Kathiriya, D Srivastava, J C Rodriguez-Rey, and M A Ros. Role of dHAND in the anterior-posterior polarization of the limb bud: implications for the Sonic hedgehog pathway. *Development (Cambridge, England)*, 127(10):2133–2142, may 2000. ISSN 0950-1991 (Print). doi:10.1242/dev.127.10.2133.

Anna Ferrer-Vaquer, Manuel Viotti, and Anna-Katerina Hadjantonakis. Transitions between epithelial and mesenchymal states and the morphogenesis of the early mouse embryo. *Cell adhesion & migration*, 4(3):447–457, 2010. ISSN 1933-6926 (Electronic). doi:10.4161/cam.4.3.10771.

W. Fitzgerald, M. L. Freeman, M. M. Lederman, J. Vasquez, and et al. A system of cytokines encapsulated in extracellular vesicles. *Scientific Reports*, 8(1):8973, 2018. doi:10.1038/s41598-018-27190-x. URL https://nature.com.

Christian Frantz, Kathleen M Stewart, and Valerie M Weaver. The extracellular matrix at a glance. *Journal of cell science*, 123(Pt 24):4195–4200, dec 2010. ISSN 1477-9137 (Electronic). doi:10.1242/jcs.023820.

I. Fujiwara, M. E. Zweifel, N. Courtemanche, and T. D. Pollard. Latrunculin A accelerates actin filament depolymerization in addition to sequestering actin monomers. *Current Biology*, 28(19):3183–3192.e2, 2018. doi:10.1016/j.cub.2018.07.082.

Mirco Galiè. Mesenchymal Traits as an Intrinsic Feature of Undifferentiated Cells. *Journal of developmental biology*, 13(1), dec 2024. ISSN 2221-3759 (Electronic). doi:10.3390/jdb13010001.

Antonella Galli, Dimitri Robay, Marco Osterwalder, Xiaozhong Bao, Jean-Denis Bénazet, Muhammad Tariq, Renato Paro, Susan Mackem, and Rolf Zeller. Distinct Roles of Hand2 in Initiating Polarity and Posterior Shh Expression during the Onset of Mouse Limb Bud Development. *PLOS Genetics*, 6(4):e1000901, apr 2010. URL `https://doi.org/10.1371/journal.pgen.1000901`.

Raluca E Ghebosu, Lawrence Hui, and Joy Wolfram. Increasing the biomolecular relevance of cell culture practice. *Journal of biomedical science*, 32(1):3, jan 2025. ISSN 1423-0127 (Electronic). doi:10.1186/s12929-024-01095-6.

Domenica Giannandrea, Natalia Platonova, Michela Colombo, Matteo Mazzola, Valentina Citro, Raffaella Adami, et al. Extracellular vesicles mediate the communication between multiple myeloma and bone marrow microenvironment in a notch dependent way. *Haematologica*, 107(9):2183, 2022.

Theresa V Gibney and Ariel M Pani. FGF diffusion is required for directed migration of postembryonic muscle progenitors in C. elegans. *Development*, 152(18):dev204802, sep 2025. ISSN 0950-1991. doi:10.1242/dev.204802. URL `https://doi.org/10.1242/dev.204802`.

A Gierer and H Meinhardt. A theory of biological pattern formation. *Kybernetik*, 12(1): 30–39, 1972. ISSN 1432-0770. doi:10.1007/BF00289234. URL `https://doi.org/10.1007/BF00289234`.

Greta Giordano-Attianese, Pablo Gainza, Elise Gray-Gaillard, Elisabetta Cribioli, Sailan Shui, Seonghoon Kim, Mi Jeong Kwak, Sabrina Vollers, Angel De Jesus Corria Osorio, Patrick Reichenbach, Jaume Bonet, Byung Ha Oh, Melita Irving, George Coukos, and Bruno E. Correia. A computationally designed chimeric antigen receptor provides a small-molecule safety switch for T-cell therapy. *Nature Biotechnology*, 38(4):426–432, 2020. ISSN 15461696. doi:10.1038/s41587-019-0403-9. URL `http://dx.doi.org/10.1038/s41587-019-0403-9`.

Sarah C Goetz and Kathryn V Anderson. The primary cilium: a signalling centre during vertebrate development. *Nature reviews. Genetics*, 11(5):331–344, may 2010. ISSN 1471-0064 (Electronic). doi:10.1038/nrg2774.

L V Goodrich, R L Johnson, L Milenkovic, J A McMahon, and M P Scott. Conservation of the hedgehog/patched signaling pathway from flies to mice: induction of a mouse patched

gene by Hedgehog. *Genes & development*, 10(3):301–312, feb 1996. ISSN 0890-9369 (Print). doi:10.1101/gad.10.3.301.

Ana-Citlali Gradilla and Isabel Guerrero. Chapter One - Hedgehog on track: Long-distant signal transport and transfer through direct cell-to-cell contact. In Thomas B T Current Topics in Developmental Biology Kornberg, editor, *Cell-Cell Signaling in Development*, volume 150, pages 1–24. Academic Press, 2022. ISBN 0070-2153. doi:https://doi.org/10.1016/bs.ctdb.2022.03.002. URL https://www.sciencedirect.com/science/article/pii/S007021532200045X.

Ana Citlali Gradilla, Esperanza González, Irene Seijo, German Andrés, Marcus Bischoff, Laura González-Mendez, Vanessa Sánchez, Ainhoa Callejo, Carmen Ibáñez, Milagros Guerra, João Ramalho Ortigão-Farias, James D. Sutherland, Monika González, Rosa Barrio, Juan M. Falcón-Pérez, and Isabel Guerrero. Exosomes as Hedgehog carriers in cytoneme-mediated transport and secretion. *Nature Communications*, 5, 2014. ISSN 20411723. doi:10.1038/ncomms6649.

Ana-Citlali Gradilla, Eléanor Simon, Gustavo Aguilar, and Isabel Guerrero. From intra- to extracellular vesicles: extracellular vesicles in developmental signalling. *Essays in Biochemistry*, 62(2):215–223, may 2018. ISSN 0071-1365. doi:10.1042/EBC20180001. URL https://doi.org/10.1042/EBC20180001.

Jeremy B.A. Green and James Sharpe. Positional information and reaction-diffusion: Two big ideas in developmental biology combine. *Development (Cambridge)*, 142(7):1203–1211, apr 2015. ISSN 14779129. doi:10.1242/dev.114991. URL https://dev.biologists.org/content/142/7/1203https://dev.biologists.org/content/142/7/1203.abstract.

Amel Gritli-Linde, Paula Lewis, Andrew P McMahon, and Anders Linde. The Whereabouts of a Morphogen: Direct Evidence for Short- and Graded Long-Range Activity of Hedgehog Signaling Peptides. *Developmental Biology*, 236(2):364–386, 2001. ISSN 0012-1606. doi:https://doi.org/10.1006/dbio.2001.0336. URL https://www.sciencedirect.com/science/article/pii/S0012160601903367.

Julia Christina Gross, Varun Chaudhary, Kerstin Bartscherer, and Michael Boutros. Active Wnt proteins are secreted on exosomes. *Nature Cell Biology*, 14(10):1036–1045, 2012. ISSN 1476-4679. doi:10.1038/ncb2574. URL https://doi.org/10.1038/ncb2574.

Vandana K. Grover, J. Gerardo Valadez, Aaron B. Bowman, and Michael K. Cooper. Lipid modifications of Sonic hedgehog ligand dictate cellular reception and signal response. *PLoS ONE*, 6(7), 2011. ISSN 19326203. doi:10.1371/journal.pone.0021353.

J B Gurdon, A Mitchell, and D Mahony. Direct and continuous assessment by cells of their position in a morphogen gradient. *Nature*, 376(6540):520–521, 1995. ISSN 1476-4687. doi:10.1038/376520a0. URL https://doi.org/10.1038/376520a0.

C. M. Gustafson, J. Roffers-Agarwal, and L. S. Gammill. Chick cranial neural crest cells release extracellular vesicles that are critical for their migration. *Journal of Cell Science*, 135(12):jcs260272, 2022. doi:10.1242/jcs.260272.

H. T. Haigler, J. A. McKanna, and S. Cohen. Direct visualization of the binding and internalization of a ferritin conjugate of epidermal growth factor in human carcinoma cells A-431. *Journal of Cell Biology*, 81(2):382–395, 1979.

Eric T. Hall, Miriam E. Dillard, Daniel P. Stewart, Yan Zhang, Ben Wagner, Rachel M. Levine, Shondra M. Pruett-Miller, April Sykes, Jamshid Temirov, Richard E. Cheney, Motomi Mori, Camenzind G. Robinson, and Stacey K. Ogden. Cytoneme delivery of sonic hedgehog from ligand-producing cells requires myosin 10 and a dispatched-boc/cdon co-receptor complex. *eLife*, 10:e61432, 2021. doi:10.7554/eLife.61432. URL `https://doi.org/10.7554/eLife.61432`.

Eric T Hall, Miriam E Dillard, Elizabeth R Cleverdon, Yan Zhang, Christina A Daly, Shariq S Ansari, Randall Wakefield, Daniel P Stewart, Shondra M Pruett-Miller, Alfonso Lavado, Alex F Carisey, Amanda Johnson, Yong-Dong Wang, Emma Selner, Michael Tanes, Young Sang Ryu, Camenzind G Robinson, Jeffrey Steinberg, and Stacey K Ogden. Cytoneme signaling provides essential contributions to mammalian tissue patterning. *Cell*, 187(2):276–293.e23, jan 2024. ISSN 1097-4172 (Electronic). doi:10.1016/j.cell.2023.12.003.

V. Hamburger and H. L. Hamilton. A series of normal stages in the development of the chick embryo. *Journal of Morphology*, 88(1), 1951.

Qing Fang Han, Wen Jia Li, Kai Shun Hu, Jie Gao, Wen Long Zhai, Jing Hua Yang, and Shui Jun Zhang. Exosome biogenesis: machinery, regulation, and therapeutic implications in cancer. *Molecular Cancer*, 21(1):1–26, 2022. ISSN 14764598. doi:10.1186/s12943-022-01671-0. URL `https://doi.org/10.1186/s12943-022-01671-0`.

John T Happ, Corvin D Arveseth, Jessica Bruystens, Daniela Bertinetti, Isaac B Nelson, Cristina Olivieri, Jingyi Zhang, Danielle S Hedeen, Ju-Fen Zhu, Jacob L Capener, Jan W Bröckel, Lily Vu, C C King, Victor L Ruiz-Perez, Xuecai Ge, Gianluigi Veglia, Friedrich W Herberg, Susan S Taylor, and Benjamin R Myers. A PKA inhibitor motif within SMOOTHENED controls Hedgehog signal transduction. *Nature structural & molecular biology*, 29(10):990–999, oct 2022. ISSN 1545-9985 (Electronic). doi:10.1038/s41594-022-00838-z.

Brian D Harfe, Paul J Scherz, Sahar Nissim, Haiming Tian, Andrew P McMahon, and Clifford J Tabin. Evidence for an expansion-based temporal shh gradient in specifying vertebrate digit identities. *Cell*, 118(4):517–528, 2004. doi:10.1016/j.cell.2004.07.024.

Yoshinori Hirano, Taiki Hatano, Aya Takahashi, Michinori Toriyama, Naoyuki Inagaki, and Toshio Hakoshima. Structural basis of cargo recognition by the myosin-X MyTH4-FERM domain. *EMBO Journal*, 30(13):2734–2747, 2011. ISSN 02614189. doi:10.1038/emboj.2011.177. URL `http://dx.doi.org/10.1038/emboj.2011.177`.

Alexander M Holtz, Kevin A Peterson, Yuichi Nishi, Steves Morin, Jane Y Song, Frédéric Charron, Andrew P McMahon, and Benjamin L Allen. Essential role for ligand-dependent feedback antagonism of vertebrate hedgehog signaling by PTCH1, PTCH2 and HHIP1 during neural patterning. *Development (Cambridge, England)*, 140(16):3423–3434, aug 2013. ISSN 1477-9129 (Electronic). doi:10.1242/dev.095083.

Bo Hu, Juan J Rodriguez, Anurag Kakkerla Balaraju, Yuanyuan Gao, Nhan T Nguyen, Heston Steen, Saeb Suhaib, Songhai Chen, and Fang Lin. Glypican 4 mediates Wnt transport between germ layers via signaling filopodia. *Journal of Cell Biology*, 220(12): e202009082, sep 2021. ISSN 0021-9525. doi:10.1083/jcb.202009082. URL `https://doi.org/10.1083/jcb.202009082`.

Diane Hu and Jill A. Helms. The role of sonic hedgehog in normal and abnormal craniofacial morphogenesis. *Development*, 126(21):4873–4884, 11 1999. ISSN 0950-1991. doi:10.1242/dev.126.21.4873. URL `https://doi.org/10.1242/dev.126.21.4873`.

Hai Huang and Thomas B Kornberg. Myoblast cytonemes mediate Wg signaling from the wing imaginal disc and Delta-Notch signaling to the air sac primordium. *eLife*, 4:e06114, 2015. ISSN 2050-084X. doi:10.7554/eLife.06114. URL `https://doi.org/10.7554/eLife.06114`.

Ilse Hurbain, Anne-Sophie Macé, Maryse Romao, Elodie Prince, Lucie Sengmanivong, Laurent Ruel, Renata Basto, Pascal P Thérond, Graça Raposo, and Gisela D'Angelo. Microvilli-derived extracellular vesicles carry Hedgehog morphogenic signals for *Drosophila* wing imaginal disc development. *Current Biology*, 32(2):361–373.e6, jan 2022. ISSN 0960-9822. doi:10.1016/j.cub.2021.11.023. URL `https://doi.org/10.1016/j.cub.2021.11.023`.

Luisa Izzi, Martin Lévesque, Steves Morin, Dominique Laniel, Brian C Wilkes, Frédéric Mille, Robert S Krauss, Andrew P McMahon, Benjamin L Allen, and Frédéric Charron. Boc and Gas1 each form distinct Shh receptor complexes with Ptch1 and are required for Shh-mediated cell proliferation. *Developmental cell*, 20(6):788–801, jun 2011. ISSN 1878-1551 (Electronic). doi:10.1016/j.devcel.2011.04.017.

Jin Jiang and Chi-Chung Hui. Hedgehog signaling in development and cancer. *Developmental cell*, 15(6):801–812, dec 2008. ISSN 1878-1551 (Electronic). doi:10.1016/j.devcel.2008.11.010.

Jennifer L Johnson, Mahalakshmi Ramadass, Jing He, Steven J Brown, Jinzhong Zhang, Lusine Abgaryan, Nikolaos Biris, Evripidis Gavathiotis, Hugh Rosen, and Sergio D Catz. Identification of Neutrophil Exocytosis Inhibitors (Nexinhibs), Small Molecule Inhibitors of Neutrophil Exocytosis and Inflammation: DRUGGABILITY OF THE SMALL GTPase Rab27a. *The Journal of biological chemistry*, 291(50):25965–25982, dec 2016. ISSN 1083-351X (Electronic). doi:10.1074/jbc.M116.741884.

G Jürgens, E Wieschaus, C Nüsslein-Volhard, and H Kluding. Mutations affecting the pattern of the larval cuticle inDrosophila melanogaster : II. Zygotic loci on the third chromosome. *Wilhelm Roux's archives of developmental biology*, 193(5):283–295, sep 1984. ISSN 0340-0794 (Print). doi:10.1007/BF00848157.

Raghu Kalluri and Kathleen M McAndrews. The role of extracellular vesicles in cancer. *Cell*, 186(8):1610–1626, apr 2023. ISSN 1097-4172 (Electronic). doi:10.1016/j.cell.2023.03.010.

Yasuhiro Kawai, Junko Noguchi, Kouyou Akiyama, Yuriko Takeno, Yasuhiro Fujiwara, Shimpei Kajita, Takehito Tsuji, Kazuhiro Kikuchi, Hiroyuki Kaneko, and Tetsuo Kunieda. A missense mutation of the Dhh gene is associated with male pseudohermaphroditic rats showing impaired Leydig cell development. *Reproduction (Cambridge, England)*, 141(2): 217–225, feb 2011. ISSN 1741-7899 (Electronic). doi:10.1530/REP-10-0006.

T. Kawakami, T. N. Kawcak, Y. Li, W. Zhang, Y. Hu, and P. Chuang. Mouse dispatched mutants fail to distribute hedgehog proteins and are defective in hedgehog signaling. *Development*, 129(24):5753–5765, 2002. doi:10.1242/dev.00178.

Meng-Tsen Ke and Takeshi Imai. Optical Clearing and Index Matching of Tissue Samples for High-resolution Fluorescence Imaging Using SeeDB2. *Bio-protocol*, 8(20):e3046, 2018. ISSN 2331-8325. doi:10.21769/BioProtoc.3046. URL `https://doi.org/10.21769/BioProtoc.3046`.

Anna Kicheva, Periklis Pantazis, Tobias Bollenbach, Yannis Kalaidzidis, Thomas Bittig, Frank Jülicher, and Marcos González-Gaitán. Kinetics of morphogen gradient formation. *Science*, 315(5811):521–525, 2007. doi:10.1126/science.1135774. URL `https://www.science.org/doi/10.1126/science.1135774`.

Maia Kinnebrew, Giovanni Luchetti, Ria Sircar, Sara Frigui, Lucrezia Vittoria Viti, Tomoki Naito, Francis Beckert, Yasunori Saheki, Christian Siebold, Arun Radhakrishnan, and Rajat Rohatgi. Patched 1 reduces the accessibility of cholesterol in the outer leaflet of membranes. *eLife*, 10:e70504, 2021. doi:10.7554/eLife.70504. URL `https://elifesciences.org/articles/70504`.

Thomas B Kornberg. Cytonemes and the dispersion of morphogens. *Wiley interdisciplinary reviews. Developmental biology*, 3(6):445–463, 2014. ISSN 1759-7692 (Electronic). doi:10.1002/wdev.151.

Joanna Kowal, Mercedes Tkach, and Clotilde Théry. Biogenesis and secretion of exosomes. *Current Opinion in Cell Biology*, 29:116–125, 2014. ISSN 0955-0674. doi:https://doi.org/10.1016/j.ceb.2014.05.004. URL `https://www.sciencedirect.com/science/article/pii/S095506741400057X`.

Henry M Kronenberg. Developmental regulation of the growth plate. *Nature*, 423(6937): 332–336, 2003. ISSN 1476-4687. doi:10.1038/nature01657. URL `https://doi.org/10.1038/nature01657`.

Lucas Leclère, Markus Bause, Chiara Sinigaglia, Julia Steger, and Fabian Rentzsch. Development of the aboral domain in Nematostella requires β-catenin and the opposing activities of Six3/6 and Frizzled5/8. *Development (Cambridge, England)*, 143(10):1766–1777, may 2016. ISSN 1477-9129 (Electronic). doi:10.1242/dev.120931.

T Lecuit, W J Brook, M Ng, M Calleja, H Sun, and S M Cohen. Two distinct mechanisms for long-range patterning by Decapentaplegic in the Drosophila wing. *Nature*, 381(6581): 387–393, may 1996. ISSN 0028-0836 (Print). doi:10.1038/381387a0.

Jeffrey D Lee, Petra Kraus, Nicholas Gaiano, Susana Nery, Jhumku Kohtz, Gord Fishell, Cynthia A Loomis, and Jessica E Treisman. An Acylatable Residue of Hedgehog Is Differentially Required in Drosophila and Mouse Limb Development. *Developmental Biology*, 231(1):122–136, 2001. doi:10.1006/dbio.2001.0218.

Laura A Lettice, Simon J H Heaney, Lorna A Purdie, Li Li, Philippe de Beer, Ben A Oostra, Debbie Goode, Greg Elgar, Robert E Hill, and Esther de Graaff. A long-range Shh enhancer regulates expression in the developing limb and fin and is associated with preaxial polydactyly. *Human Molecular Genetics*, 12(14):1725–1735, jul 2003. ISSN 0964-6906. doi:10.1093/hmg/ddg180. URL `https://doi.org/10.1093/hmg/ddg180`.

J Lewis, J M Slack, and L Wolpert. Thresholds in development. *Journal of theoretical biology*, 65(3):579–590, apr 1977. ISSN 0022-5193 (Print). doi:10.1016/0022-5193(77)90216-8.

Paula M Lewis, Matthew P Dunn, Jill A McMahon, Malcolm Logan, James F Martin, Benoit St-Jacques, and Andrew P McMahon. Cholesterol Modification of Sonic Hedgehog Is Required for Long-Range Signaling Activity and Effective Modulation of Signaling by Ptc1. *Cell*, 105(5):599–612, jun 2001. ISSN 0092-8674. doi:10.1016/S0092-8674(01)00369-5. URL `https://doi.org/10.1016/S0092-8674(01)00369-5`.

Dongliang Li, Jianjian Sun, and Tao P Zhong. Wnt Signaling in Heart Development and Regeneration. *Current cardiology reports*, 24(10):1425–1438, oct 2022. ISSN 1534-3170 (Electronic). doi:10.1007/s11886-022-01756-8.

Li Li, Jing Zhao, Quanbao Zhang, and Zhengxin Wang. Cancer cell-derived exosomes promote hcc tumorigenesis through hedgehog pathway. *Frontiers in Oncology*, 11:756205, 2021. doi:10.3389/fonc.2021.756205. URL `https://www.frontiersin.org/journals/oncology/articles/10.3389/fonc.2021.756205/full`.

P. Li, J. S. Markson, S. Wang, S. Chen, V. Vachharajani, and M. B. Elowitz. Morphogen gradient reconstitution reveals Hedgehog pathway design principles. *Science*, 360(6388): 543–548, 2018.

Yina Li, Huimin Zhang, Ying Litingtung, and Chin Chiang. Cholesterol modification restricts the spread of Shh gradient in the limb bud. *Proceedings of the National Academy of Sciences*, 103(17):6548–6553, apr 2006. doi:10.1073/pnas.0600124103. URL `https://doi.org/10.1073/pnas.0600124103`.

Yongxing Li, Fengshuo Liu, Qingjin Cai, Lijun Deng, Qin Ouyang, Xiang H.-F. Zhang, and Ji Zheng. Invasion and metastasis in cancer: molecular insights and therapeutic targets. *Signal Transduction and Targeted Therapy*, 10(1):58, Feb 2025. doi:10.1038/s41392-025-02148-4. URL https://www.nature.com/articles/s41392-025-02148-4.

Xinhong Lim and Roel Nusse. Wnt signaling in skin development, homeostasis, and disease. *Cold Spring Harbor perspectives in biology*, 5(2), feb 2013. ISSN 1943-0264 (Electronic). doi:10.1101/cshperspect.a008029.

Yuh Charn Lin, Binay K. Sahoo, Shiang Shin Gau, and Ruey-Bing Yang. The biology of scube. *Journal of Biomedical Science*, 30(1):33, 2023. doi:10.1186/s12929-023-00925-3. URL https://doi.org/10.1186/s12929-023-00925-3.

Ying Litingtung, Randall D Dahn, Yina Li, John F Fallon, and Chin Chiang. Shh and Gli3 are dispensable for limb skeleton formation but regulate digit number and identity. *Nature*, 418(6901):979–983, aug 2002. ISSN 0028-0836 (Print). doi:10.1038/nature01033.

Yu Liu, Yun Peng, Peng-Gao Dai, Quan-Sheng Du, Lin Mei, and Wen-Cheng Xiong. Differential regulation of myosin X movements by its cargos, DCC and neogenin. *Journal of cell science*, 125(Pt 3):751–762, feb 2012. ISSN 1477-9137 (Electronic). doi:10.1242/jcs.094946.

K. J. Livak and T. D. Schmittgen. Analysis of relative gene expression data using real-time quantitative PCR and the $2^{-\Delta\Delta C_T}$ method. *Methods*, 25(4):402–408, 2001. doi:10.1006/meth.2001.1262.

Huaixi Luo, Hao Zhou, Shengyao Jiang, Chuan He, Ke Xu, Jinmei Ding, Jiajia Liu, Chao Qin, Kangchun Chen, Wenchuan Zhou, Liyuan Wang, Wenhao Yang, Wenqi Zhu, and He Meng. Gene Expression Profiling Reveals Potential Players of Sex Determination and Asymmetrical Development in Chicken Embryo Gonads, 2023.

Jiayue Ma, Honglin Yu, Shuo Yao, Yan Yan, Zhaoyu Gu, Ziqi Wang, Hai Huang, and Di Chen. Making cells inter-connected for signaling communication: a developmental view of cytonemes. *Cell communication and signaling : CCS*, 23(1):241, may 2025. ISSN 1478-811X (Electronic). doi:10.1186/s12964-025-02229-5.

Y. Ma, A. Erkner, R. Gong, S. Yao, J. Taipale, K. Basler, and P. A. Beachy. Hedgehog-mediated patterning of the mammalian embryo requires transporter-like function of Dispatched. *Cell*, 111(1):63–75, 2002.

Sheikh Faisal Asadullah Mahdi and Eric T. Hall. Emerging roles of cytoneme-mediated signaling in cancer. *International Journal of Molecular Sciences*, 27(17):7600, 2026. doi:10.3390/ijms27177600. URL https://www.mdpi.com/1422-0067/27/17/7600.

Randall K Mann and Philip A Beachy. Novel lipid modifications of secreted protein signals. *Annual review of biochemistry*, 73:891–923, 2004. ISSN 0066-4154 (Print). doi:10.1146/annurev.biochem.73.011303.073933.

Valeria Marigo, Robert A. Davey, Yi Zuo, James M. Cunningham, and Clifford J. Tabin. Biochemical evidence that patched is the hedgehog receptor. *Nature*, 384(6605):176–179, Nov 1996a. doi:10.1038/384176a0. URL https://www.nature.com/articles/384176a0.

Valeria Marigo, Randy L Johnson, Andrea Vortkamp, and Clifford J Tabin. Sonic hedgehog Differentially Regulates Expression ofGLIandGLI3during Limb Development. *Developmental Biology*, 180(1):273–283, 1996b. ISSN 0012-1606. doi:https://doi.org/10.1006/dbio.1996.0300. URL https://www.sciencedirect.com/science/article/pii/S0012160696903000.

Mathilde Mathieu, Nathalie Névo, Mabel Jouve, José Ignacio Valenzuela, Mathieu Maurin, Frederik J. Verweij, Roberta Palmulli, Danielle Lankar, Florent Dingli, Damarys Loew, Eric Rubinstein, Gaëlle Boncompain, Franck Perez, and Clotilde Théry. Specificities of exosome versus small ectosome secretion revealed by live intracellular tracking of CD63 and CD9. *Nature Communications*, 12(1), 2021. ISSN 20411723. doi:10.1038/s41467-021-24384-2. URL http://dx.doi.org/10.1038/s41467-021-24384-2.

M. E. Matlashov, D. M. Shcherbakova, J. Alvelid, M. Baloban, F. Pennacchietti, A. A. Shemetov, I. Testa, and V. V. Verkhusha. A set of monomeric near-infrared fluorescent proteins for multicolor imaging across scales. *Nature Communications*, 11(1):239, 2020. doi:10.1038/s41467-019-13897-6.

Benjamin Mattes, Yonglong Dang, Gediminas Greicius, Lilian Tamara Kaufmann, Benedikt Prunsche, Jakob Rosenbauer, Johannes Stegmaier, Ralf Mikut, Suat Özbek, Gerd Ulrich Nienhaus, Alexander Schug, David M Virshup, and Steffen Scholpp. Wnt/PCP controls spreading of Wnt/β-catenin signals by cytonemes in vertebrates. *eLife*, 7, jul 2018. ISSN 2050-084X (Electronic). doi:10.7554/eLife.36953.

David Q Matus, Craig R Magie, Kevin Pang, Mark Q Martindale, and Gerald H Thomsen. The Hedgehog gene family of the cnidarian, Nematostella vectensis, and implications for understanding metazoan Hedgehog pathway evolution. *Developmental biology*, 313(2): 501–518, jan 2008. ISSN 1095-564X (Electronic). doi:10.1016/j.ydbio.2007.09.032.

T. Matusek, F. Wendler, S. Polès, S. Pizette, G. D'Angelo, M. Fürthauer, and P. Thérond. The ESCRT machinery regulates the secretion and long-range activity of Hedgehog. *Nature*, 516(7529):99–103, 2014. doi:10.1038/nature13847.

Tamás Matusek, Julien Marcetteau, and Pascal P Thérond. Functions of Wnt and Hedgehog-containing extracellular vesicles in development and disease. *Journal of Cell Science*, 133 (18):jcs209742, sep 2020. ISSN 0021-9533. doi:10.1242/jcs.209742. URL https://doi.org/10.1242/jcs.209742.

Andrew P McMahon, Philip W Ingham, and Clifford J Tabin. Developmental roles and clinical significance of hedgehog signaling. *Current topics in developmental biology*, 53: 1–114, 2003. ISSN 0070-2153 (Print). doi:10.1016/s0070-2153(03)53002-2.

Caitlin McQueen and Matthew Towers. Establishing the pattern of the vertebrate limb. *Development*, 147(17):dev177956, sep 2020. ISSN 0950-1991. doi:10.1242/dev.177956. URL https://doi.org/10.1242/dev.177956.

Patrick Mehlen, Fréderic Mille, and Chantal Thibert. Morphogens and cell survival during development. *Journal of Neurobiology*, 64(4):357–366, sep 2005. ISSN 0022-3034. doi:https://doi.org/10.1002/neu.20167. URL https://doi.org/10.1002/neu.20167.

Felix A Mic, I Ovidiu Sirbu, and Gregg Duester. Retinoic acid synthesis controlled by Raldh2 is required early for limb bud initiation and then later as a proximodistal signal during apical ectodermal ridge formation. *The Journal of biological chemistry*, 279(25): 26698–26706, jun 2004. ISSN 0021-9258 (Print). doi:10.1074/jbc.M401920200.

Peter O Mulhair, Alessandro Pennati, Carlos Herrera-Ubeda, and Peter W H Holland. Revised evolutionary relationships within Brachycera and the early origin of bicoid in flies. *Current Biology*, 35(21):5308–5319.e3, 2025. ISSN 0960-9822. doi:https://doi.org/10.1016/j.cub.2025.09.051. URL https://www.sciencedirect.com/science/article/pii/S0960982225012515.

Patrick Müller, Katherine W Rogers, Shuizi R Yu, Michael Brand, and Alexander F Schier. Morphogen transport. *Development (Cambridge, England)*, 140(8):1621–1638, apr 2013. ISSN 1477-9129 (Electronic). doi:10.1242/dev.083519.

Vandhana Muralidharan-Chari, James Clancy, Carolyn Plou, Maryse Romao, Philippe Chavrier, Graca Raposo, and Crislyn D'Souza-Schorey. ARF6-regulated shedding of tumor cell-derived plasma membrane microvesicles. *Current biology : CB*, 19(22):1875–1885, dec 2009. ISSN 1879-0445 (Electronic). doi:10.1016/j.cub.2009.09.059.

Vandhana Muralidharan-Chari, James W Clancy, Alanna Sedgwick, and Crislyn D'Souza-Schorey. Microvesicles: mediators of extracellular communication during cancer progression. *Journal of cell science*, 123(Pt 10):1603–1611, may 2010. ISSN 1477-9137 (Electronic). doi:10.1242/jcs.064386.

Kaisa Mäki-Mantila et al. Extracellular vesicles derived from pro-inflammatory m1 macrophages induce an inflammatory and invasive phenotype in melanoma cells. *University of Eastern Finland / Research Portal*, 2026. URL https://researchportal.helsinki.fi/en/publications/extracellular-vesicles-derived-from-pro-inflammatory-m1-macrophag/.

Joseph Needham, Conrad Hal Waddington, and Dorothy Mary Moyle Needham. Physico-chemical experiments on the amphibian organizer. *Proceedings of the Royal Society of London. Series B, Containing Papers of a Biological Character*, 114(789):393–422, feb 1934. ISSN 0950-1193. doi:10.1098/rspb.1934.0014. URL https://doi.org/10.1098/rspb.1934.0014.

D Nellen, R Burke, G Struhl, and K Basler. Direct and long-range action of a DPP morphogen gradient. *Cell*, 85(3):357–368, may 1996. ISSN 0092-8674 (Print). doi:10.1016/s0092-8674(00)81114-9.

C J Neumann and S M Cohen. Long-range action of Wingless organizes the dorsal-ventral axis of the Drosophila wing. *Development (Cambridge, England)*, 124(4):871–880, feb 1997. ISSN 0950-1991 (Print). doi:10.1242/dev.124.4.871.

Sylvia Neumann, Damien Y M Coudreuse, Deneys R Van Der Westhuyzen, Erik R M Eckhardt, Hendrik C Korswagen, Gerd Schmitz, and Hein Sprong. Mammalian Wnt3a is Released on Lipoprotein Particles. *Traffic*, 10(3):334–343, mar 2009. ISSN 1398-9219. doi:https://doi.org/10.1111/j.1600-0854.2008.00872.x. URL `https://doi.org/10.1111/j.1600-0854.2008.00872.x`.

Charles Nicholson and Eva Syková. Extracellular space structure revealed by diffusion analysis. *Trends in Neurosciences*, 21(5):207–215, may 1998. ISSN 0166-2236. doi:10.1016/S0166-2236(98)01261-2. URL `https://doi.org/10.1016/S0166-2236(98)01261-2`.

Christof Niehrs. On growth and form: a Cartesian coordinate system of Wnt and BMP signaling specifies bilaterian body axes. *Development*, 137(6):845–857, mar 2010. ISSN 0950-1991. doi:10.1242/dev.039651. URL `https://doi.org/10.1242/dev.039651`.

E Nieuwenhuis and C-c Hui. Hedgehog signaling and congenital malformations. *Clinical genetics*, 67(3):193–208, mar 2005. ISSN 0009-9163 (Print). doi:10.1111/j.1399-0004.2004.00360.x.

L Niswander, C Tickle, A Vogel, I Booth, and G R Martin. FGF-4 replaces the apical ectodermal ridge and directs outgrowth and patterning of the limb. *Cell*, 75(3):579–587, nov 1993. ISSN 0092-8674 (Print). doi:10.1016/0092-8674(93)90391-3.

Lee Niswander, Susan Jeffrey, Gail R Martin, and Cheryll Tickle. A positive feedback loop coordinates growth and patterning in the vertebrate limb. *Nature*, 371(6498):609–612, 1994. ISSN 1476-4687. doi:10.1038/371609a0. URL `https://doi.org/10.1038/371609a0`.

C Nüsslein-Volhard and E Wieschaus. Mutations affecting segment number and polarity in Drosophila. *Nature*, 287(5785):795–801, oct 1980. ISSN 0028-0836 (Print). doi:10.1038/287795a0.

C Nüsslein-Volhard, E Wieschaus, and H Kluding. Mutations affecting the pattern of the larval cuticle inDrosophila melanogaster : I. Zygotic loci on the second chromosome. *Wilhelm Roux's archives of developmental biology*, 193(5):267–282, sep 1984. ISSN 0340-0794 (Print). doi:10.1007/BF00848156.

C Nüsslein-Volhard, H G Frohnhöfer, and R Lehmann. Determination of anteroposterior polarity in Drosophila. *Science (New York, N.Y.)*, 238(4834):1675–1681, dec 1987. ISSN 0036-8075 (Print). doi:10.1126/science.3686007.

Shinsuke Ohba. Hedgehog Signaling in Skeletal Development: Roles of Indian Hedgehog and the Mode of Its Action. *International Journal of Molecular Sciences*, 21(18), 2020. ISSN 1422-0067. doi:10.3390/ijms21186665. URL https://www.mdpi.com/1422-0067/21/18/6665.

D M Ornitz and N Itoh. Fibroblast growth factors. *Genome biology*, 2(3):REVIEWS3005, 2001. ISSN 1474-760X (Electronic). doi:10.1186/gb-2001-2-3-reviews3005.

Matias Ostrowski, Nuno B Carmo, Sophie Krumeich, Isabelle Fanget, Graça Raposo, Ariel Savina, Catarina F Moita, Kristine Schauer, Alistair N Hume, Rui P Freitas, Bruno Goud, Philippe Benaroch, Nir Hacohen, Mitsunori Fukuda, Claire Desnos, Miguel C Seabra, François Darchen, Sebastian Amigorena, Luis F Moita, and Clotilde Thery. Rab27a and Rab27b control different steps of the exosome secretion pathway. *Nature cell biology*, 12 (1):13–19, jan 2010. ISSN 1476-4679 (Electronic). doi:10.1038/ncb2000.

Leif Oxburgh, Gerald C Chu, Simon K Michael, and Elizabeth J Robertson. TGFbeta superfamily signals are required for morphogenesis of the kidney mesenchyme progenitor population. *Development (Cambridge, England)*, 131(18):4593–4605, sep 2004. ISSN 0950-1991 (Print). doi:10.1242/dev.01324.

Kasturi Pal, Sun-Hee Hwang, Bandarigoda Somatilaka, Hemant Badgandi, Peter K Jackson, Kathryn DeFea, and Saikat Mukhopadhyay. Smoothened determines β-arrestin-mediated removal of the G protein-coupled receptor Gpr161 from the primary cilium. *The Journal of cell biology*, 212(7):861–875, mar 2016. ISSN 1540-8140 (Electronic). doi:10.1083/jcb.201506132.

Wilhelm Palm, Marta M. Swierczynska, Veena Kumari, Monika Ehrhart-Bornstein, Stefan R. Bornstein, and Suzanne Eaton. Secretion and signaling activities of lipoprotein-associated hedgehog and non-sterol-modified hedgehog in flies and mammals. *PLoS Biology*, 11(3): e1001505, 03 2013. doi:10.1371/journal.pbio.1001505. URL https://journals.plos.org/plosbiology/article?id=10.1371/journal.pbio.1001505.

Yong Pan, Chunyang Brian Bai, Alexandra L Joyner, and Baolin Wang. Sonic hedgehog signaling regulates Gli2 transcriptional activity by suppressing its processing and degradation. *Molecular and cellular biology*, 26(9):3365–3377, may 2006. ISSN 0270-7306 (Print). doi:10.1128/MCB.26.9.3365-3377.2006.

Daniela Panáková, Hein Sprong, Eric Marois, Christoph Thiele, and Suzanne Eaton. Lipoprotein particles are required for Hedgehog and Wingless signalling. *Nature*, 435 (7038):58–65, 2005. ISSN 1476-4687. doi:10.1038/nature03504. URL https://doi.org/10.1038/nature03504.

A. Parchure, N. Vyas, C. Ferguson, R. G. Parton, and S. Mayor. Oligomerization and endocytosis of Hedgehog is necessary for its efficient exovesicular secretion. *Molecular Biology of the Cell*, 26(25):4700–4717, 2015. doi:10.1091/mbc.E15-09-0671.

Eric Parmantier, Bruce Lynn, Durward Lawson, Mark Turmaine, Soheila Sharghi Namini, Lisa Chakrabarti, Andrew P McMahon, Kristjan R Jessen, and Rhona Mirsky. Schwann Cell–Derived Desert Hedgehog Controls the Development of Peripheral Nerve Sheaths. *Neuron*, 23(4):713–724, 1999. ISSN 0896-6273. doi:https://doi.org/10.1016/S0896-6273(01)80030-1. URL https://www.sciencedirect.com/science/article/pii/S0896627301800301.

A Patapoutian and L F Reichardt. Roles of Wnt proteins in neural development and maintenance. *Current opinion in neurobiology*, 10(3):392–399, jun 2000. ISSN 0959-4388 (Print). doi:10.1016/s0959-4388(00)00100-8.

Akshay Patel, Yicong Wu, Xiaofei Han, Yijun Su, Tim Maugel, Hari Shroff, and Sougata Roy. Cytonemes coordinate asymmetric signaling and organization in the Drosophila muscle progenitor niche. *Nature Communications*, 13(1):1185, 2022. doi:10.1038/s41467-022-28587-z. URL https://www.nature.com/articles/s41467-022-28587-z.

R V 2nd Pearse, P J Scherz, J K Campbell, and C J Tabin. A cellular lineage analysis of the chick limb bud. *Developmental biology*, 310(2):388–400, oct 2007. ISSN 0012-1606 (Print). doi:10.1016/j.ydbio.2007.08.002.

R B Pepinsky, C Zeng, D Wen, P Rayhorn, D P Baker, K P Williams, S A Bixler, C M Ambrose, E A Garber, K Miatkowski, F R Taylor, E A Wang, and A Galdes. Identification of a palmitic acid-modified form of human Sonic hedgehog. *The Journal of biological chemistry*, 273(22):14037–14045, may 1998. ISSN 0021-9258 (Print). doi:10.1074/jbc.273.22.14037.

Madelen Persson, Despina Stamataki, Pascal te Welscher, Elisabet Andersson, Jens Böse, Ulrich Rüther, Johan Ericson, and James Briscoe. Dorsal-ventral patterning of the spinal cord requires Gli3 transcriptional repressor activity. *Genes & development*, 16(22):2865–2878, nov 2002. ISSN 0890-9369 (Print). doi:10.1101/gad.243402.

Christian P Petersen and Peter W Reddien. Wnt Signaling and the Polarity of the Primary Body Axis. *Cell*, 139(6):1056–1068, dec 2009. ISSN 0092-8674. doi:10.1016/j.cell.2009.11.035. URL https://doi.org/10.1016/j.cell.2009.11.035.

Kostadin Petrov, Bradley M Wierbowski, Jingjing Liu, and Adrian Salic. Distinct Cation Gradients Power Cholesterol Transport at Different Key Points in the Hedgehog Signaling Pathway. *Developmental cell*, 55(3):314–327.e7, nov 2020. ISSN 1878-1551 (Electronic). doi:10.1016/j.devcel.2020.08.002.

Ralitsa Petrova and Alexandra L. Joyner. Roles for hedgehog signaling in adult organ homeostasis and repair. *Development*, 141(18):3445–3457, 09 2014. ISSN 0950-1991. doi:10.1242/dev.083691. URL https://doi.org/10.1242/dev.083691.

Joseph Pickering, Kavitha Chinnaiya, and Matthew Towers. An autoregulatory cell cycle timer integrates growth and specification in chick wing digit development. *eLife*, 8:e47625, 2019. doi:10.7554/eLife.47625.

Autumn P Pomreinke, Gary H Soh, Katherine W Rogers, Jennifer K Bergmann, Alexander J Bläßle, and Patrick Müller. Dynamics of BMP signaling and distribution during zebrafish dorsal-ventral patterning. *eLife*, 6:e25861, 2017. ISSN 2050-084X. doi:10.7554/eLife.25861. URL `https://doi.org/10.7554/eLife.25861`.

J A Porter, K E Young, and P A Beachy. Cholesterol modification of hedgehog signaling proteins in animal development. *Science (New York, N.Y.)*, 274(5285):255–259, oct 1996a. ISSN 0036-8075 (Print). doi:10.1126/science.274.5285.255.

Jeffery A. Porter, Stephen C. Ekker, Woong-Jin Park, Derek P. von Kessler, Karen E. Young, Chieh-Ju Chen, Yan Ma, Amina S. Woods, Robert J. Cotter, Eugene V. Koonin, and Philip A. Beachy. Hedgehog patterning activity: role of a lipophilic modification mediated by the carboxy-terminal autoprocessing domain. *Cell*, 86(1):21–34, 1996b. doi:10.1016/s0092-8674(00)80074-4.

J Puschmann, G Steffes, J Froese, D Manikowski, K Ehring, J Wittke, C Garbers, S V Wegner, and K Grobe. Scube2 primes Dispatched and ADAM10-mediated Shh release by recruiting HDL acceptors to the plasma membrane. *Communications biology*, 9(1):189, jan 2026. ISSN 2399-3642 (Electronic). doi:10.1038/s42003-025-09466-x.

Xiaofeng Qi, Philip Schmiege, Elias Coutavas, Jiawei Wang, and Xiaochun Li. Structures of human Patched and its complex with native palmitoylated sonic hedgehog. *Nature*, 560 (7716):128–132, aug 2018. ISSN 1476-4687 (Electronic). doi:10.1038/s41586-018-0308-7.

Hongwu Qian, Pingping Cao, Miaohui Hu, Shuai Gao, Nieng Yan, and Xin Gong. Inhibition of tetrameric Patched1 by Sonic Hedgehog through an asymmetric paradigm. *Nature communications*, 10(1):2320, may 2019. ISSN 2041-1723 (Electronic). doi:10.1038/s41467-019-10234-9.

Luis Quijada and Isabel Guerrero. Detecting Tagged Hedgehog with Intracellular and Extracellular Immunocytochemistry for Functional Analysis. In Jamila I Horabin, editor, *Hedgehog Signaling Protocols*, pages 91–103. Humana Press, Totowa, NJ, 2007. ISBN 978-1-59745-516-9. doi:10.1007/978-1-59745-516-9_8. URL `https://doi.org/10.1007/978-1-59745-516-9_8`.

J. Rädler, D. Gupta, A. Zickler, and S. El Andaloussi. Exploiting the biogenesis of extracellular vesicles for bioengineering and therapeutic cargo loading. *Molecular Therapy*, 31(5): 1231–1250, 2023. doi:10.1016/j.ymthe.2023.02.013.

Felipe Andrés Ramírez-Weber and Thomas B. Kornberg. Cytonemes: Cellular processes that project to the principal signaling center in Drosophila imaginal discs. *Cell*, 97(5): 599–607, 1999. ISSN 00928674. doi:10.1016/S0092-8674(00)80771-0.

Mingyue Ren, Guihua Song, Yan Xu, Suping Yu, Yan Zhang, Mengmeng Sun, and Bingxue Zhang. Temporal regulation of wnt signaling in alveolar development and regeneration: mechanistic insights and therapeutic advances in chronic lung diseases. *Frontiers in Cell*

and Developmental Biology, Volume 14 - 2026, 2026. ISSN 2296-634X. URL https://www.frontiersin.org/journals/cell-and-developmental-biology/articles/10.3389/fcell.2026.1914253.

Vanessa Ribes and James Briscoe. Establishing and interpreting graded Sonic Hedgehog signaling during vertebrate neural tube patterning: the role of negative feedback. *Cold Spring Harbor perspectives in biology*, 1(2):a002014, aug 2009. ISSN 1943-0264 (Electronic). doi:10.1101/cshperspect.a002014.

Robert D. Riddle, Randy L. Johnson, Ed Laufer, and Cliff Tabin. Sonic hedgehog mediates the polarizing activity of the ZPA. *Cell*, 75(7):1401–1416, 1993. ISSN 00928674. doi:10.1016/0092-8674(93)90626-2.

Drucilla J Roberts, Randy L Johnson, Ann C Burke, Craig E Nelson, Bruce A Morgan, and Cliff Tabin. Sonic hedgehog is an endodermal signal inducing Bmp-4 and Hox genes during induction and regionalization of the chick hindgut. *Development*, 121(10):3163–3174, oct 1995. ISSN 0950-1991. doi:10.1242/dev.121.10.3163. URL https://doi.org/10.1242/dev.121.10.3163.

H Roelink, J A Porter, C Chiang, Y Tanabe, D T Chang, P A Beachy, and T M Jessell. Floor plate and motor neuron induction by different concentrations of the amino-terminal cleavage product of sonic hedgehog autoproteolysis. *Cell*, 81(3):445–455, may 1995. ISSN 0092-8674 (Print). doi:10.1016/0092-8674(95)90397-6.

Katherine W. Rogers and Alexander F. Schier. Morphogen gradients: from generation to interpretation. *Annual Review of Cell and Developmental Biology*, 27(1):377–407, 2011. doi:10.1146/annurev-cellbio-092910-154148. URL https://doi.org.

S. Rogers, C. Zhang, V. Anagnostidis, C. Liddle, M. L. Fishel, F. Gielen, and S. Scholpp. Cancer associated fibroblasts influence Wnt/PCP signaling in gastric cancer cells by cytoneme based dissemination of ROR2. *Proceedings of the National Academy of Sciences of the United States of America*, 120(39), 2023.

Patricia Rojas-Ríos, Isabel Guerrero, and Acaimo González-Reyes. Cytoneme-mediated delivery of hedgehog regulates the expression of bone morphogenetic proteins to maintain germline stem cells in Drosophila. *PLoS biology*, 10(4):e1001298, 2012. ISSN 1545-7885 (Electronic). doi:10.1371/journal.pbio.1001298.

Maria A Ros, Randall D Dahn, Marian Fernandez-Teran, Kay Rashka, Nicholas C Caruccio, Sean M Hasso, J James Bitgood, Joseph J Lancman, and John F Fallon. The chick oligozeugodactyly (ozd) mutant lacks sonic hedgehog function in the limb. *Development*, 130(3):527–537, feb 2003. ISSN 0950-1991. doi:10.1242/dev.00245. URL https://doi.org/10.1242/dev.00245.

Andreas Sagner and James Briscoe. Morphogen interpretation: concentration, time, competence, and signaling dynamics. *Wiley Interdisciplinary Reviews: Developmental Biology*, 6(4):e271, 2017. doi:10.1002/wdev.271.

Patricia Saiz-Lopez, Kavitha Chinnaiya, Victor M Campa, Irene Delgado, Maria A Ros, and Matthew Towers. An intrinsic timer specifies distal structures of the vertebrate limb. *Nature Communications*, 6(1):8108, 2015. ISSN 2041-1723. doi:10.1038/ncomms9108. URL `https://doi.org/10.1038/ncomms9108`.

Timothy A. Sanders, Esther Llagostera, and Maria Barna. Specialized filopodia direct long-range transport of shh during vertebrate tissue patterning. *Nature*, 497(7451):628–632, May 2013. doi:10.1038/nature12157. URL `https://nature.com`.

Lisette Sandoval, Mariana Labarca, Claudio Retamal, Paula Sánchez, Juan Larraín, and Alfonso González. Sonic hedgehog is basolaterally sorted from the TGN and transcytosed to the apical domain involving Dispatched-1 at Rab11-ARE. *Frontiers in Cell and Developmental Biology*, 10(December):1–24, 2022. ISSN 2296634X. doi:10.3389/fcell.2022.833175.

John W Saunders. The proximo-distal sequence of origin of the parts of the chick wing and the role of the ectoderm. *Journal of Experimental Zoology*, 108(3):363–403, 1948. doi:10.1002/jez.1401080304.

John W. Saunders, Jr. and Mary T. Gasseling. Ectodermal-mesenchymal interactions in the origin of limb symmetry. In Raúl Fleischmajer and Rupert E. Billingham, editors, *Epithelial-Mesenchymal Interactions*, pages 78–97. Williams & Wilkins, Baltimore, MD, 1968.

Madison B Schank, Juan Zhao, Ling Wang, Jonathan P Moorman, and Zhi Q Yao. Extracellular Vesicles: A Comprehensive Review of Their Origins, Functions, and Therapeutic Potential, 2026.

Paul J. Scherz, Edwina McGlinn, Sahar Nissim, and Clifford J. Tabin. Extended exposure to Sonic hedgehog is required for patterning the posterior digits of the vertebrate limb. *Developmental Biology*, 308(2):343–354, aug 2007. ISSN 00121606. doi:10.1016/j.ydbio.2007.05.030.

Thomas F Schilling, Qing Nie, and Arthur D Lander. Dynamics and precision in retinoic acid morphogen gradients. *Current opinion in genetics & development*, 22(6):562–569, dec 2012. ISSN 1879-0380 (Electronic). doi:10.1016/j.gde.2012.11.012.

G. Schlissel, M. Meziane, and D. Narducci. Diffusion barriers imposed by tissue topology shape Hedgehog morphogen gradients. *Proceedings of the National Academy of Sciences of the United States of America*, 121(36), 2024.

Gerald Schwank, Sascha Dalessi, Schu-Fee Yang, Ryohei Yagi, Aitana Morton de Lachapelle, Markus Affolter, Sven Bergmann, and Konrad Basler. Formation of the long range dpp morphogen gradient. *PLoS Biology*, 9(7):e1001111, Jul 2011. doi:10.1371/journal.pbio.1001111. URL `https://doi.org`.

D. Segal, N. Dhanyasi, E. D. Schejter, and B. Shilo. Adhesion and fusion of muscle cells are promoted by filopodia. *Developmental Cell*, 38(3):291–304, 2016. doi:10.1016/j.devcel.2016.07.010.

K Sekine, H Ohuchi, M Fujiwara, M Yamasaki, T Yoshizawa, T Sato, N Yagishita, D Matsui, Y Koga, N Itoh, and S Kato. Fgf10 is essential for limb and lung formation. *Nature genetics*, 21(1):138–141, jan 1999. ISSN 1061-4036 (Print). doi:10.1038/5096.

Julia Shangguan and Ronald S Rock. Hundreds of myosin 10s are pushed to the tips of filopodia and could cause traffic jams on actin. *eLife*, 12:RP90603, 2024. ISSN 2050-084X. doi:10.7554/eLife.90603. URL `https://doi.org/10.7554/eLife.90603`.

Soheila Sharghi-Namini, Mark Turmaine, Carola Meier, Vishal Sahni, Fujio Umehara, Kristjan R Jessen, and Rhona Mirsky. The Structural and Functional Integrity of Peripheral Nerves Depends on the Glial-Derived Signal Desert Hedgehog. *The Journal of Neuroscience*, 26(23):6364 LP – 6376, jun 2006. doi:10.1523/JNEUROSCI.0157-06.2006. URL `http://www.jneurosci.org/content/26/23/6364.abstract`.

Helen Sheldon, Elena Heikamp, Helen Turley, Robert Dragovic, Paul Thomas, Choo-Ean Oon, Russell Leek, Michael Edelmann, Benedikt Kessler, Shazia Din, et al. New mechanism for notch signaling to endothelium at a distance by delta-like 4 incorporation into exosomes. *Blood*, 116(13):2385–2394, 2010. doi:10.1182/blood-2010-04-279091.

Sailan Shui, Pablo Gainza, Leo Scheller, Che Yang, Yoichi Kurumida, Stéphane Rosset, Sandrine Georgeon, Raphaël B. Di Roberto, Rocío Castellanos-Rueda, Sai T. Reddy, and Bruno E. Correia. A rational blueprint for the design of chemically-controlled protein switches. *Nature Communications*, 12(1):1–12, 2021. ISSN 20411723. doi:10.1038/s41467-021-25735-9. URL `http://dx.doi.org/10.1038/s41467-021-25735-9`.

C H Sloop, L Dory, and P S Roheim. Interstitial fluid lipoproteins. *Journal of lipid research*, 28(3):225–237, mar 1987. ISSN 0022-2275 (Print).

J. C. Smith. The time required for positional signalling in the chick wing bud. *Journal of Embryology and Experimental Morphology*, 60:321–328, 1980.

M. Solursh, C. Singley, and R. Sreiter. The influence of epithelia on cartilage and loose connective tissue formation by limb mesenchyme cultures. *Developmental Biology*, 86(2): 471–482, 1981.

H Spemann and Hilde Mangold. über Induktion von Embryonalanlagen durch Implantation artfremder Organisatoren. *Archiv für mikroskopische Anatomie und Entwicklungsmechanik*, 100(3):599–638, 1924. ISSN 1432-041X. doi:10.1007/BF02108133. URL `https://doi.org/10.1007/BF02108133`.

Eliana Stanganello and Steffen Scholpp. Role of cytonemes in Wnt transport. *Journal of cell science*, 129(4):665–672, feb 2016. ISSN 1477-9137 (Electronic). doi:10.1242/jcs.182469.

Eliana Stanganello, Anja I.H. Hagemann, Benjamin Mattes, Claude Sinner, Dana Meyen, Sabrina Weber, Alexander Schug, Erez Raz, and Steffen Scholpp. Filopodia-based Wnt transport during vertebrate tissue patterning. *Nature Communications*, 6, 2015. ISSN 20411723. doi:10.1038/ncomms6846.

Oskar Staufer, Jochen Estebano Hernandez Bücher, Julius Fichtler, Martin Schröter, Ilia Platzman, and Joachim P Spatz. Vesicle Induced Receptor Sequestration: Mechanisms behind Extracellular Vesicle-Based Protein Signaling. *Advanced science (Weinheim, Baden-Wurttemberg, Germany)*, 9(13):e2200201, may 2022. ISSN 2198-3844 (Electronic). doi:10.1002/advs.202200201.

Harald Stenmark. Rab gtpases as coordinators of vesicle traffic. *Nature Reviews Molecular Cell Biology*, 10(8):513–525, 2009. doi:10.1038/nrm2728.

Maura Strigini and Stephen M Cohen. A Hedgehog activity gradient contributes to AP axial patterning of the Drosophila wing. *Development*, 124(22):4697–4705, nov 1997. ISSN 0950-1991. doi:10.1242/dev.124.22.4697. URL `https://doi.org/10.1242/dev.124.22.4697`.

Xin Sun, Francesca V Mariani, and Gail R Martin. Functions of FGF signalling from the apical ectodermal ridge in limb development. *Nature*, 418(6897):501–508, aug 2002. ISSN 0028-0836 (Print). doi:10.1038/nature00902.

B. H. Sung, A. von Lersner, J. Guerrero, E. S. Krystofiak, D. Inman, R. Pelletier, A. Zijlstra, S. M. Ponik, and A. M. Weaver. A live cell reporter of exosome secretion and uptake reveals pathfinding behavior of migrating cells. *Nature Communications*, 11(1):1–15, 2020. doi:10.1038/s41467-020-15747-2.

Miriam Fussae Suzuki, João Ezequiel Oliveira, Renata Damiani, Eliana Rosa Lima, Kleicy Cavalcante Amaral, Anderson Maikon de Souza Santos, Geraldo Santana Magalhães, Leonardo Perez Faverani, Luis Antonio Violin Dias Pereira, Fabiana Medeiros Silva, and Paolo Bartolini. Human bone morphogenetic protein-2 (hBMP-2) characterization by physical-chemical, immunological and biological assays. *AMB Express*, 10(1):34, feb 2020. ISSN 2191-0855 (Print). doi:10.1186/s13568-020-0964-5.

Tetsuya Tabata and Thomas B Kornberg. Hedgehog is a signaling protein with a key role in patterning Drosophila imaginal discs. *Cell*, 76(1):89–102, jan 1994. ISSN 0092-8674. doi:10.1016/0092-8674(94)90175-9. URL `https://doi.org/10.1016/0092-8674(94)90175-9`.

Ritsuko Takada, Yoshinori Satomi, Tomoko Kurata, Naoto Ueno, Shigemi Norioka, Hisato Kondoh, Toshifumi Takao, and Shinji Takada. Monounsaturated Fatty Acid Modification of Wnt Protein: Its Role in Wnt Secretion. *Developmental Cell*, 11(6):791–801, 2006. ISSN 1534-5807. doi:https://doi.org/10.1016/j.devcel.2006.10.003. URL `https://www.sciencedirect.com/science/article/pii/S1534580706004552`.

Ayumi Taniguchi and Toshiaki Watanabe. Roles of biotin in growing ovarian follicles and embryonic development in domestic fowl. *Journal of Nutritional Science and Vitaminology*, 53(6):457–463, 2007. ISSN 03014800. doi:10.3177/jnsv.53.457.

Pascal te Welscher, Marian Fernandez-Teran, Marian A Ros, and Rolf Zeller. Mutual genetic antagonism involving GLI3 and dHAND prepatterns the vertebrate limb bud mesenchyme

prior to SHH signaling. *Genes & development*, 16(4):421–426, feb 2002. ISSN 0890-9369 (Print). doi:10.1101/gad.219202.

C. Tickle, D. Summerbell, and L. Wolpert. Positional signalling and specification of digits in chick limb morphogenesis. *Nature*, 254(5497):199–202, 1975. doi:10.1038/254199a0. URL https://www.nature.com/articles/254199a0.

Cheryll Tickle. How the embryo makes a limb: determination, polarity and identity. *Journal of anatomy*, 227(4):418–430, oct 2015. ISSN 1469-7580 (Electronic). doi:10.1111/joa.12361.

Bryan P Toole. Hyaluronan: from extracellular glue to pericellular cue. *Nature reviews. Cancer*, 4(7):528–539, jul 2004. ISSN 1474-175X (Print). doi:10.1038/nrc1391.

Matthew Towers, Ruth Mahood, Yili Yin, and Cheryll Tickle. Integration of growth and specification in chick wing digit-patterning. *Nature*, 452(7189):882–886, apr 2008. ISSN 1476-4687 (Electronic). doi:10.1038/nature06718.

Matthew Towers, Jason Signolet, Adrian Sherman, Helen Sang, and Cheryll Tickle. Insights into bird wing evolution and digit specification from polarizing region fate maps. *Nature communications*, 2:426, aug 2011. ISSN 2041-1723 (Electronic). doi:10.1038/ncomms1437.

Bipin Kumar Tripathi and Kenneth D Irvine. The wing imaginal disc. *Genetics*, 220(4): iyac020, 04 2022. doi:10.1093/genetics/iyac020. URL https://doi.org/10.1093/genetics/iyac020.

H. Tukachinsky, R. P. Kuzmickas, C. Y. Jao, J. Liu, and A. Salic. Dispatched and Scube mediate the efficient secretion of the cholesterol-modified Hedgehog ligand. *Cell Reports*, 2(2):308–320, 2012. doi:10.1016/j.celrep.2012.07.010.

Hanna Tukachinsky, Lyle V. Lopez, and Adrian Salic. A mechanism for vertebrate hedgehog signaling: recruitment to cilia and dissociation of sufu–gli protein complexes. *The Journal of Cell Biology*, 191(2):415–428, 2010. doi:10.1083/jcb.201004108. URL https://doi.org/10.1083/jcb.201004108.

Sarah Tulin and Angelike Stathopoulos. Analysis of Thisbe and Pyramus functional domains reveals evidence for cleavage of Drosophila FGFs. *BMC developmental biology*, 10:83, aug 2010. ISSN 1471-213X (Electronic). doi:10.1186/1471-213X-10-83.

Alan Mathison Turing. The chemical basis of morphogenesis. *Philosophical Transactions of the Royal Society of London. B, Biological Sciences*, 237(641):37–72, aug 1952. ISSN 0080-4622. doi:10.1098/rstb.1952.0012. URL https://doi.org/10.1098/rstb.1952.0012.

Giuseppina Turturici, Rosaria Tinnirello, Gabriella Sconzo, and Fabiana Geraci. Extracellular membrane vesicles as a mechanism of cell-to-cell communication: advantages and disadvantages. *American Journal of Physiology-Cell Physiology*, 306(7):C621–C633, 2015. doi:10.1152/ajpcell.00228.2013. URL https://journals.physiology.org/doi/full/10.1152/ajpcell.00228.2013.

Guillaume van Niel, Gisela D'Angelo, and Graça Raposo. Shedding light on the cell biology of extracellular vesicles. *Nature Reviews Molecular Cell Biology*, 19(4):213–228, apr 2018. doi:10.1038/nrm.2017.125. URL https://doi.org.

Markku Varjosalo and Jussi Taipale. Hedgehog: functions and mechanisms. *Genes & development*, 22(18):2454–2472, sep 2008. ISSN 0890-9369 (Print). doi:10.1101/gad.1693608.

F. J. Verweij, M. P. Bebelman, C. R. Jimenez, J. J. Garcia-Vallejo, H. Janssen, J. Neefjes, J. C. Knol, R. de Goeij-de Haas, S. R. Piersma, S. R. Baglio, M. Verhage, J. M. Middeldorp, A. Zomer, J. van Rheenen, M. G. Coppolino, I. Hurbain, G. Raposo, M. J. Smit, R. F. G. Toonen, et al. Quantifying exosome secretion from single cells reveals a modulatory role for GPCR signaling. *Journal of Cell Biology*, 217(3):1129–1142, 2018. doi:10.1083/jcb.201703206.

Michael P Verzi and Ramesh A Shivdasani. Wnt signaling in gut organogenesis. *Organogenesis*, 4(2):87–91, apr 2008. ISSN 1547-6278 (Print). doi:10.4161/org.4.2.5854.

Jean-Paul Vincent and James Briscoe. Morphogens. *Current Biology*, 11(21):R851–R854, oct 2001. ISSN 0960-9822. doi:10.1016/S0960-9822(01)00514-0. URL https://doi.org/10.1016/S0960-9822(01)00514-0.

S. Vincent, A. Thomas, B. Brasher, and J. D. Benson. Targeting of proteins to membranes through hedgehog auto-processing. *Nature Biotechnology*, 21:936–941, 2003.

C. S. von Bartheld and A. L. Altick. Multivesicular bodies in neurons: Distribution, protein content, and trafficking functions. *Progress in Neurobiology*, 93(3):313–340, 2011. doi:10.1016/j.pneurobio.2011.01.003.

Neha Vyas, Debanjan Goswami, A. Manonmani, Priti Sharma, Riya Raghupathy, S. Vijayakumar, Bhushan Madan, L. S. Shashidhara, R. Sowdhamini, and Satyajit Mayor. Nanoscale organization of hedgehog is essential for long-range signaling. *Cell*, 133(7): 1214–1227, 2008. doi:10.1016/j.cell.2008.05.026. URL https://www.cell.com/fulltext/S0092-8674(08)00685-5.

Neha Vyas, Ankita Walvekar, Dhananjay Tate, Vairavan Lakshmanan, Dhiru Bansal, Alessandra Lo Cicero, Graca Raposo, Dasaradhi Palakodeti, and Jyotsna Dhawan. Vertebrate Hedgehog is secreted on two types of extracellular vesicles with different signaling properties. *Scientific Reports*, 4(1):1–12, dec 2014. ISSN 20452322. doi:10.1038/srep07357. URL www.nature.com/scientificreports.

A. Walvekar, S. Pandey, S. S. Kamat, R. K. Ladher, and N. Vyas. The patterning and proliferation roles of Shh are partitioned on distinct exosomes. *Developmental Biology*, 528:239–254, 2025. doi:10.1016/j.ydbio.2025.09.017.

B Wang, J F Fallon, and P A Beachy. Hedgehog-regulated processing of Gli3 produces an anterior/posterior repressor gradient in the developing vertebrate limb. *Cell*, 100(4): 423–434, feb 2000. ISSN 0092-8674 (Print). doi:10.1016/s0092-8674(00)80678-9.

Chengbing Wang, Ulrich Rüther, and Baolin Wang. The Shh-independent activator function of the full-length Gli3 protein and its role in vertebrate limb digit patterning. *Developmental biology*, 305(2):460–469, may 2007. ISSN 0012-1606 (Print). doi:10.1016/j.ydbio.2007.02.029.

Shuo Wang, Yosuke Tanaka, Ying Xu, Sen Takeda, and Nobutaka Hirokawa. KIF3B promotes a PI3K signaling gradient causing changes in a Shh protein gradient and suppressing polydactyly in mice. *Developmental Cell*, 57(19):2273–2289.e11, 2022. ISSN 18781551. doi:10.1016/j.devcel.2022.09.007. URL `https://doi.org/10.1016/j.devcel.2022.09.007`.

Xu Wang, Siqi Li, Yuan Liu, Xiangyu Kuang, Jianxin Chen, Pei Yu, Lianzheng Zhao, Ze Zhang, Meimei Huang, Liansheng Liu, Mengxian Zhang, Yalong Wang, Weizhi Ji, Jinsong Li, Lei Zhang, and Ye-Guang Chen. Positional BMP signaling orchestrates villus length in the small intestine. *Nature communications*, 16(1):5461, jul 2025. ISSN 2041-1723 (Electronic). doi:10.1038/s41467-025-60643-2.

Yin Wang, Xi Wang, Thorsten Wohland, and Karuna Sampath. Extracellular interactions and ligand degradation shape the nodal morphogen gradient. *eLife*, 5:e13879, 2016. ISSN 2050-084X. doi:10.7554/eLife.13879. URL `https://doi.org/10.7554/eLife.13879`.

Ortrud Wartlick, Anna Kicheva, and Marcos González-Gaitán. Morphogen gradient formation. *Cold Spring Harbor perspectives in biology*, 1(3):a001255, sep 2009. ISSN 1943-0264 (Electronic). doi:10.1101/cshperspect.a001255.

Joshua A Welsh, Deborah C I Goberdhan, Lorraine O'Driscoll, Edit I Buzas, Cherie Blenkiron, Benedetta Bussolati, Houjian Cai, Dolores Di Vizio, Tom A P Driedonks, Uta Erdbrügger, Juan M Falcon-Perez, Qing-Ling Fu, Andrew F Hill, Metka Lenassi, Sai Kiang Lim, Mỹ G Mahoney, Sujata Mohanty, Andreas Möller, Rienk Nieuwland, Takahiro Ochiya, Susmita Sahoo, Ana C Torrecilhas, Lei Zheng, Andries Zijlstra, Sarah Abuelreich, Reem Bagabas, Paolo Bergese, Esther M Bridges, Marco Brucale, Dylan Burger, Randy P Carney, Emanuele Cocucci, Rossella Crescitelli, Edveena Hanser, Adrian L Harris, Norman J Haughey, An Hendrix, Alexander R Ivanov, Tijana Jovanovic-Talisman, Nicole A Kruh-Garcia, Vroniqa Ku'ulei-Lyn Faustino, Diego Kyburz, Cecilia Lässer, Kathleen M Lennon, Jan Lötvall, Adam L Maddox, Elena S Martens-Uzunova, Rachel R Mizenko, Lauren A Newman, Andrea Ridolfi, Eva Rohde, Tatu Rojalin, Andrew Rowland, Andras Saftics, Ursula S Sandau, Julie A Saugstad, Faezeh Shekari, Simon Swift, Dmitry Ter-Ovanesyan, Juan P Tosar, Zivile Useckaite, Francesco Valle, Zoltan Varga, Edwin van der Pol, Martijn J C van Herwijnen, Marca H M Wauben, Ann M Wehman, Sarah Williams, Andrea Zendrini, Alan J Zimmerman, Clotilde Théry, and Kenneth W Witwer. Minimal information for studies of extracellular vesicles (MISEV2023): From basic to advanced approaches. *Journal of extracellular vesicles*, 13(2):e12404, feb 2024. ISSN 2001-3078 (Electronic). doi:10.1002/jev2.12404.

Bradley M Wierbowski, Kostadin Petrov, Laura Aravena, Garrick Gu, Yangqing Xu, and Adrian Salic. Hedgehog Pathway Activation Requires Coreceptor-Catalyzed, Lipid-

Dependent Relay of the Sonic Hedgehog Ligand. *Developmental Cell*, 55(4):450–467.e8, nov 2020. ISSN 1534-5807. doi:10.1016/j.devcel.2020.09.017. URL https://doi.org/10.1016/j.devcel.2020.09.017.

Karl Willert, Jeffrey D Brown, Esther Danenberg, Andrew W Duncan, Irving L Weissman, Tannishtha Reya, John R 3rd Yates, and Roel Nusse. Wnt proteins are lipid-modified and can act as stem cell growth factors. *Nature*, 423(6938):448–452, may 2003. ISSN 0028-0836 (Print). doi:10.1038/nature01611.

L. Wolpert. Positional information and the spatial pattern of cellular differentiation. *Journal of Theoretical Biology*, 25(1):1–47, 1969. ISSN 10958541. doi:10.1016/S0022-5193(69)80016-0.

Lewis Wolpert. The french flag problem: A contribution to the discussion on pattern development and regeneration. In Conrad Hal Waddington, editor, *Towards a Theoretical Biology: 1. Prolegomena*, pages 125–140. Edinburgh University Press, Edinburgh, 1968.

M. Xu, J. Ji, D. Jin, Y. Wu, T. Wu, R. Lin, S. Zhu, F. Jiang, Y. Ji, B. Bao, M. Li, W. Xu, and M. Xiao. The biogenesis and secretion of exosomes and multivesicular bodies (MVBs): Intercellular shuttles and implications in human diseases. *Genes and Diseases*, 10(5):1894–1907, 2023. doi:10.1016/j.gendis.2022.03.021.

Yukiko M. Yamashita, Michiyuki Inaba, and Michael Buszczak. Specialized intercellular communications via cytonemes and nanotubes. *Annual Review of Cell and Developmental Biology*, 34(1):59–84, 2018. doi:10.1146/annurev-cellbio-100617-062932. URL https://doi.org.

Yasuo Yamazaki, Lucy Palmer, Cyrille Alexandre, Satoshi Kakugawa, Karen Beckett, Isabelle Gaugue, Ruth H Palmer, and Jean-Paul Vincent. Godzilla-dependent transcytosis promotes Wingless signalling in Drosophila wing imaginal discs. *Nature cell biology*, 18 (4):451–457, apr 2016. ISSN 1476-4679 (Electronic). doi:10.1038/ncb3325.

Yifang Yan and Qiang Wang. BMP Signaling: Lighting up the Way for Embryonic Dorsoventral Patterning. *Frontiers in Cell and Developmental Biology*, Volume 9 -, 2021. ISSN 2296-634X. URL https://www.frontiersin.org/journals/cell-and-developmental-biology/articles/10.3389/fcell.2021.799772.

Dakai Yang, Jing Liu, Hui Qian, and Qin Zhuang. Cancer-associated fibroblasts: from basic science to anticancer therapy. *Experimental & Molecular Medicine*, 55(7):1322–1332, Jul 2023. doi:10.1038/s12276-023-01013-0. URL https://doi.org.

Yingzi Yang. Growth and patterning in the limb: Signaling gradients make the decision. *Science Signaling*, 2(53):pe3–pe3, 2009. doi:10.1126/scisignal.253pe3. URL https://www.science.org/doi/abs/10.1126/scisignal.253pe3.

Yingzi Yang, Ourania Drossopoulou, Pao-Tien Chuang, Delphine Duprez, Elsa Marti, David Bumcrot, Neil Vargesson, Jon Clarke, Lee Niswander, Andrew McMahon, and Cheryll

Tickle. Relationship between dose, distance and time in sonic hedgehog-mediated regulation of anteroposterior polarity in the chick limb. *Development*, 124(21):4393–4404, 1997. doi:10.1242/dev.124.21.4393. URL https://biologists.com.

S Yonei-Tamura, T Endo, H Yajima, H Ohuchi, H Ide, and K Tamura. FGF7 and FGF10 directly induce the apical ectodermal ridge in chick embryos. *Developmental biology*, 211 (1):133–143, jul 1999. ISSN 0012-1606 (Print). doi:10.1006/dbio.1999.9290.

Shuizi Rachel Yu, Markus Burkhardt, Matthias Nowak, Jonas Ries, Zdeněk Petrášek, Steffen Scholpp, Petra Schwille, and Michael Brand. Fgf8 morphogen gradient forms by a source-sink mechanism with freely diffusing molecules. *Nature*, 461(7263):533–536, 2009. ISSN 1476-4687. doi:10.1038/nature08391. URL https://doi.org/10.1038/nature08391.

Shen Yue, Liu-Ya Tang, Ying Tang, Yi Tang, Qiu-Hong Shen, Jie Ding, Yan Chen, Zengdi Zhang, Ting-Ting Yu, Ying E Zhang, and Steven Y Cheng. Requirement of Smurf-mediated endocytosis of Patched1 in sonic hedgehog signal reception. *eLife*, 3:e02555, 2014. ISSN 2050-084X. doi:10.7554/eLife.02555. URL https://doi.org/10.7554/eLife.02555.

K. Yusa, L. Zhou, M. Amy, A. Bradley, and N. L. Craig. A hyperactive piggyBac transposase for mammalian applications. *Proceedings of the National Academy of Sciences of the United States of America*, 108(4):1531–1536, 2011. doi:10.1073/pnas.1008322108.

Chengting Zhang and Steffen Scholpp. Cytonemes in development. *Current Opinion in Genetics & Development*, 57:25–30, 2019. ISSN 0959-437X. doi:https://doi.org/10.1016/j.gde.2019.06.005. URL https://www.sciencedirect.com/science/article/pii/S0959437X19300255.

Hongquan Zhang, Jonathan S Berg, Zhilun Li, Yunling Wang, Pernilla Lång, Aurea D Sousa, Aparna Bhaskar, Richard E Cheney, and Staffan Strömblad. Myosin-X provides a motor-based link between integrins and the cytoskeleton. *Nature cell biology*, 6(6):523–531, jun 2004. ISSN 1465-7392 (Print). doi:10.1038/ncb1136.

Zijian Zhang, Nicolas Denans, Yingfei Liu, Olena Zhulyn, Hannah D. Rosenblatt, Marius Wernig, and Maria Barna. Optogenetic manipulation of cellular communication using engineered myosin motors. *Nature Cell Biology*, 23(2):198–208, 2021. ISSN 14764679. doi:10.1038/s41556-020-00625-2. URL http://dx.doi.org/10.1038/s41556-020-00625-2.

Shaohua Zhou, Wang-Che Lo, Jeffrey L Suhalim, Michelle A Digman, Enrico Gratton, Qing Nie, and Arthur D Lander. Free extracellular diffusion creates the dpp morphogen gradient of the drosophila wing disc. *Current Biology*, 22(8):668–675, 2012. doi:10.1016/j.cub.2012.02.065.

Jianjian Zhu, Eiichiro Nakamura, Minh-Thanh Nguyen, Xiaozhong Bao, Haruhiko Akiyama, and Susan Mackem. Uncoupling Sonic Hedgehog Control of Pattern and Expansion of

the Developing Limb Bud. *Developmental Cell*, 14(4):624–632, 2008. ISSN 1534-5807. doi:https://doi.org/10.1016/j.devcel.2008.01.008. URL https://www.sciencedirect.com/science/article/pii/S1534580708000361.

Jianjian Zhu, Rashmi Patel, Anna Trofka, Brian D Harfe, and Susan Mackem. Sonic hedgehog is not a limb morphogen but acts as a trigger to specify all digits in mice. *Developmental cell*, 57(17):2048–2062.e4, sep 2022. ISSN 1878-1551 (Electronic). doi:10.1016/j.devcel.2022.07.016.

Shiwen Zhu, Yi Ting Loo, Sapthaswaran Veerapathiran, Tricia Y J Loo, Bich Ngoc Tran, Cathleen Teh, Jun Zhong, Paul Matsudaira, Timothy E Saunders, and Thorsten Wohland. Receptor binding and tortuosity explain morphogen local-to-global diffusion coefficient transition. *Biophysical journal*, 124(6):963–979, mar 2025. ISSN 1542-0086 (Electronic). doi:10.1016/j.bpj.2024.07.024.

Tenghan Zhuang. Hedgehog pathway, cell cycle, and primary cilium. *Cell Death Discovery*, 11(1):302, 2025. ISSN 2058-7716. doi:10.1038/s41420-025-02605-7. URL https://doi.org/10.1038/s41420-025-02605-7.